PERFORMANCE EVALUATION OF PV DRIVEN NF-RO HYBRID WATER TREATMENT SYSTEM

Ph.D. THESIS

by

MANOJ CHANDRA GARG

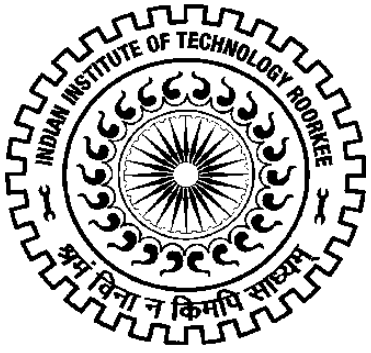

DEPARTMENT OF HYDROLOGY
INDIAN INSTITUTE OF TECHNOLOGY ROORKEE
ROORKEE-247 667 (INDIA)
FEBRUARY, 2015

PERFORMANCE EVALUATION OF PV DRIVEN NF-RO HYBRID WATER TREATMENT SYSTEM

A THESIS
Submitted in partial fulfilment of the requirements for the award of the degree of

DOCTOR OF PHILOSOPHY
in
HYDROLOGY

by

MANOJ CHANDRA GARG

DEPARTMENT OF HYDROLOGY
INDIAN INSTITUTE OF TECHNOLOGY ROORKEE
ROORKEE-247 667 (INDIA)
FEBRUARY, 2015

INDIAN INSTITUTE OF TECHNOLOGY ROORKEE
ROORKEE

CANDIDATE'S DECLARATION

I hereby certify that the work which is being presented in the thesis entitled "**PERFORMANCE EVALUATION OF PV DRIVEN NF-RO HYBRID WATER TREATMENT SYSTEM"** in partial fulfilment of the requirements for the award of the Degree of Doctor of Philosophy and submitted in the **Department of Hydrology of the Indian Institute of Technology Roorkee** is an authentic record of my own work carried out during a period from July, 2009 to February, 2015 under the supervision of Dr. Himanshu Joshi, Professor, Department of Hydrology, Indian Institute of Technology Roorkee.

The matter presented in the thesis has not been submitted by me for the award of any other degree of this or any other Institute.

(MANOJ CHANDRA GARG)

This is to certify that the above statement made by the candidate is correct to the best of my knowledge.

Dated**:** February , 2015

(HIMANSHU JOSHI)
Supervisor

Abstract

Inland salinity of groundwater, having a total dissolved solids (TDS) of 1500–3000 mg/L, has been found in substantial volumes throughout the majority of India. However, these parts of the India also receive a 5.5 – 6 kWh/m^2/day of annual average global horizontal irradiance (GHI) making the photovoltaic (PV) the apparent selection as a renewable energy source. Nanofiltration (NF) and Reverse Osmosis (RO) membrane are processes used for the removal of divalent ions (Calcium, Magnesium, Sulphate etc.) and monovalent ions (Sodium, Chloride etc.) respectively [131, 215, 220]. Integration of renewable energy (PV) with desalination technologies (NF and RO) may provide the solution of drinking water problem in areas suffering from brackish ground water sources as well as having non-existent or limited electricity accessibility.

Several solar powered membrane filtration systems have been investigated earlier. The performance and overall cost of such systems has been based on water productivity, rejection capability and power consumption. As a higher feed water recovery would result in smaller installation size of the membrane unit as well as have less capital and operating costs, many attempts have been made to increase the water recovery of membrane processes. In addition to this, increase in recovery by using concentrate staging has also been investigated earlier resulting in a significant reduction in Specific Energy Consumption (SEC), henceforth the overall system cost. Although some researchers had shown an influence of NF-RO hybridization on plant performance in terms of water quality in permeate staging configuration but, similar studies with concentrate staging configuration were not reported to minimize the SEC enabling its integration with solar PV system.

In view of the above, NF-RO hybrid systems with both the configurations apparently need to be studied with an aim to increase water recovery, minimize the SEC and assessment of its compatibility with the PV system.The main objectives of this research work are:

1. Process optimization for NF and RO membrane systems in isolation and hybrid modes for both the staging configurations.
2. To check the operational feasibility of PV system driven NF-RO hybrid system and evaluate seasonal fluctuation of solar radiation on plant performance.
3. Economic assessment and recommendation for up-scaling to pilot studies.

This thesis is composed of seven chapters. Chapter 1 deals with the introduction which includes problem statement, research gaps, objectives, research design and methodology, significance and organisation of thesis. Chapter 2 presents the literature review, discussing the studies carried out in the field of solar desalination with special interest of PV-RO technology and related issues along with the need of research in the present scenario.

Chapter 3 presents methodology of the research work performed in this thesis. Overview of the system configuration and experimental procedure has been discussed in detail. A laboratory scale hybrid membrane unit was designed and procured to perform various membrane experiments in isolation and hybrid modes. A 1.5 kWp grid connected PV system consisting of multi-crystalline silicon PV modules was employed in combination with grid connected solar inverter capable to supply loads of up to 3 kWp, metering devices and distribution system. Optimization experiments were carried out to maximize water recovery and TDS rejection and to minimize SEC of small scale brackish water RO process [116] using pH, feed temperature, feed pressure and concentration of feed solution as input parameters. Six TFC RO and NF (molecular weight cut off-MWCO 100, 250 and 400 Da) membranes from four leading manufacturing companies (CSM, Dow, Vontron and Permionics) in spiral wound configuration were used to perform laboratory scale experiments. In present study, synthetic water was formulated in the laboratory on the basis of major ionic elements of actual groundwater and further used for performing different membrane experiments. Furthermore, to validate the accuracy of this formulation, concentrations of elements of the synthetic groundwater were analysed experimentally and compared with that of actual ground water. The two results displayed a net correlation of 0.9982.

Chapter 4 deals with membrane characterization and optimization of input process parameters. This chapter presents the details of characterization of six commercially available small scale RO and NF membranes and also the optimization experiments using central composite design (CCD) of response surface methodology (RSM). Physical aspects of characterizing NF and RO membranes from various manufacturing brand were investigated. Physical surface characteristics including surface roughness, occurrence of functional groups and hydrophobicity/hydrophilicity properties were determined by atomic force microscopy (AFM), fourier transform infrared spectroscopy (FTIR) and contact angle measurement, respectively. A correlation between surface properties and membrane filtration results were obtained. From AFM analysis, it was revealed that the CSM RO membrane was the smoothest, with an RMS (Rq)

value of 33.99 µm. From FTIR analysis graphs it could be predicted that all RO and NF membranes contained thin polyamide layer with polysulfone support [152]. The smaller contact angle (higher hydrophilicity) and smoother surface of CSM membrane among RO membranes and NF250 among NF membranes could be the reason of its better performance. In the present study, optimization was performed employing RSM using CCD. Furthermore, experiments to validate these RO results were conducted employing the optimized process variables values derived from RSM prediction. Since RSM proposes the surface plots offering a better approach to envisage relations between independent and dependent variables, both the RSM and artificial neural network (ANN) methods were applied for modelling using the same experimental data. Finally, the validation of optimized process conditions suggested by the RSM was also carried out by the generated ANN model in MATLAB. After employing RSM models for process parameters optimisation on all NF and RO membranes, CSM membrane (among RO membranes) showed the best performance at 31.92^{o}C temperature, 0.79 MPa pressure, 1500 mg/l feed salt concentration and 6.53 pH (very near to the actual i.e. 6.7) with 19.25% water recovery, 89.2% salt rejection and 17.6 kWh/m^3 of SEC. Also, NF250 showed the best performance (among NF membranes) at 30^{o}C temperature, 1.08 MPa pressure, 1500 mg/l feed salt concentration and pH 7.15 with 18.98% water recovery, 70.64% salt rejection and 9.35 kWh/m^3 of SEC. Removal efficiency of major ions of validation experiment was observed. The removal efficiency of divalent ions (Ca^{2+}<Mg^{2+}<SO_4^{2+}) was found to be higher as compared to monovalent ions (NO_3^- <Na^+<Cl^-) through RO and NF membranes. However, the overall removal efficiency of ions was generally higher in RO membranes than the NF membranes. Furthermore, ANN model was used to validate the RSM predicted optimized process conditions. Feed water temperature (31.94 ^{o}C), pressure (0.78 MPa), salt concentration (1500 mg/L) and pH (6.53) were used as input parameters for the ANN model. ANN predicted 19.51% and 18.59% of water recovery, 88.92% and 71.4% of TDS rejection and 16.60 kWh/m^3 9.43 kWh/m^3 of SEC for CSM and NF250 membranes respectively, at optimal process conditions. A comparison of the predicted values between ANN and RSM revealed that the values predicted by both RSM and ANN model were much closer to experimental values.

Chapter 5 deals with the RO - NF hybrid experiments with PV system. After RSM optimization, best RO and NF membranes were selected to perform validation runs followed by NF-RO hybrid experiments. According to the operating conditions of feed, concentrate and permeate flow streams, the membrane performance data in isolation and hybrid configurations

were analysed. The membrane filtration unit was designed to operate for about 6 to 8 hrs./day, depending on peak sun shine hours (PSSH). Monthly variation in current generation mainly depends on the sunny or cloudy nature of sky. Generated current was compared with the current required by hybrid membrane system. It was apparent that the amount of current generated during the PSSH was enough to operate the NF-C-RO hybrid membrane unit. Excess energy, which was not utilized by membrane filtration system,could be utilized in maintaing the temperature of feed water and/or for pumping the water. The chemical analysis by scanning electron microscope-energy dispersive using X-Ray (SEM-EDX) demonstrated that Ca, Mg, Cl, O, C and S were the major elements of the inorganic deposits. The next highest cation was Mg involved in the inorganic fouling process. The SEM-EDX analysis of inorganically fouled membranes signified that substantial quantity of deposits contained inorganic material and minerals. For every possible compound initial search was performed using X-Ray diffraction analysis (XRD) data base. The XRD patterns of the all inorganically fouled membranes were almost similar. Calcite ($CaCO_3$) was observed as a common element of the crystalline phase deposits observed on the all membrane surface

The aim of the chapter 6 is the economic assessment to estimate the water production cost. For estimation of water production cost, common technical assumptions, specifications and design parameters were considered for PV assisted RO and NF membrane systems in isolation and hybrid mode. The water production cost of NF-RO hybrid system (Rs.99.81/m^3) was about 1.6 times lesser than NF (Rs.158.46/m^3) and 4 times lesser than RO (Rs.400.49/m^3) system in isolation. Moreover, this cost could be further reduced on increasing the capacity of the membrane system and by providing more subsidy on solar system as an incentive to its users. The water production cost of Rs.146.5/m^3, Rs.370.26/m^3 and Rs.92.87/m^3 for the PV-NF, PV-RO and PV-NF/RO hybrid membrane systems respectively could be reached when the plant life increases to 30 years.

Finally chapter 7 presents the conclusions and contributions made by the research work as well as the recommendation for future work.

Acknowledgements

This thesis could not have been in its present form without the assistance and support of many people who deserve special mention. First, I would like to thank my supervisor, Prof. Himanshu Joshi for his excellent guidance and support. He spent his precious time and effort directing this research work. His constant encouragement and stimulating discussions were helpful in taking this research to its fruitful ending.

I am also thankful to Head of the Department, Prof. M. Perumal for providing all the necessary facilities. This acknowledgement will be incomplete without mentioning the names of chairman of my research committee, Dr. N.K. Goel; Dr. Manoj K. Jain and Prof. Pradeep Kumar, the members of my research committee for their valuable suggestions and healthy criticism during my research work.

I would like to thank Ministry of Human Resource and Development (MHRD), Government of India, New Delhi, India and Ministry of Drinking Water and Sanitation, New Delhi, India for providing me financial assistance to carry out this research work. My deepest regards goes to Indian Institute of Technology Roorkee, Roorkee for providing me research platform and well equipped laboratory in Department of Hydrology.

Special thanks go to Mr. J. K. Sharma for making arrangement of chemicals and equipments required for research work. I would like to thank Shyam for his helping hand during the experimental work. I would also like to thank my colleagues Pinki, Reshu, Asmita, Ajay and Sunil for the round of discussions we had altogether sometimes regarding research, sometime social and philosophical.

I extend my gratitude to my parents Mrs. Krishna Garg and Mr. Satish Garg for their assistance in various ways. It was their patience, encouragement and faith in me that I could complete this work. The study would not be possible without the loving support of my wife, Smriti. I appreciate her for love and patience during all these years. To my beloved daughter Gauri, I would like to express my thanks for being such a good girl always cheering me up.

Last but not least I am thankful to all those who were associated with my research work directly or indirectly. My thesis has been a wonderful experience and I cherish the educational and personal growth it has provided.

Manoj Chandra Garg

Table of Contents

List of Figures

List of Tables

Acronyms and Notations

Acronyms

AC	Alternate current
ACDB	AC distribution board
AFM	Atomic force microscopy
ANN	Artificial neural network
ANOVA	Analysis of variance
ATR-FTIR	Attenuated total reflectance-Fourier transform infrared spectroscopy
BP	Back propagation
CCD	Central composite design
CSP	Concentrated solar power
DC	Direct current
EC	Electrical conductivity
ED	Electrodialysis
EDR	Electrodialysis reversal
EDX	Energy dispersive using X-Ray
EPF	Energy production factor
FE-SEM	Field emission scanning electron microscopy
FTIR	Fourier transform infrared spectroscopy
GHI	Global horizontal irradiance
GW	Giga watt
HFF	Hollow fine-fiber
I	Current intensity
IC	Ion Chromatography
ICP-MS	Inductive Coupled Plasma-Mass spectrometry
IGRAC	International groundwater resources assessment centre
IW	Input weight matrix
LCCE	Life cycle conversion efficiency
LDCs	Least developing countries

LPH	Liter per hour
LW	Layer weight matrix
MD	Membrane distillation
MED	Multi-effect distillation
MF	Microfiltration
MPPT	Maximum power point tracker
MSF	Multi-stage flash distillation
MWCO	Molecular weight cut off
NASA	National aeronautics and space administration
NF	Nanofiltration
NF-C-RO	Nanofiltration-concentrate-reverse osmosis
NF-P-RO	Nanofiltration-permeate-reverse osmosis
NTU	Nephelometric turbidity units
O&M	Operation and maintenance
PAC	Powdered activated carbon
PES	Polyethersulfone
PSSH	Peak sun shine hours
PV	Photovoltaic
PVDF	Polyvinylidene fluoride
PV-ED	Photovoltaic-electrodialysis
PV-RO	Photovoltaic-reverse osmosis
RMS	Root mean square
RO	Reverse osmosis
ROIFA	Reverse osmosis inorganic fouling assessment
RS	Response surface
RSM	Response surface methodology
SEC	Specific energy consumption
SSE	Surface meteorology and solar energy
STC	Standard test conditions
SW	Spiral-wound
TDS	Total dissolve solids
TFC	Thin film composite

UF	Ultrafiltration
V	Voltage, Volts
VC	Vapor compression
XPS	X-ray photoelectron spectroscopy
XRD	X-Ray diffraction analysis
ZLD	Zero liquid discharge

Notations

A	Periodic amortization payment,
Al	Aluminium
As	Arsenic
b	Bias
B	Boron
C	Carbon
Ca	Calcium
Cd	Cadmium
C_f	Feed concentration
Cl	Chloride
C_p	Permeate concentration
Cr	Chromium
Cu	Copper
Da	Dalton
f	RO plant availability
F	Fluoride
Fe	Iron
Hg	Mercury
I_{mp}	Current at Pmpp, Amps
I_{sc}	Short Circuit Current, Amps
K	Potassium
logsis	Log sigmoid transfer functions
Mg	Magnesium

Mn	Manganese
n	Number of variables
N	Total number of experiments required
Na	Sodium
n_c	Replicate number at the central point
NO_3	Nitrate
O	Oxygen
P	Principal amount borrowed
Pb	Lead
purelin	Linear transfer functions
Q_f	Feed flowrate
Q_p	Permeate flowrate
r	Periodic interest rate
R^2	Coefficient of determination
R_q	RMS roughness
S	Sulphur
Se	Selenium
SO_4	Sulphate
V_{mp}	Voltage at Pmpp, Volts
V_{oc}	Open Circuit Voltage, Volts
w	Weights
x_i	Coded levels of input variables
y	Predicted response
Zn	Zinc

Greek Symbols

β_0	Constant term
β_i,	Linear regression coefficients
β_{ii}	Quadratic regression coefficients
β_{ij}	Interaction regression coefficients
^oC	Degree Celsius
ε	Experimental error
2θ	Scanning angle

Chapter 1.
Introduction

1.1 Background

Fresh water and power availability are the two major issues that mankind will have to face and solve in 21st century [250]. Fresh water crisis is affected by many factors including climatic and geographical condition, population growth, rapid urbanization, industrial growth etc. [101]. Concurrently, renewable energy is strongly emerging as a viable and more environment-friendly option to supplement and at times, replace the conventional power generation options, which may observe a continuous decline in coming decades [200].

Inland salinity of groundwater, having total dissolve solids (TDS) of 1500–3000 mg/l, has been found in substantial volumes (over 1.90 lakh km^2) throughout the major parts in India (Haryana, Delhi, Uttar Pradesh, Karnataka, Punjab, Rajasthan, Gujarat and Tamil Nadu) [161]. However, these parts incidentally also receive a 5.5 – 6 kWh/m^2/day of annual average global horizontal irradiance (GHI), making photovoltaic (PV) the apparent selection as a renewable energy source [173]. For the removal of salinity in drinking water, pressure driven reverse osmosis (RO), a relatively new and less energy intensive process that was first commercialized in 1970s, has found more favour in comparison to the thermal processes [51, 213]. Nanofiltration (NF) and RO membrane process are used for the removal of divalent (Calcium, Magnesium, Sulphate etc.) and monovalent ions (Sodium, Chloride etc.), respectively [134].

Rural areas in many parts of developing countries suffer from power crisis, due to insufficient resources and heavy installation requirements for electric power generation. Use of solar power can be a boon for these residents, which provides renewable source of energy with comparatively lesser installation prerequisites and almost maintenance free operation. In view of the above, integration of renewable energy (*i.e.* PV) with membrane filtration based desalination technologies (NF and RO) may be the solution to drinking water problem in areas suffering from brackish ground water sources as well as non-existent or limited electricity accessibility.

1.2 Problem Statement

Various configurations of solar powered membrane filtration systems have been investigated earlier [28, 35, 43, 62, 64, 79, 136, 190, 204, 205, 232]. The performance and overall cost of such systems have also been evaluated on the basis of water productivity, rejection capability and power consumption [91, 156, 190, 192].

As a higher feed water recovery would result in smaller installation size of the membrane unit as well as have less capital and operating costs, several attempts have been made to enhance water recovery in the membrane processes. Many studies have used NF membrane as a water softener to increase the performance of RO membrane [15, 188, 221, 231, 254]. In addition to this, increase in recovery employing concentrate staging has also been investigated earlier [16, 19, 174] resulting in a significant reduction in specific energy consumption (SEC), henceforth the reduction in overall system cost. However, membrane fouling and inorganic scaling have been major challenges for concentrate staging configuration [19]. A number of tools are available today to predict the fouling potential of feed water which enable the users to improve the operation and cleaning efficiency of their plant [109].

Mehdizadeh [157] explained the advantage of integration of NF-RO desalination plant for minimization of energy requirement and several other researchers had also shown that plant performance was influenced by NF-RO hybridization in permeate staging configuration [70, 71, 165, 187, 206]. However, none of these works were carried out on NF - RO hybrid units with concentrate staging configuration to minimize SEC. Hence, the present study was designed to optimize the operating conditions of commercially available small scale NF and RO membranes and to investigate the effect of their hybridization on the overall system cost along with PV.

1.3 Research Gaps

- The drawbacks of NF-RO system in permeate staging configuration (reduction in overall recovery and increase in cost and SEC) need to be investigated and rectified.
- Small-scale NF-RO systems in concentrate staging configuration for the treatment of brackish groundwater have not been given much attention and need to be studied.
- Integration of PV with hybrid NF-RO system for the treatment of brackish water is needed to be researched with a view point of feasibility and compatibility of the overall system.

- Refinement in economic assessment of PV assisted NF-RO systems is needed along with finding solutions for cost reduction.

1.4 Objectives

The main goal of this study is to evaluate the performance of a PV driven NF-RO hybrid water treatment system.

The broad objectives of this study are:

i. Process optimization for NF and RO membrane systems in isolation and hybrid modes for both the staging configurations.
ii. To check the operational feasibility of PV driven NF-RO hybrid system and evaluate seasonal fluctuation of solar radiation on plant performance.
iii. Economic assessment of the system and providing recommendation for up-scaling to pilot study.

1.5 Research Design and Methodology

A laboratory scale hybrid membrane unit was designed and set up to perform various membrane experiments in isolation and hybrid modes. Six thin film composite (TFC) RO and NF membranes (MWCO 100, 250 and 400 Da) from four leading manufacturing companies (CSM, Dow, Vontron and Permionics) were used in spiral wound configuration to perform laboratory scale experiments. The experiments were conducted with synthetic water that was formulated on the basis of major ionic elements of actual brackish groundwater [157].

Response surface methodology (RSM) using central composite design (CCD) was employed to investigate mutual effect of factors on the performance of RO process [129]. Response surface (RS) model was solved to maximize water recovery and salt rejection while minimizing SEC. The validation of optimized process conditions suggested by RSM was also carried out by artificial neural network (ANN) model in MATLAB [127, 129]. Further, experiments were performed employing the derived optimal levels of the input parameters and the results compared against the predicted values of the RSM and ANN.

Characterization of membranes was carried out by atomic force microscopy (AFM) analysis, fourier transform infrared spectroscopy (FTIR) analysis and contact angle measurement.

Thereafter, experiments were carried out on RO – NF hybrid membrane system in concentrate (NF-C-RO) and permeate (NF-P-RO) staging configurations. Reverse osmosis inorganic fouling assessment (ROIFA) software was used to calculate inorganic fouling load of feed and concentrate water.

The current generated by PV system was compared with the current required by the hybrid membrane system.

Lastly, economic assessment of the full process was carried out to estimate per unit water production cost.

1.6 Significance

Many remote communities in both developed and developing countries lack electricity and clean drinking water. The solution, for such communities that have to survive on brackish groundwater, is a PV powered hybrid NF and RO membrane filtration system.

Developed RSM and ANN methodology will provide a holistic approach for the optimization of different RO membranes available in the market in terms of increased water recovery and salt rejection with least energy consumption.

Application of NF-RO hybrid membrane system in concentrate staging configuration will improve the performance of overall system and will helps to reduce the water production cost significantly.

Output of this work may be practically implemented in non-electrified rural areas having drinking water problems due to brackish groundwater.

1.7 Organization of Thesis

The Thesis is divided into seven chapters.

Chapter One presents an introduction, problem statement, aims and objectives along with the significance of work.

Chapter Two presents the literature review, discussing the earlier studies carried on solar assisted desalination systems, and their limitations along with the research gaps.

Chapter Three presents the methodology related to the experimental work carried out *viz.* analytical techniques, laboratory scale experimental setup, optimization of process parameters, hybrid membrane experiments, solar PV system installation and experiments.

Chapter Four deals with the results and discussions regarding the membrane characterization and optimization of process parameters by RSM and ANN methods for NF and RO membranes.
Chapter Five presents the results related to NF-RO hybrid membrane experiments, solar PV setup and comparison of PV generated current vs required current by membrane systems.
Chapter Six presents the economic assessment of the proposed system and effect of fluctuation in different parameters on performance of the membrane system.
Chapter seven presents conclusions. Scope of future work is also outlined.

Chapter 2.
Literature Review

2.1 Quality and Availability of Drinking Water

2.1.1 Physical and Economic Water Scarcity

It is estimated that the world's population has exceeded seven billion and will reach around eight billion by 2025 [50]. Limited resources and rapid urban growth has made population especially in Africa, parts of the Middle East and Asia more vulnerable to water shortage. Whereas the minimum water requirement of about 1.2 billion people is unable to be met as they live in areas of physical water scarcity, about 1.6 billion people face economic water scarcity, as the economic deficiencies in water supply make it infeasible to meet their minimum water demand (Figure 2.1). In a general sense, ubiquitous availability and apparently better quality of groundwater make it preferable over surface water [176]. which is more readily exposed to pollutants from various sources than groundwater [82]. In view of this, groundwater is being exhausted by millions of water pumps throughout the world, especially in Bangkok (Thailand), Manila (Philippines), Beijing, Shanghai (China) and Chennai (India) [234], causing a 10 to 50 meters drop in their aquifer water level [87].

2.1.2 Genesis and Worldwide Occurrence of Groundwater Salinity

All over the world, a largest amount of fresh groundwater is found at shallow and intermediate depths (200-500 m below ground surface). However, at greater depth, fresh groundwater may turn brackish due to slower rate of recharge and mineralization due to long residence time alongwith few other geologic processes. In few cases, such situations arises at shallower depth. International Groundwater Resources Assessment Centre (IGRAC) has prepared a sketch of groundwater salinity at different depths of the soil [255]. It represents the worldwide occurrence (amount and depth) and the genesis (oceanic, terrestrial, anthropogenic) of the groundwater salinity (Figure 2.2). Most of the saline groundwater can be categorized as follows:

- Saline groundwater of marine origin

- Saline groundwater of terrestrial origin (natural)
- Saline groundwater of terrestrial origin (anthropogenic)

2.1.2.1 Saline Groundwater of Marine Origin

Connate saline groundwater can result from accumulation of seawater within rock matrix and be present in the spaces. Coastal freshwater in aquifer may turn into saline groundwater as coastal area becomes flooded by the seawater during marine transgression periods. Genesis of saline groundwater can also occur in coastal zones because of interaction between the seas and hydraulically connected coastal aquifers [255].

2.1.2.2 Saline Groundwater of Terrestrial Origin – Natural

The origin of mineral enriched groundwater occurred due to the evaporation of water near land surface of shallow groundwater table [258]. Groundwater can also get enriched in mineral content by dissolution of naturally occurring soluble minerals, when flowing through such subsurface bodies. Groundwater percolating through a compacted layer of soil works as a salt filtering membrane that leads to building up of high groundwater salinity near the inflow side of the membrane.

2.1.2.3 Saline Groundwater of Terrestrial Origin – Anthropogenic

Evaporation of irrigation water leaves behind the water enriched in mineral content. Large scale irrigation may lead to water-logging and shallow groundwater table, resulting in the residue of mineralized water in the soil. It may reach the aquifer and contribute to a progressive increase in salinity of its groundwater. Groundwater may also get enriched in mineral content by anthropogenic pollution such as road salt (applied in winter), fertilizers, industrial, domestic and agricultural effluents, spilled oil and brines from desalinization plants [209, 255].

The quality of brackish groundwater may vary from location to location but, due to natural filtration through the earth, it generally lacks in suspended sediments. Less than 5,000 mg/l TDS makes it suitable for economic treatment by RO process.

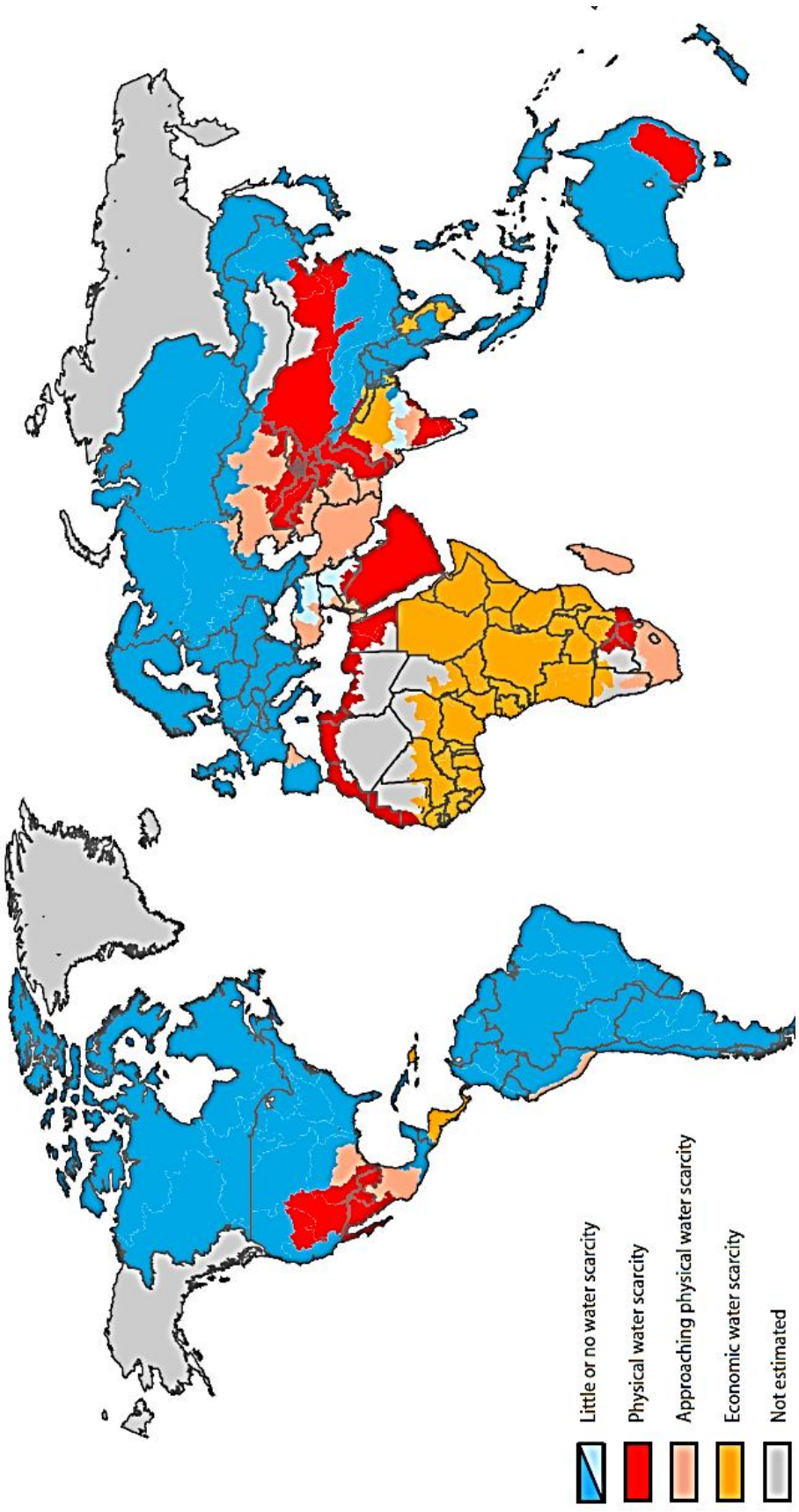

Figure 2.1. Areas of physical and economic water scarcity.

Source: Molden [166]

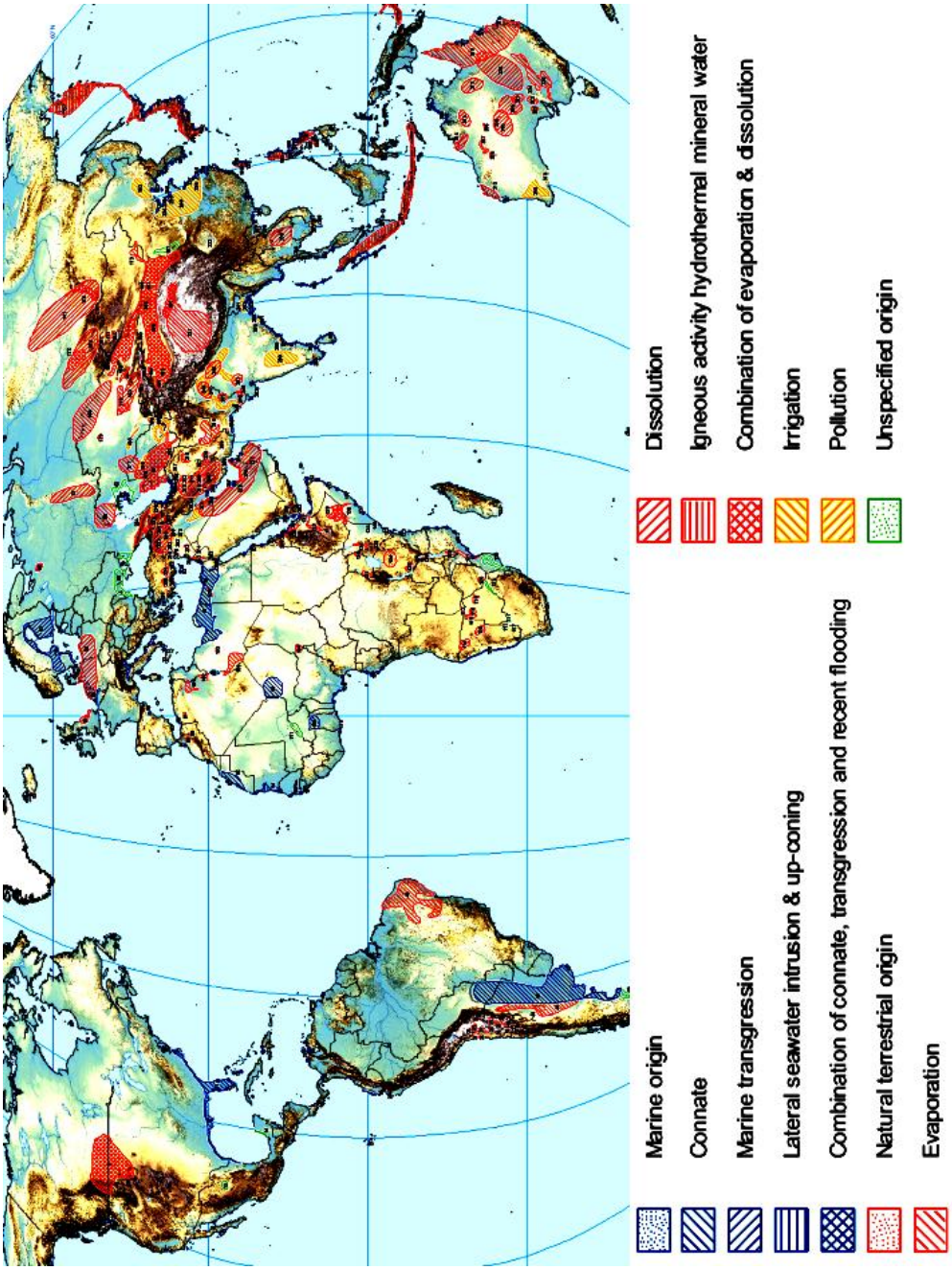

Figure 2.2. Global overview of saline groundwater occurrence and genesis.

Source: Weert et al. [255]

2.2 Commonly Employed Desalination Technologies

In order to make water fit for drinking and irrigation, the five most commonly adopted desalination technologies are as follows:

- Distillation
- Multi-stage flash distillation (MSF)
- Vapor compression (VC)
- Multi-effect distillation (MED)
- Electrodialysis (ED)
- Reverse osmosis (RO)

The first three processes viz. MED, MSF and VC induce physical changes in the state of water. MED and MSF are thermal distillation processes which are very effective if industrial high quality waste heat energy is available [1]. ED can treat the higher level of charged, suspended and dissolved solids but other impurities remaining in the product water need further treatment. On the other hand, RO process is cheaper than the distillation plants of upto 300 to 400 kL/day capacity. In general, RO plants use lesser energy than thermal distillation process to separate salts from water, which help in the reduction of the overall cost of desalination. The following section provides a brief introduction about these processes.

2.2.1 Distillation

Heating water in a tank causes it to vaporise, leaving behind any salt. After cooling vapour condenses as freshwater, which may be collected in a separate tank. A simple still of this type is easy to construct, but very inefficient in energy terms. The heat energy required is the latent heat of evaporation, which is around 627 kWh/m^3, plus losses [31, 92, 218].

2.2.2 Multi-Stage Flash (MSF)

In flash distillation, the water is heated under pressure to prevent vaporisation. Unlike MED, sections on flash-distillation systems are known as stages, hence the term Multi-Stage Flash (MSF). A typical MSF plant can contain from 4 to about 40 stages. Water passes into a next stage at lower pressure and temperature than the earlier one, which allows it to again vaporise by reduction in its boiling point and it gets more concentrated in the successive stages

[13]. Multiple boiling is thus possible without the supply of additional heat after the brine heater. When first introduced in the 1960's, MSF presented considerably lesser energy efficiency than MED, but this was compensated by scaling considerations, which made it the industry standard [65].

2.2.3 Vapour Compression (VC)

Compressing water vapour raises its temperature, which allows it to be used at a heat source for the same tank of water that produced it [66]. This allows heat recycling in a single effect distillation process. In Thermal Vapour Compression, the compressor is driven by steam, and such systems are popular for medium-scale desalination because they are simple in comparison to MSF. In Mechanical Vapour Compression, the compressor is driven by a diesel engine or electric motor [9, 27].

2.2.4 Multi-Effect Distillation (MED)

Most of the heat energy consumed in a simple still ends up in the coolant of the condenser. Recycling this heat energy can improve efficiency several fold. The temperature of the condenser is not high enough to heat the saltwater in the original tank, but it can be used to heat a second tank at a lesser pressure[218]. Generally, practical distillation systems have many tanks, known as effects, hence the term Multi-Effect Distillation (MED). MED was developed for desalination purposes during the first half of the twentieth century, but had a major practical problem with the buildup of scale on the outside of the heating pipes, rather like the scaling of the heating element in an electric kettle [10, 259].

2.2.5 Electrodialysis (ED)

ED also uses membranes, but it differs from pressure-driven membrane processes by utilizing electrical current as the main driving force in salt separation. The charged particles must be mobile, and the separation media must be able to transfer the electrical current with relatively low resistance. ED is almost exclusively carried out on liquids [11, 256].

Two different types of membranes are stacked alternately and held apart by spacers. A DC voltage is applied to the stack after feeding brackish or seawater into spacer layers on one

side of the stack. Depending on polarity of salt ions, it is attracted by membranes and at the same time water comes out of the other side of the stack [142, 171].

In order to reduce fouling, reversing of polarity of the applied voltage can be done frequently as it reverse the freshwater and concentrate layers. This ED process is now termed as Electrodialysis Reversal (EDR). ED was commercialised during the 1960's and is commonly used for desalination of brackish water. The energy consumption changes with the concentration of the feed water and so ED is rarely used for seawater desalination [22].

2.2.6 Reverse Osmosis (RO)

Reverse Osmosis (RO) is a membrane filtration process and, in contrast to the distillation processes just described, does not involve vaporising the water [16, 165]. This generally leads to it being much more energy efficient. RO is the technology chosen for the system described in this thesis.

2.3 Membrane Processes

Drinking water contaminants are presented as inorganic, organic and biological contaminants, as well as radionuclides, particulates, and other groupings.

The ionic range in Figure 2.3 encompasses potable water solutes such as sodium, chloride, total hardness, most total dissolved solids, and disinfection by-product precursor matter. The macromolecular range includes large and small colloids, bacteria, viruses, and color. The fine particle range includes larger turbidity producing particles, most total suspended solids, cysts, and larger bacteria.

Membrane systems have experienced significant development in water quality functions in the past few years, and are now offered in a variety of forms that can differ in shape, size, and process, and each is exclusively capable to resolve a specific need. A number of applications have been described on water treatment [177, 197].

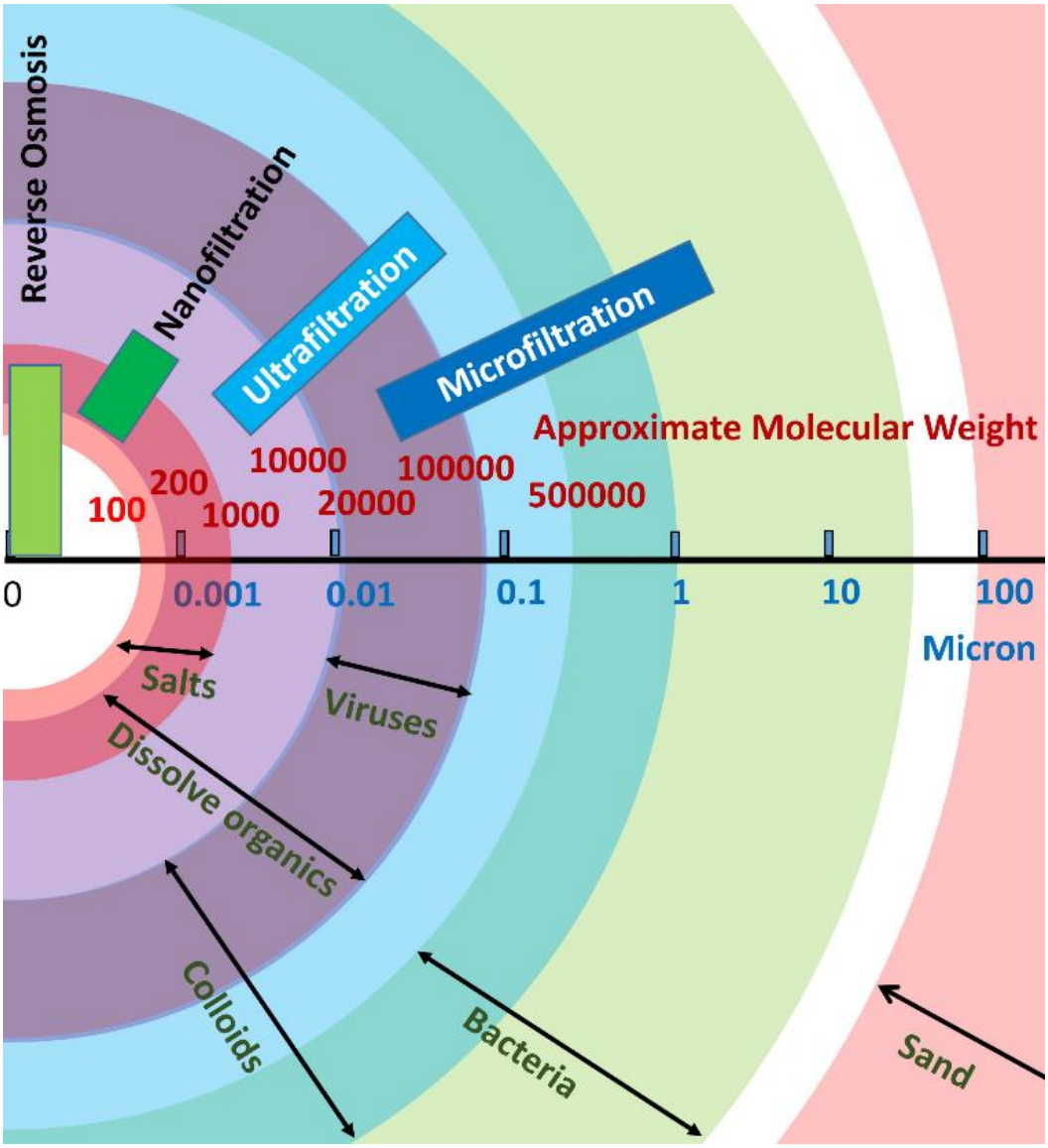

Figure 2.3. Size range of membrane processes and contaminants.

Source: Chen et al. [59]

Although many factors affect solute separation by these processes, a general understanding of drinking water applications can be attained by associating minimum size of solute rejection with membrane process and regulated contaminants [51, 202]. One correct interpretation of Figure 2.3 is to assume that each membrane process has the capability of rejecting solutes larger than the size shown in the exclusion column. The membrane processes normally used in the ionic range remove macromolecules and fine particles [26].

Contaminants larger than the maximum pore size of the membrane are completely removed by a diffusion-controlled process. Contaminant rejection by diffusion-controlled membrane processes increases as species charge and size increases [45, 70]. Consequently, satisfactory removal of metals, TDS, biota, radionuclides, and disinfection by-product precursors can be attained by membrane processes [151, 202].

Many membrane manufacturers specify the molecular weight cut off (MWCO) values for membranes. The MWCO represents a molecular weight of a known ionic species that would be rejected in a fixed percentage, using a specific membrane and experimental conditions [26, 151].

Membrane processes with the greatest immediate application to drinking water treatment are microfiltration (MF), ultrafiltration (UF), nanofiltration (NF), reverse osmosis (RO), and ED/EDR [181, 235, 240]. In the broadest sense, a membrane, the common element of all these processes, could be defined as "any barrier to the flow of suspended, colloidal, or dissolved species in any solvent" [36, 40, 56, 59].

All membrane processes can reject contaminants such as turbidity or pathogens, but UF and MF are the most cost effective processes for control of large particles [67, 197, 210, 226].

ED and EDR methods can efficiently remove the smallest charged ionic contaminants upto 0.0001 μm. Therefore, ED and EDR are restricted to treatment of ionic contaminants and are ineffective for most organic applications and pathogen removal [142, 171].

Desalting methods by NF and RO membrane are intended for the removal of TDS that usually cannot be removed by conventional treatment methods. RO and NF perform both diffusion and sieving. They can remove all pathogens and many organic contaminants by sieving; by diffusion, they can achieve almost total removal of ionic contaminants [216]. RO and NF processes have the widest limit of treatment capabilities [165, 197]. Consequently, these processes effectively remove turbidity and microbiological contaminants, making them ideal for treating the greater part of drinking water sources [142, 171]. Typically, the cost of membrane treatment increases as the size of the solute removed decreases [71].

2.3.1 Classification and Configurations of Membrane Processes

Some membrane processes rely on pressure as the driving force to transport fluid across the membranes. They can be classified by the types of materials they reject and the mechanisms by which rejection occurs [29]. The progression of MF to UF to NF to RO corresponds to a decreasing minimum size of components rejected by membranes as well as increasing transmembrane pressures required to transport fluid across the membranes and decreasing recoveries [109, 197, 227, 228].

While pressure driven processes like RO pass water through the membranes, ED involves the passage of the solute rather than the solvent through the membrane. As a consequence, both the mechanism of separation and the physical characteristics of membranes in ED differ substantially from those in pressure driven processes [15, 22]. ED membranes are fundamentally porous sheets of ion exchange resin with a relatively low permeability for water.

Membranes are classified by solute exclusion size, which is sometimes referred to as pore size. A RO or hyperfiltration membrane is capable to reject solutes as small as 0.0001 µm, which is in the ionic or molecular size range [151, 197]. An NF membrane rejects solutes as small as 0.001 µm, which is also in the ionic and molecular size range. Solute mass transport in these processes is diffusion controlled [165, 254]. UF and MF membranes have a smallest solute rejection size of 0.01 and 0.10 µm, respectively [197]. These membranes reject colloidal particles, bacteria, and suspended solids by size exclusion and are not diffusion controlled. Pressure drives the transport of water (the solvent) through these membranes. MF and UF require the use of pretreatment processes such as coagulation and/or oxidation or powdered activated carbon (PAC) to remove dissolved organic and inorganic constituents [197]. ED relies on charge for solute separation and pulls ions through ED membranes, so it is unaffected by pore size.

Membranes can be classified by molecular weight cut offs (MWCO), solute and solvent permeability, solute and solvent solubility in the membrane film, active film material, active film thickness, surface charge, and active film surface [19]. The molecular weight cut off is the degree of exclusion of a known solute, as determined for a given set of test conditions in the laboratory. Typical known solutes used for determination of molecular weight cut off are sodium chloride, magnesium sulfate, dextrose, and some dyes. Solute mass transport through a diffusion-controlled membrane is influenced by solute type and aqueous environment, so attempts to

characterize them benefit from the use of additional organic solutes such as aromatic and aliphatic compounds of known molecular weight and structure [253].

Common MF and UF membrane materials used today include polyvinylidene fluoride (PVDF), polyethersulfone (PES), polysulfone, and cellulose triacetate [24, 63, 93, 179]. Recently, the use of ceramic materials made by sintering inorganic materials such as aluminum oxide, titanium oxide, or a carbon nanocomposite formulation have been considered for MF applications [153, 170]. Common NF and RO materials include polyaramide and polyamide for spiral-wound (SW) configurations, and cellulose triacetate for RO hollow fine fiber membranes [12, 46]. The development of the cross-linked fully aromatic polyamide thin-film composite membrane in the late 1970s represented a major advance in membrane technology [185].

Membranes for drinking water treatment have either SW or hollow fine-fiber (HFF) configurations [46]. The SW configuration is most commonly used for production of potable water [120]. The HFF configuration was used widely for desalination of seawater and brackish water in the Middle and Far East. However, the use of SW configurations has increased over time [184]. The geometry of a SW membrane is subject to fewer "dead areas" than that of a HFF membrane, it can be cleaned more thoroughly, and it is less subject to fouling. The ratio of surface area to volume is higher for a HFF element than a SW element. The recovery from a HFF element ranges from 10 to 50 percent and is typically higher than that from a SW element [46].

SW thin-film composite RO membranes were introduced in the mid to late 1970s and were designed for brackish and seawater applications [104, 150]. SW elements are manufactured using flat-sheet membranes, as opposed to bundles of fibers. A typical SW element consists of envelopes attached to a center tube that collects the permeate stream (Figure 2.4). Designs of SW elements differ among manufacturers; however, the following description is applicable to Filmtec, Toray, Hydranautics, and Koch SW membranes [120, 121].

Typically, in a SW element, an envelope is formed by folding one flat sheet over a permeate stream spacer. The sheet itself consists of two layers, a nonporous active membrane film and a porous membrane support. The active layer is on the outside of the fold. The envelope is glued along three open sides and near the fold, completely enclosing the permeate spacer. The glue line on the fold end is a short distance away from the fold, because the fold end is attached to the center collection tube [212]. Therefore, the remaining pressure in the permeate stream drives it through the membrane into the centre collection tube . A feedstream spacer is attached to each envelope prior to establishing the fold end glue line [212]. Several envelopes and

feedstream spacers are attached to the center collection tube and wrapped in a spiral mode around it. An epoxy shell or tape wraps are applied around the envelopes, completing the SW element [196]. An anti-telescoping device is attached to both ends of the element to maintain a fixed space between elements and facilitate flow from one element to the next.

The feed stream enters the end of the SW element in the channel created by the feed stream spacer. The feed stream can flow either in a path parallel to the center collection tube or through the active membrane film and membrane supports into a channel created by the permeate-stream spacers [51, 151]. The permeate stream follows a spiral path into the center collection tube and is taken away as product water in a drinking water application.

2.3.2 Membrane Properties

Characterization of membrane properties is desirable because of the potential of relating these characteristics to solute rejection and membrane-fouling studies [48, 253]. This information could be used to modify existing membranes or develop new membranes that would effectively reject inorganic and organic solutes from drinking water sources without fouling the membranes [77].

Currently, techniques are capable of measuring membrane surface charge, pore size, thickness, roughness, surface energy, and surface atomic composition. These techniques are presented in Table 2.1.

2.3.3 Staging Configuration in Membrane System

For most membrane methods, the conversion of feed water into product water is restricted through a single module [107]. Therefore, to produce more product than that attainable by a single passage, most RO methods employ sequential staging configuration [192].

2.3.3.1 Concentrate Staging Configuration

RO and NF membrane elements cannot generally attain a recovery of much more than 15%. Further, the beginning of concentration polarisation and the scaling typically restricts the conversion to well below this (Figure 2.5). Therefore, it is normal for them to be positioned in series, with the concentrate stream from one element being passed on to the feed water stream of

the next element [247]. This is commonly known as concentrate staging, and is very common for the brackish water treatment by RO process [16].

2.3.3.2 Permeate Staging Configuration

It is not essentially practical or required for the concentrate to be staged in order to maximise the overall water recovery. For high TDS feed waters or seawater, where osmotic pressures in the range of tens of bar prevail, further concentration of these waters would demand uneconomically high operating pressures [192]. Therefore, for these type of brackish waters, permeate staging is practiced, and permeate from the first stage is fed to the second stage (Figure 2.6). This system is found suitable for high-purity water production [206].

Table 2.1. Techniques to Characterize Membrane Surfaces.

SN	**Techniques**	**Application on membrane research**	**References**
1	Scanning electron microscopy (SEM)	High resolution image to characterize roughness and pore size for clean and fouled membrane	[54, 119]
2	Attenuated total reflectance Fourier transform infrared spectroscopy (ATR-FTIR)	Kinetics study on membrane-solute solvent interface	[8, 238]
3	Contact angle	Surface energy to distinguish hydrophilic and hydrophobic membranes	[8]
4	Scanning probe microscopy/AFM	Topological information to characterize roughness and pore size for clean and fouled membrane	[138, 139]
5	Streaming potential	Charge on membrane surface to determine electrostatic interactions.	[76, 238]
6	X-ray photoelectron spectroscopy (XPS)	Chemical analysis for sorption and fouling for clean and fouled membrane	[238]

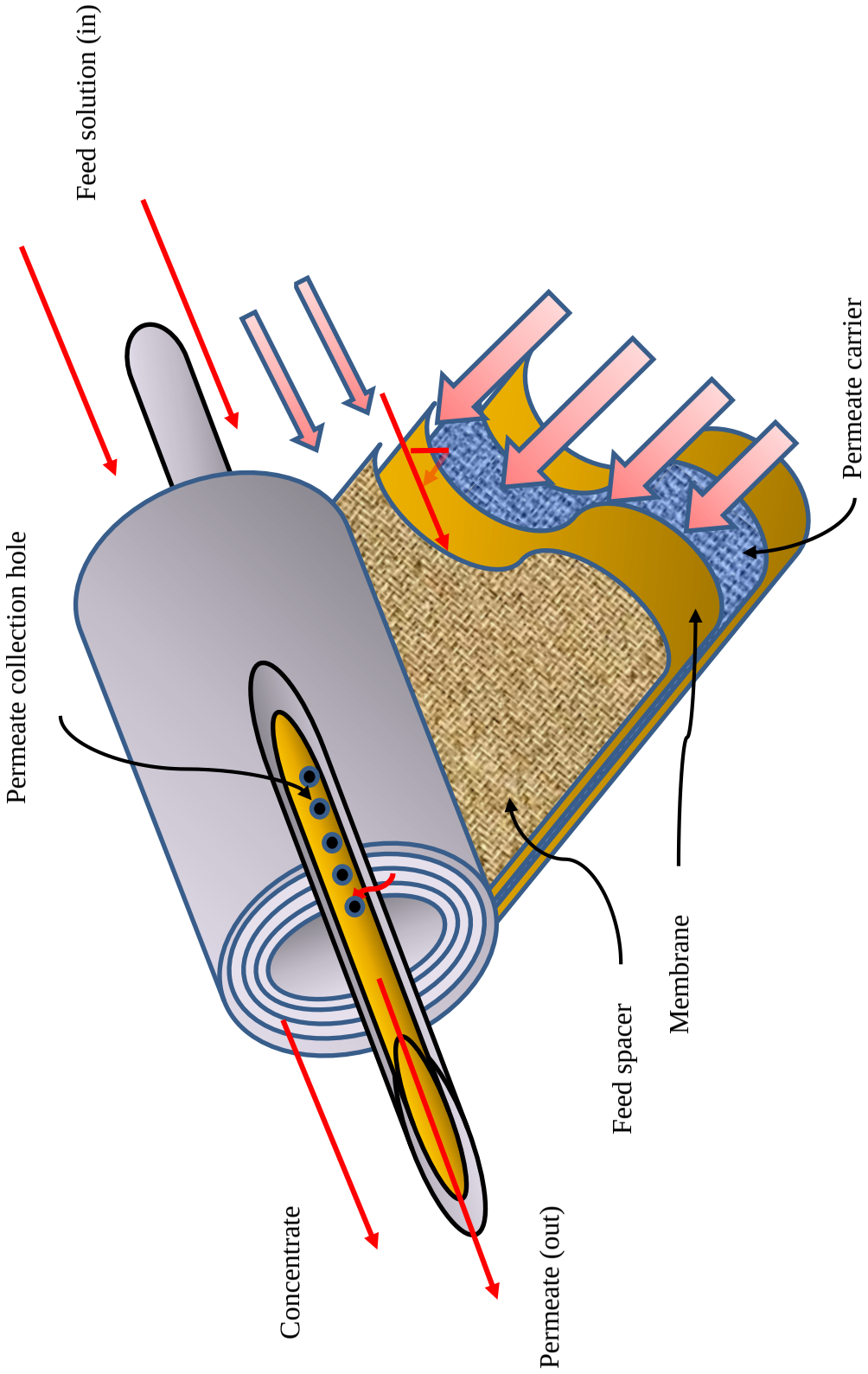

Figure 2.4. Spiral wound membrane module.

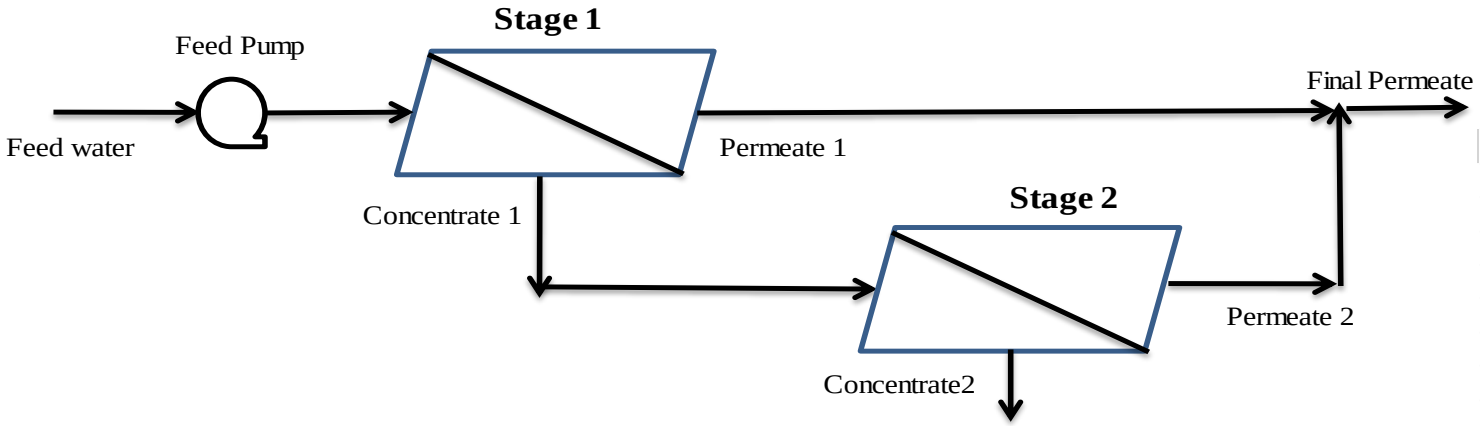

Figure 2.5. Concentrate flow through the membrane module (Concentrate staging configuration).

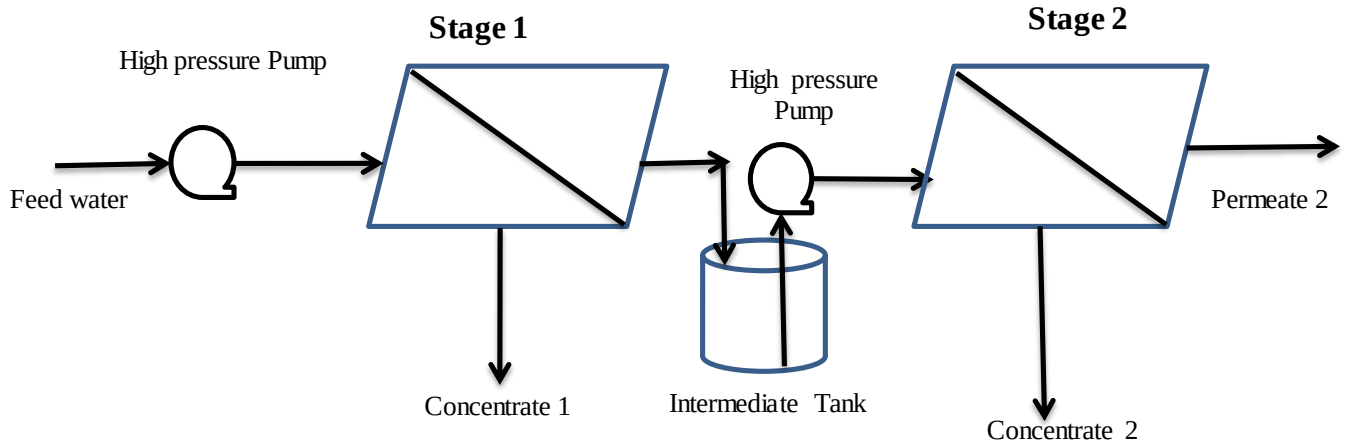

Figure 2.6. Permeate flow through the membrane module (Permeate staging configuration).

2.4 Status and Potential of Solar Energy

2.4.1 Worldwide Non-Renewable and Renewable Energy Scenario

The occurence and availability of electricity are also uneven worldwide. According to the report of UNDP/WHO, 2009 [144], the least developing countries (LDCs) and Sub-Saharan Africa have a lower percentage of people with access to electricity (21% and 26%) than those in developing countries (72%). This problem is more severe in rural areas of LDCs and sub-Saharan Africa (87% and 89%) than in developing countries (41%) (Figure 2.7). In addition to this, many parts of the world, especially remote areas, are suffering from shortages in modern fuels (electricity, liquid and gaseous fuels). In developing countries, more than 40% of people rely on modern fuels; however, in LDCs and sub-Saharan Africa, only 9% and 17%, respectively, have access to modern fuels (Figure 2.8). About 70% of urban people in developing countries rely on modern fuels as the primary cooking fuels and about 19% of rural people use modern fuels as their primary fuel [144].

According to the global oil depletion report, peak oil production is forecasted [233], to decline by 2020 or later, after which the rate of petroleum extraction is expected to enter in terminal decline [61, 97].

Solar, wind, geothermal, tidal, hydroelectric and nuclear power are considered to be cleaner alternatives to meet the growing energy demand. It is a known fact that the solar radiation is unevenly distributed, and that it varies in intensity from one geographic location to another. The reason of uneven distribution of solar radiation throughout the world is the variable solar altitude, degree of pollution and cloud coverage [106].

2.4.2 Distribution of Solar Radiation on Earth Surface

Solar irradiance or insolation is described as an amount of solar radiant energy incident on a surface per unit area and per unit time. However, some parts of the earth get higher solar flux than the annual average flux. Many of the developing nations in Northern Africa and southern parts of Asia (falling between 15-35^{o} N) receive the highest flux of solar radiation. Scattered radiation increases due to high atmospheric humidity and cloud formation in equatorial belts (0-15° N), which still make them favorable for reception of solar radiation. Further, in regions falling between 35-45^{o} N, higher latitude and lower altitude results in the enhancement of dispersion of the solar radiation making them less favorable for receiving the solar radiation

[106]. Beyond 45^{o} N, it is very difficult to exploit almost half of the solar radiation, as it is in the form of scattered radiation and makes this belt much less favourable (Figure 2.9).

Similar distribution of the earth's latitude zones for the southern hemisphere influences the reception of solar radiation [3]. Most of the developing countries fall between latitude 35° N and 35° S and receive adequate flux of sunlight that may be used economically in various forms by both rural and urban households. Capturing even 1% of the total solar insolation on the surface of earth can supply more than the world's energy requirements [114].

2.4.3 Progress in Photovoltaics

Photovoltaic (PV) technology has made substantial progress in recent years, resulting in an increase in the conversion efficiency and a decrease in the capital and also O&M costs of the PV system. The global capacity of solar PV modules was expected to reach 54 GW by the end of the year 2012 as shown in Figure 2.10. The Jawaharlal Nehru National Solar Mission (National Solar Mission) is a major initiative of Government of India and the State Governments that aims to generate 20 GW of solar power by 2022, about 100 GW by 2030 and about 200 GW by 2050. This aims to promote ecologically sustainable growth and self-sufficiency in manufacturing of solar power systems and equipment and also make India a leader in solar energy installations [172].

Solar PV based power supply is becoming popular in rural and remote areas. Free availability, Ubiquitous and non-polluting nature of solar energy makes it a reliable source for future energy generation especially in the rural and remote areas of developing countries [5, 132, 252]. The applications of solar energy in rural areas are very wide e.g. electricity, pumping and water for drinking and irrigation, telecommunication, water purification etc. [172]. Life-time operation and maintenance costs of a solar PV system are lower than that of other existing solar based technologies. In general, overall conversion efficiency of PV cells is 7.5% with the maximum reported efficiency being 14.5%, though PV systems have generally higher initial capital cost. With the recent advancements in PV technology, however, we can expect a rise in the efficiency upto 12% to 13% [61, 97].

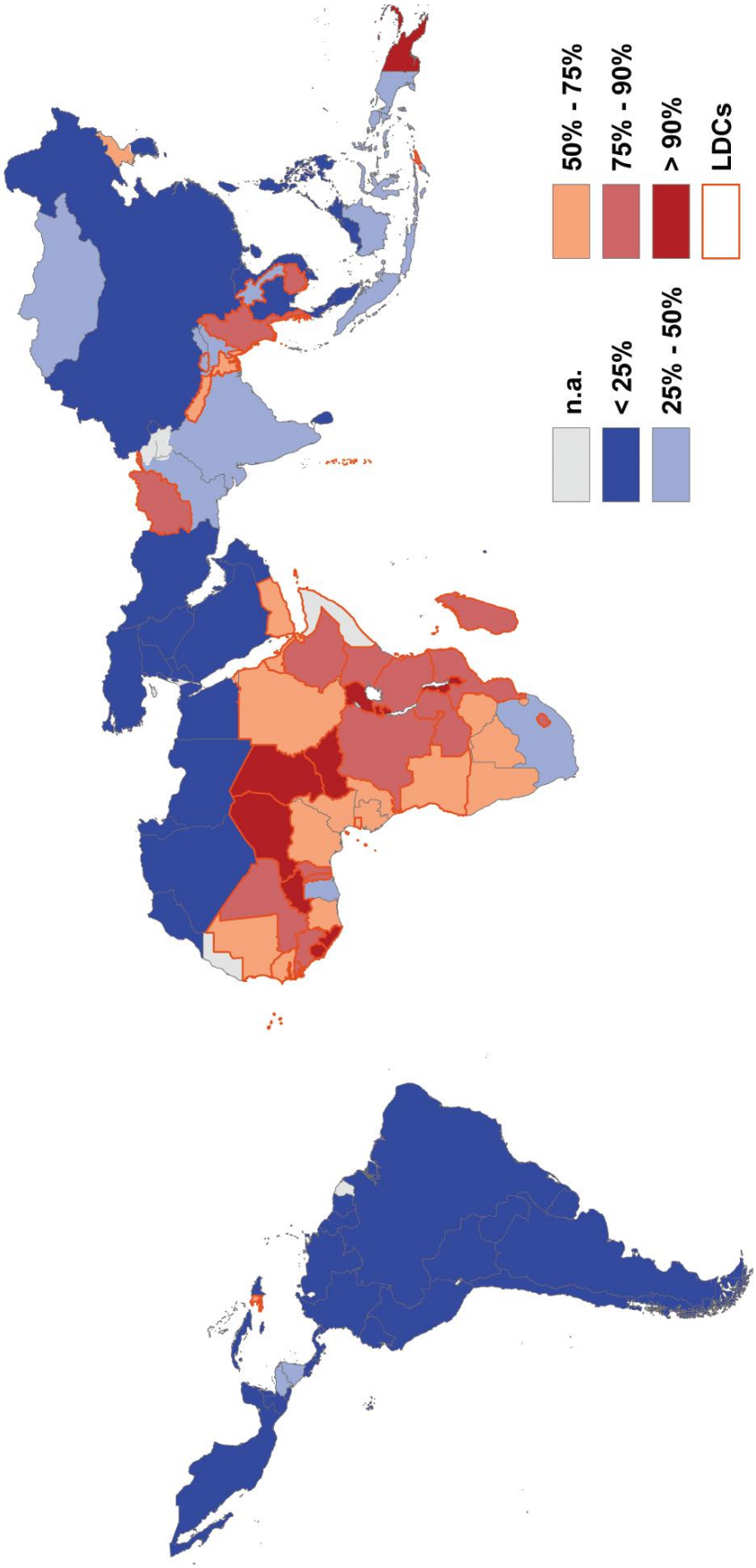

Figure 2.7. Share of people without electricity access for developing countries.

Source: Legros et al. [144]

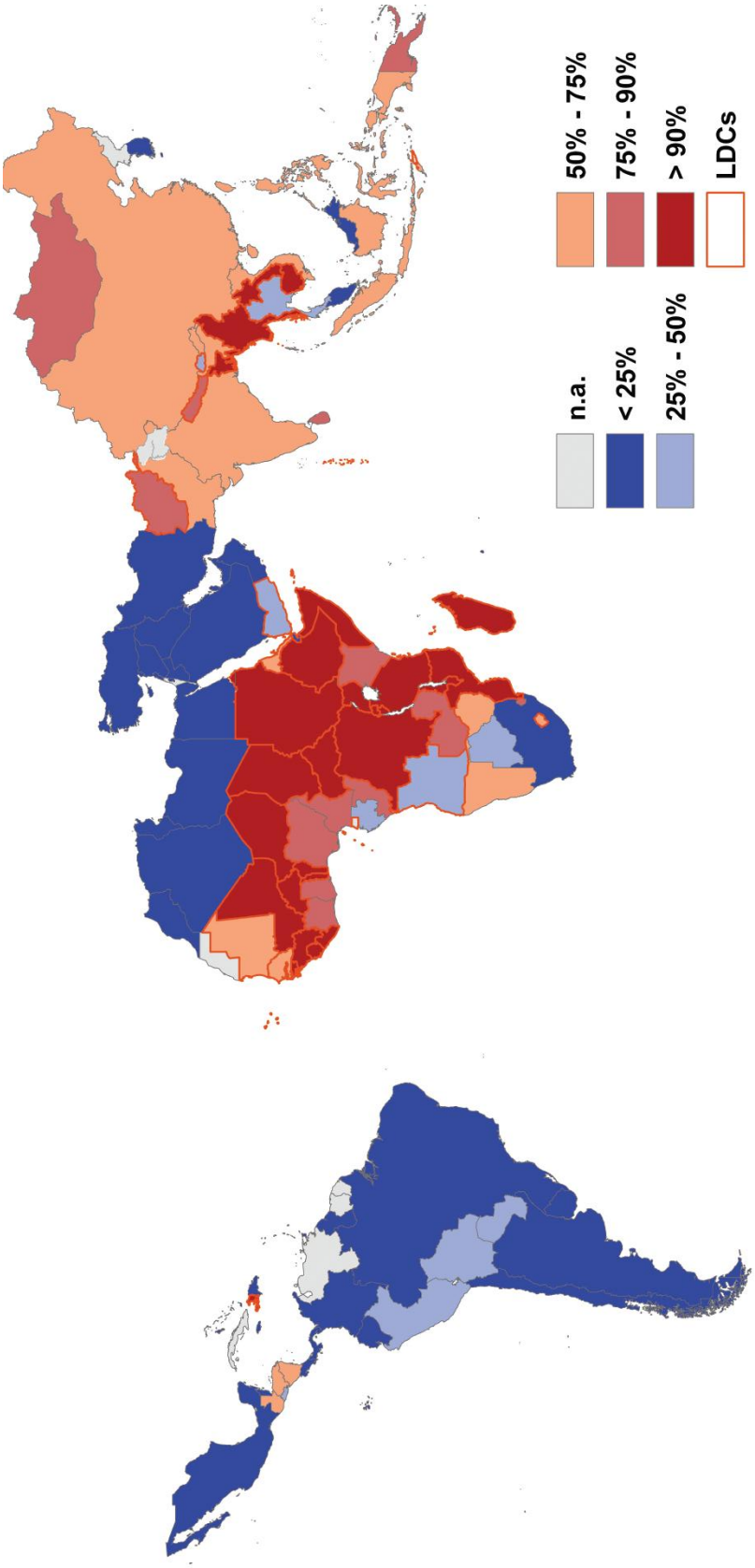

Figure 2.8. Share of population without access to modern fuels for developing countries.

Source: Legros et al. [144]

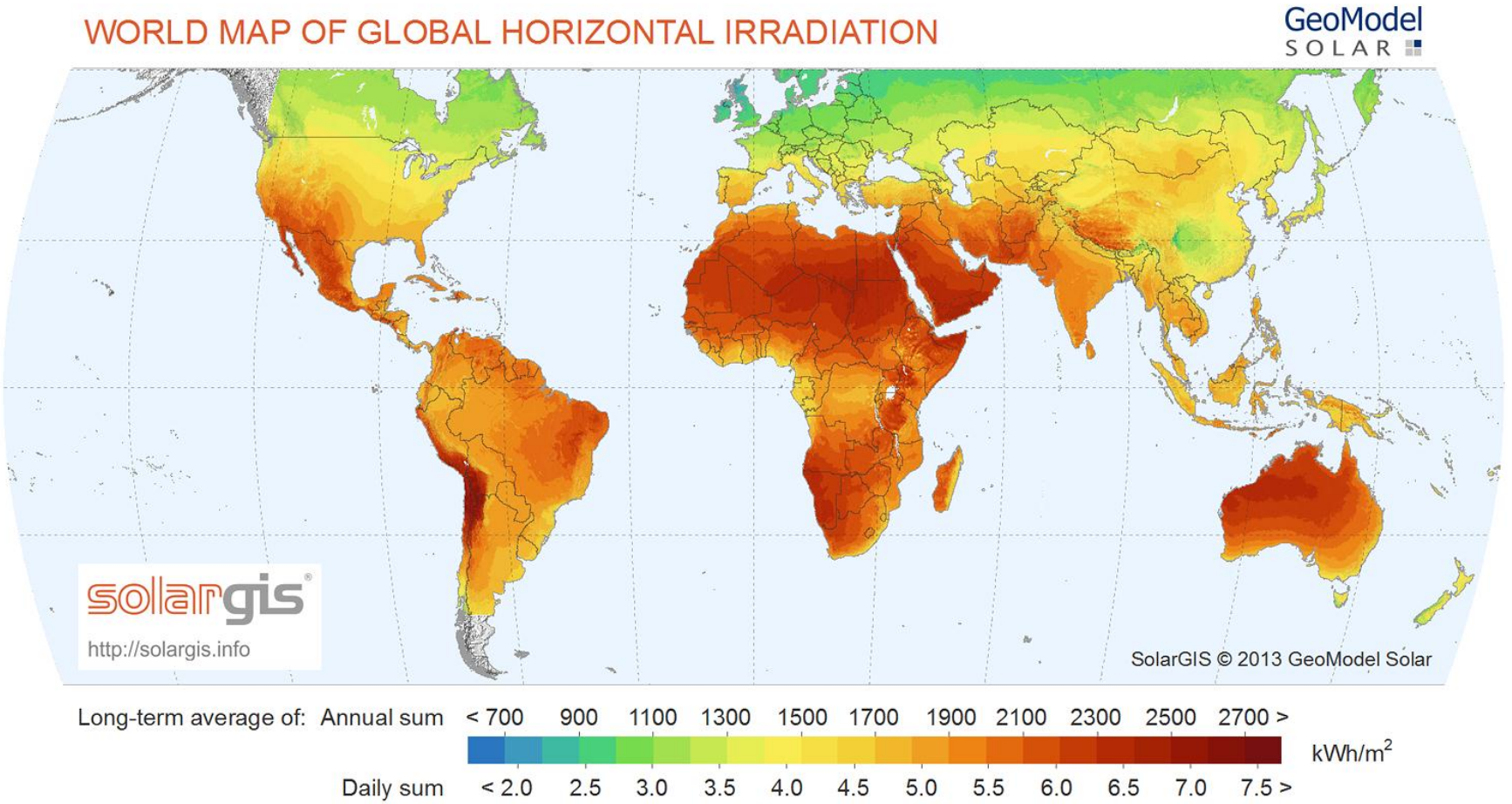

Figure 2.9. World map of global average yearly solar radiation.

Source: SolarGIS [230]

2.5 Solar Thermal Coupled Desalination Systems

Using solar energy sources (solar thermal and solar PV) to drive desalination technologies [83] is a practical way to produce drinking water in many locations of the world, in particularly remote regions, where the connection to the public electrical grid is either unavailable or not cost-effective, and where water scarcity is severe. Figure 2.11 shows the worldwide use of different desalination technologies using solar power source (s) [21].

Solar energy can be transformed to thermal as well as electrical energy. Thermal energy can be obtained using solar stills or solar thermal collection systems. Electrical energy can be produced from solar PV conversion or solar thermal power plants. The different desalination systems driven by concentrated solar power are presented below.

2.5.1 Solar Thermal Distillation

A solar still is a simple way of distilling water, consisting of a shallow basin covered by a condenser film, using the solar radiation to drive evaporation of water, and ambient air to cool a condenser film. Solar still systems give small quantities (4 to 6 L/day) of fresh water for human consumption especially in remote and rural regions. Chafidz et al. [53] developed an integrated solar-driven distillation system that uses membrane distillation process to produce potable water. This is an integrated (self-contained) system that uses solar energy for its operation by combining solar PV and solar thermal collectors. The system is intended for autonomous operation in arid remote areas where electricity and potable water are not readily available. Thermal and economic evaluation of a hybrid solar thermal distillation system has also been carried out by Kumar [135] incorporating the effect of subsidy, tax benefit, inflation, and maintenance costs for the climatic condition of New Delhi (India). This analysis was based on annualized costing and for the expected life spans of 30 years. Energy production factor (EPF) and life cycle conversion efficiency (LCCE) were found to be 5.9% and 14.5%, respectively, for expected life of 30 years. The distillate production costs was found to be Rs. 0.75/L.

2.5.2 Solar Pond

Solar ponds combine solar energy collection and thermal storage due to their chemically stratified nature. The large storage capacity of solar ponds can be useful to generate electricity for RO, MVC, and ED desalination plants or for continuous operation of MED, MSF, or TVC

desalination plants [49] during cloudy days and night-time. The waste (reject) brine from desalination units and the rejected heat from the power plant could be used to build the solar pond coupled thermal desalination plant [49]. Farahbod et al. [80] investigated the efficiency of a solar desalination pond as a second stage of proposed zero discharge desalination processes to reach fresh water and concentrated brine from the effluent wastewater of the desalination unit. In addition, Garmana and Muntasserb [92] developed a mathematical model to study the factors affecting the size of a solar pond to serve adequate thermal load enough to run the desalination unit for the entire period of operation. They could conclude that there is a linear relation between the required thermal load for the desalination unit and the surface area of the solar pond.

2.5.3 Solar Membrane Distillation

Thermally driven membrane distillation (MD) processes are gaining growing attention among emerging desalination technologies, particularly for small-scale applications and possibility of easy coupling with solar energy sources [32, 33, 49, 193]. Separation of vapour from aqueous solution achieved by passing a hot saline feed water over a hydrophobic membrane, where the trans-membrane vapour pressure difference between the two sides of the membrane cause a water to evaporate. The vapour is then passed through the membrane and condensed on the opposite side of the membrane by condenser [53]. Most existing MD projects are still in the laboratory or small-scale pilot-plant stage. Factors like reduction in overall energy efficiency due to the need of large amount of water and high cost associated with the membranes have kept this technology away from commercial markets [10]. However, membrane distillation is a promising process, especially for situations where low temperature solar, waste, or other heat is available [126].

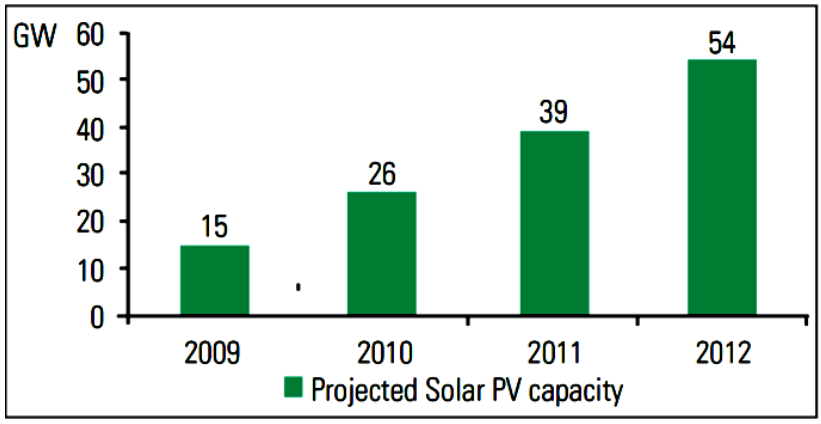

Figure 2.10. Cumulative capacity additions planned in solar PV until 2012.

Source: ISA [113]

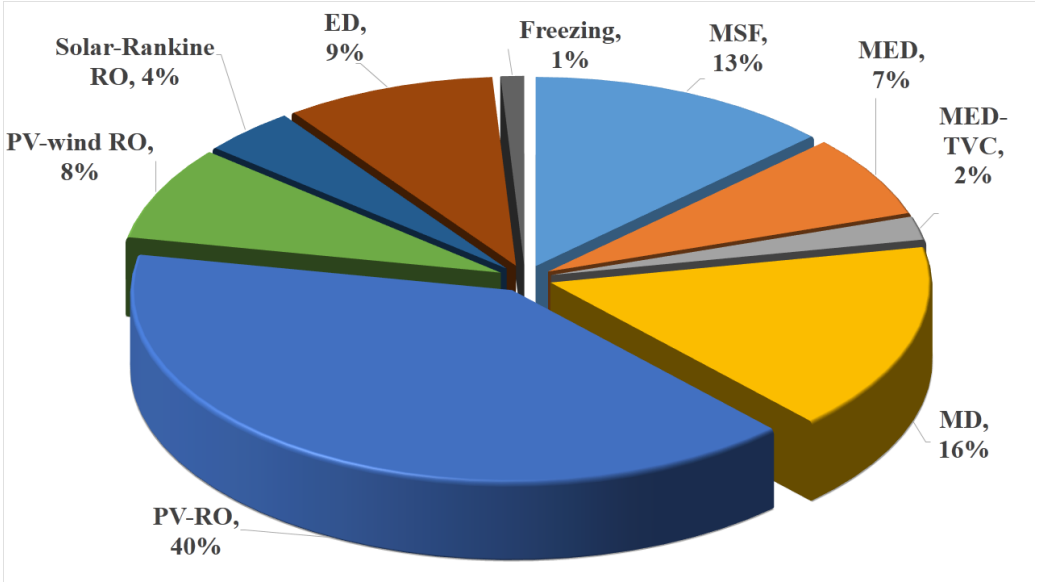

Figure 2.11. Desalination technologies powered by renewable solar energy installed worldwide.

Source: Ali et al. [21]

2.5.4 Concentrated Solar Power desalination

Integration of concentrated solar power (CSP) with MED and RO membrane desalination system is becoming more common among the existing solar-powered desalination technologies [49]. It is based on the concept of concentrating solar radiation by using glass mirror to give high temperature heat for electricity generation using steam turbines. The parabolic trough system MED and RO desalination processes [147, 180], make currently the best combination for CSP/desalination coupling. Many of the large-scale thermal desalination plants are located with power stations or industries with thermal process energy waste due to high energy requirement in the form of thermal energy [103]. An alternative scheme by an integration of CSP with MED and RO desalination processes was proposed by Iaquaniello et al. [110]. According to the proposed scheme, RO is powered by electricity produced by the steam turbine, while MED is powered by the low temperature exhaust steam delivered from the same steam turbine, and conventional gas turbine included as a thermal back up system. Main objective of the hybrid integration of desalination with CSP was to develop an energy efficient seawater desalination technology [10]. This is a mature technology, allows a continuous operation and offers an effective way to lower the total water production costs but it cannot compete economically with other conventional desalting technologies without further improvements.

For any solar thermal desalination project, proper surface design is essential for the improvement of system efficiency governed by high heat and mass transfer during evaporation and condensation. Further reducing the pressure within the reservoir by vacuum pump, significantly decreases the temperature and heat energy required for desalination [125]. This concept eliminates the challenge of achieving optimum temperature difference between solar generated vapour and the seawater cooled condenser.

2.6 Photovoltaic Assisted Membrane Systems

PV is a mature technology with modules having a life expectancy of 20 to 30 years. Membrane desalination unit can be coupled with solar PV energy [49]. A PV system could be used to power mainly two processes, RO and ED desalination units. Comparing RO and ED, water is transported through the RO membrane, while in ED process, electrolyte is transported through the membrane. Furthermore, ED uses DC electricity that supply directly from the PV system for operation of ED unit as well as low-pressure pump [2]. RO makes up a more reliable

choice for seawater desalination than ED, since it is energy-efficient when feed water salinity is higher. ED is preferable used for low concentration brackish water desalination (less than 2500 ppm). Pre-treatment is often required in RO, since RO membranes are very susceptible to fouling [247]. Considering the energy supply, RO presents lower energy consumption but ED shows better behavior considering intermittent or fluctuating electrical power, as a consequence of changes in solar resource intensity [10]. PV-RO is a lower energy consumption system in comparison to PV-ED [11]. However PV-ED shows better performance on fluctuating solar electrical power.

The main problem of these technologies is the high cost, requirement of large PV arrays and regular replacement of batteries. Furthermore, PV-powered RO or ED system is a valid option for desalination at remote sites.

Using solar PV energy sources to drive RO membrane desalination system is worthwhile to produce drinking water particularly for remote areas, where the connection to the electrical grid is either unavailable or inaccessible, and where water scarcity as well as salinity is severe.

Work on PV-RO desalination technology started in the early eighties (Table 2.2). However, efforts have been reportedly initiated recently for assessment of its technical and economical feasibility.

Table 2.2. Milestones of development of solar powered RO plant.

1982	World's first Solar PV powered seawater RO plant [44]
1985	Introduction of Energy recovery device (positive displacement energy recovery pump) in PV powered seawater RO plant [122]
1988	First brackish water RO plant powered by PV [72]
1998	Hybrid plant of PV driven brackish water RO plant with solar stills [102]
2001	First batteryless PV powered brackish RO system [116]
2002	First batteryless PV powered seawater RO system [244]

It is important to note that most of the experimental research was carried out earlier in countries (mostly southernmost part of Europe), where the yearly average solar irradiance on a horizontal surface was considerably higher than the worldwide average (Figure 2.9), and severe physical water scarcity existed (Figure 2.1).

2.6.1 Brackish-Water PV-RO Systems

Although PV-RO systems have been employed for both brackish (TDS range 1000-8000 mg/l) and seawater (TDS range 20000-45000 mg/l) desalination (Table 2.3 and Table 2.4). However, most of the PV-RO installations exist for the treatment of brackish water with the capacity of 100 to 1000 LPH (Figure 2.13).

Many working components and mechanisms are common to all design methods and they can be used to produce a basic, common design plan for PV-RO systems [189, 208] as shown in Figure 2.12. Thomson and Infield [242-244, 246] proposed a PV- RO plant that was able to operate without batteries. They performed laboratory experiments to validate the model and control of the system having capacity of 3 m^3/d with a PV array of 2.4 kWp. Joyce et al. [116] simulated and implemented a small scale RO unit operated by PV system, for remote rural sites with typical daily production of 100–500 l and functioning with pressures as low as 5 bar. Manolakos et al. [154] and Mohamed and Papadakis [162] presented the design of a stand-alone hybrid wind-PV system to power a seawater RO desalination unit, with energy recovery using a simplified spreadsheet model. The realized energy saving was close to 50% when a pressure-exchanger-type energy recovery unit was considered.

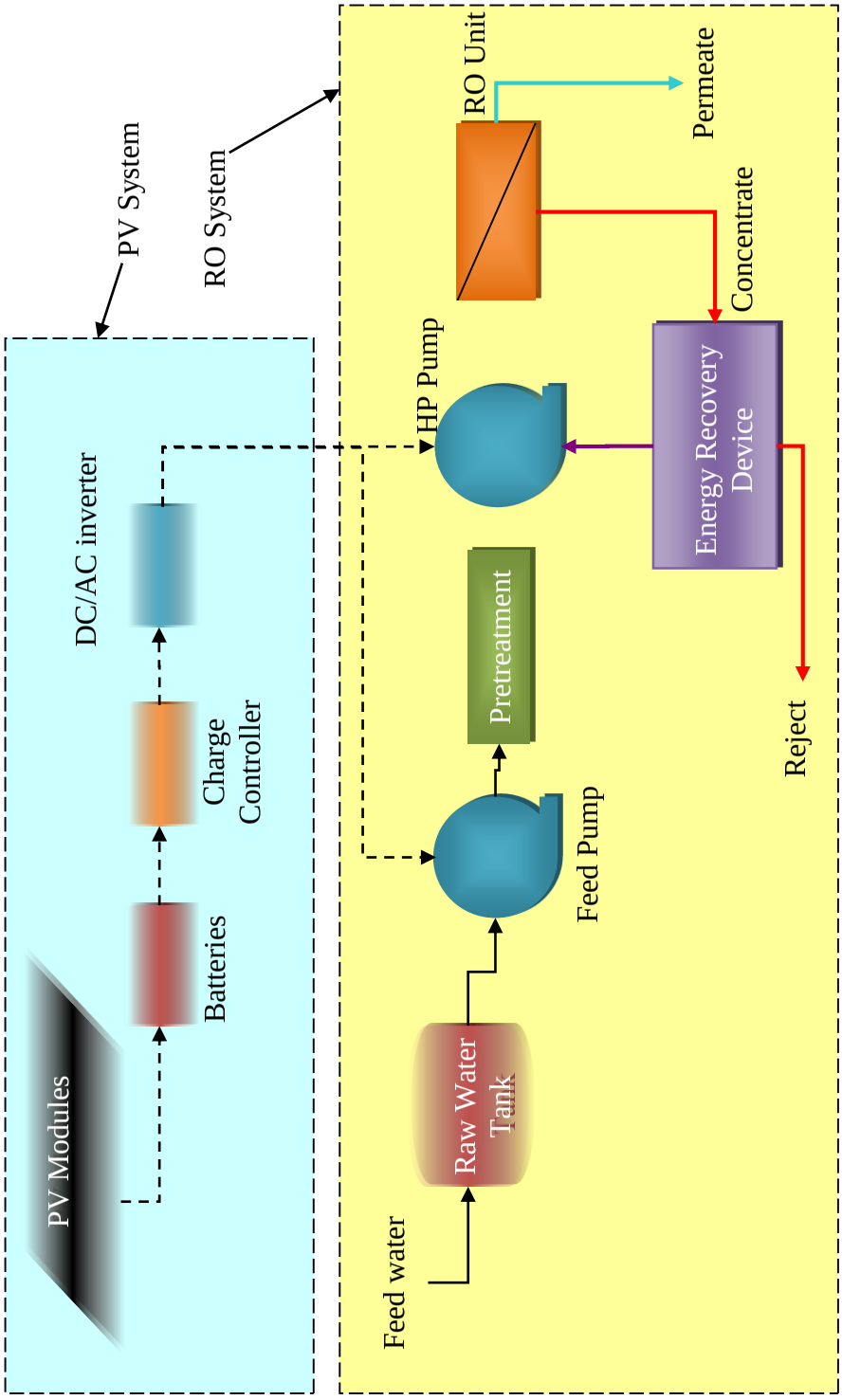

Figure 2.12. Simplified general model of a PV powered RO desalination plant.

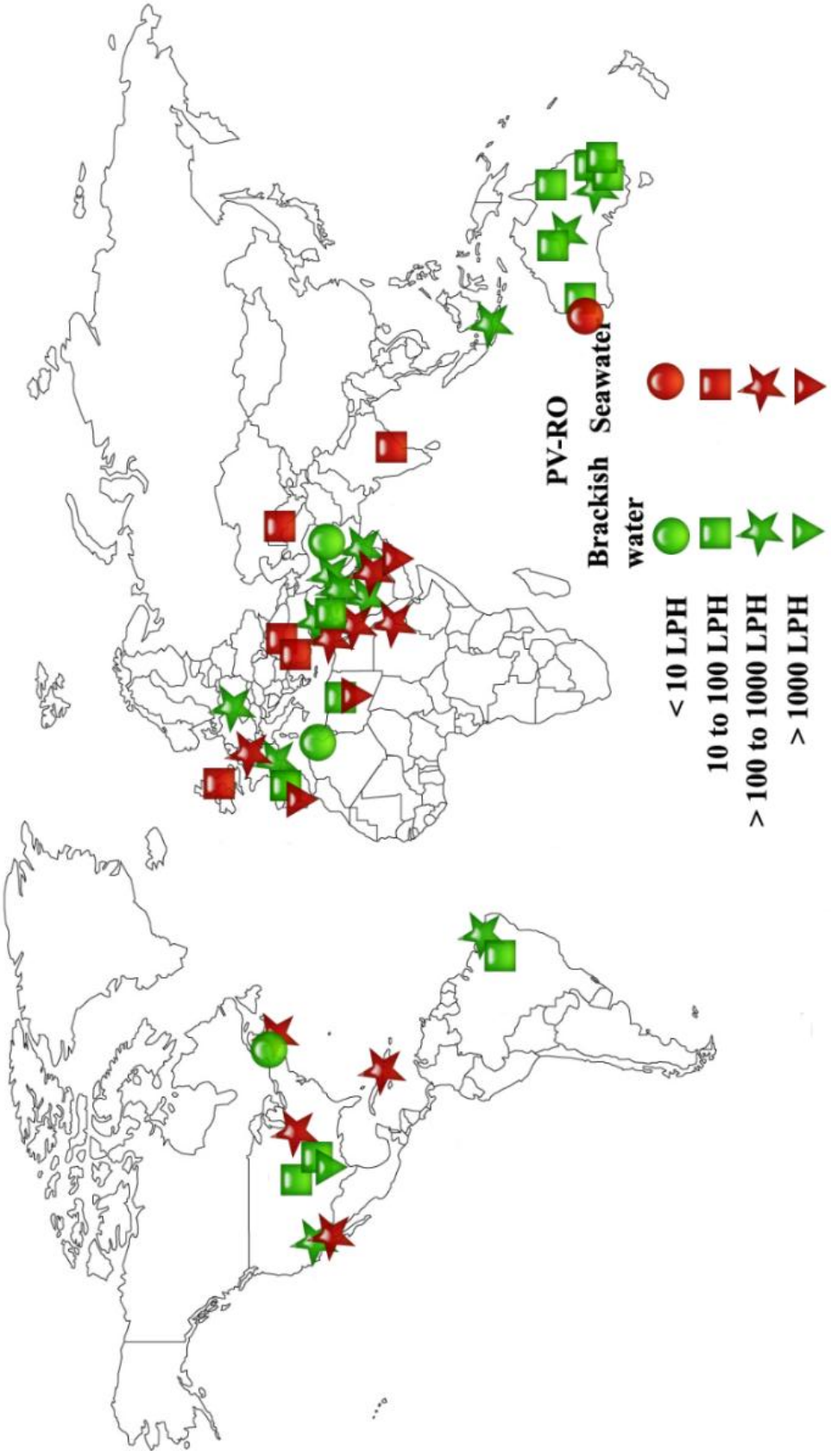

Figure 2.13. Worldwide geographical distribution of experiments on brackish and seawater PV RO.

Table 2.3. Summary of brackish water PV powered RO desalination plant.

Country	Year	Feed TDS (mg/L)	Permeate flowrate (LPH)	Pressure (Bar)	Pump drive (AC/ DC)	PV Power (kW)	Battery storage	SEC (kWh/ m^3)	Energy recovery devices	Source
Sultanate of Oman	1998	1010	1000	-	AC	11.46	Yes	-	No	[17]
Sultanate of Oman	2000	1010	1000	-	AC	3.25	Yes	-	No	[18]
Fortaleza, Brasil	2004	1200	250	8.27	AC	1.1	Yes	3.03	No	[52]
Kassel, Germany	2002	2000	143	-	AC	1.07	Yes	-	No	[6]
Jordan	2008	3000	250-300	-	AC	-	Yes	-	No	[108]
West Bank Palestine	2003	3382	2170	-	AC	8.9	Yes	2	No	[148]
Egypt	2012	3400	208	-	AC	1.8	Yes	9	No	[81]
Sydney, Australia	2003	3500	100	6-7	AC	0.255	No	2	Yes	[203]
Jakarta, Indonesia	1988	3500	500	40	AC	24.5	Yes	4-6	No	[72]
Australia	2008	5300	46	9	AC	-	No	2.3	No	[201]
Central Australia	2007	5300	250	12	AC	0.6	Yes	1.2	No	[214]
Sadous, Riyadh, Saudi Arabia	1998	5800	600	-	AC	10.08	Yes	-	No	[102]
Tunisia	2011	6000	25	15.5	AC	30.8	No	-	No	[60]
Spain	2010	6000	107-252	8-13.5	AC	0.36	Yes	1.3	No	[130]

Amman, Jordan	2005	400	11	-	DC	0.07	No	-	No	[1]
Brazil	2009	800	50	-	DC	0.165	No	1.57	No	[205]
Australia	2009	1000	150-280	4	DC	-	No	1.1	No	[202]
Australia	2005	1500-5000	42	4-15	DC	-	No	3	No	[217]
Jordan	2012	1700	21	4.5	DC	0.432	Yes	13.82	Yes	[34]
Tunisia	2005	2800	2	2-5	DC	-	No	-	No	[47]
Australia	2009	3000	17	2	DC	0.12	No	-	Yes	[64]
Colorado, USA	2004	3500	500	17.25	DC	0.44	No	1.38	No	[57]
Australia	2005	5000	42	10	DC	-	No	2.2	No	[156]
Lisbon, Portugal	2001	5000	4-20	5	DC	0.05-0.15	No	-	No	[116]
Australia	2011	-	-	12	DC	-	No	1.9	No	[204]

2.6.2 Sea-Water PV-RO Systems

According to Table 2.3 and Table 2.4, it is observed that so far, PV-RO systems for brackish water and seawater have been studied upto 11.46 kW and 60 kW AC power respectively. It is due to the fact that PV-RO systems for brackish water source have been operated at lower pressure (15 bar) in comparison to those with a sea water source (65 bar). As a result, brackish water PV-RO systems have lesser SEC (3.03 kWh/m^3) in comparsion to seawater (7.73 kWh/m^3). Maximum permeate flow rate of brackish water and seawater PV-RO desalination systems is upto 2170 LPH and 4166 LPH, respectively. These comparisons conclude that solar PV-RO desalination plants can satisfy a maximum of ~4000 LPH drinking water demand economically. Fresh water yield of more than 4000 LPH requires higher capital and labour costs, and thereby, makes non-solar desalination systems more economic [1].

Recently, Clarke et al. [62] presented the results of simulations used to investigate a small-scale, stand-alone, solar-PV powered RO system, with and without battery storage. Results showed that system performance is affected differently when including power characteristics of RO devices and by the temporal resolution used in simulations. Soric et al. [232] developed and tested a portable desalination prototype (1 m^3d^{-1}) based on a RO process powered by solar PV panels without using an intermediate storage battery. Richards et al. [204] investigated the effects of fluctuating energy and pH on retention of dissolved contaminants from real Australian groundwater using a solar PV powered UF–NF/RO system [201, 202]. They found that the renewable energy membrane system reliably removed salts and inorganic contaminants over a range of real energy and pH conditions via convection/diffusion and precipitation mechanisms. This has important implications for remote water applications where such contaminants that are difficult to remove by conventional technologies are a concern.

Table 2.4. Summary of seawater PV powered RO desalination plant.

Country	Year	Feed TDS (mg/L)	Permeate Flow rate (LPH)	Operating Pressure (Bar)	Pump drive (AC/DC)	PV Power (kW)	Battery storage	SEC (kWh/m^3)	Energy recovery devices	Source
UK	2005	32800	60	40	AC	1.53	No	4	Yes	[243]
Greece	1998	40000	500	65	AC	20.5	yes	-	No	[249]
UK	2002	40000	500	-	AC	2.4	No		Yes	[244]
Greece	2004	40000	500	65	AC	31.2	yes	6.3	Yes	[162]
Libya	2005	42000	3475	-	AC	60	yes	4.3	Yes	[124]
Saudi Arabia	2009	43500	4166	38	AC	-	yes	6.3	No	[91]
UAE	2008	45000	833	55	AC	8.59	No	7.73	Yes	[105]
India	2007	-	21	-	AC	10.47	No	-	No	[136]
Australia	2013	10000-40000	5.5	-	DC	0.7	No	-	No	[62]
Greece	2008	17500	100	16	DC	0.846	No	3.8	Yes	[154]
Greece	2008	25000	90	50	DC	1.6	No	4.6	Yes	[163]
France	2012	25000	140	17.25	DC	0.5	No	-	Yes	[232]
USA	1982	42800	270	-	DC	8	yes	-	No	[44]
Boston USA	2011	35000	12.5	-	DC	0.23	No	4	Yes	[42]
Uzbekistan	2010	-	60	5.5	DC	0.03	Yes	-	No	[28]

2.7 Issues Related to PV-RO Systems

Although PV-RO technology has been well established, but the following issues can be considered for further improvement:

a. Development of PV-RO system for household drinking purpose in non-electrified areas of developing countries.
b. Improvement of efficiency/performance of PV-RO system.
c. Economic assessment of solar PV-RO systems.

2.7.1 Need of PV-RO System for Developing Countries

It is surprising that very little research in the field of PV powered RO technology has been done in developing countries despite the fact that about 5 billion or 80% of the world's population lives in them (Table 2.3and Table 2.4). It is also remarkable that the most suitable belt (35°N-35°S) of solar radiation covers many of the developing nations in northern Africa and southern parts of Asia. Also, near about 80–90% of conventional water resources have been used for irrigation in the developing countries. Moreover, secondary salinisation is dominant in many countries [237]. Furthermore, since the economic price of water in developing and industrialized countries is comparable, water disturbs the budget of people in developing countries [186]. Hence, there is an urgent need to carry out more research for the development of PV-RO technology particularly for non-electrified areas of developing countries such that:

a. The running cost of the system could be reduced substantially to bring the final water cost within the limits of a common man's budget.
b. The operation and maintenance of the system should be simple so that an unskilled labor can also operate it.Improvements in PV-RO systems

Efficiency and performance of PV-RO system can be improved by:

2.7.1.1 Improvement in the Material of Photovoltaic Cells

Research work has been continuously going on for exploring the new materials and improving the characteristics of existing PV material. One of them is photonic crystals (optical nanostructures) that slow down movement of photons through the material of PV cell and help in absorbing more red wavelengths of light. With the help of this method, about 25%

improvement in the efficiency of traditional solar cells has been reported. On the other hand, more expensive silicon solar cells give about 15% to 25% efficiency [100].

It is possible to develop affordable materials to capture the usable solar energy by using nano scale architecture. These materials need to be low-priced and should have fast charge transfer properties as the photo generated holes can destroy the material even after efficiently generating electron-hole pairs by absorbing lots of sunlight. The scientists are increasing the light absorbing property that is needed to generate an electron hole pair by developing highly ordered nanotubes and scheming its structural design e.g. length, wall thickness and intrinsic geometry [186].

2.7.1.2 Pretreatment of Reverse Osmosis Feed Water

RO TFC membranes are subjected to scaling and fouling by many substances e.g. biological, particle, organic, mineral etc. Appropriate pretreatment before RO can improve the efficiency of the RO systems by increasing the recovery rate, rejection ratio and lowering the fouling and scaling problems. Conventional pretreatment for RO may include coarser filter (20–25 μm), main filter (5 μm), coagulation and filtration (for colloidal fouling), active carbon filtration (free chlorine removal), disinfection by chlorination (avoid biofilm development on the membrane surface), antiscalant or acidification (for inorganic fouling protection).

Pretreatment of RO feed water with ultra-filtration (UF) or micro-filtration (MF) helps in reducing the fouling potential and thus reduces overall cost by minimizing SEC. The need of RO membrane disinfection is generally eliminated after the pretreatment by UF membrane as it removes significant number of microorganisms. It also reduces RO membrane cleaning and replacement costs that compensate its higher installation cost [201, 214]. The risk of RO membrane surface scaling or inorganic fouling can be reduced after adding anti-scalents.

2.7.2 Concentrate Management

Several treatment technologies are available for treatment of RO concentrate before its discharge in water bodies. Although, to make near zero liquid discharge (ZLD), combination of treatment technologies is needed [58, 236]. The most pronounced effects of direct brine disposal from PV-RO plants to water bodies are adverse impacts on receiving water ecosystems such as eutrophication, accumulation of heavy metals, pH value variations etc. [183]. To reduce adverse

environmental effects of direct brine disposal, it can be diluted with power plant cooling waters, natural seawater or municipal wastewaters prior to discharge [158, 207]. Traditionally, options for the concentrate's disposal from PV-RO plants have been solar evaporation, deep well injection and surface water discharge [7, 25, 90, 149]. One of the major drawbacks with RO is the volume of concentrate produced during the process. Several technologies and process configurations are available to reduce the concentrate volume [95]. Thermal-based brine concentration technologies are well established, but they are capital-intensive, consume a significant amount of energy and are not cost-effective for large-scale applications. Membrane-based technologies are less energy intensive when compared to the thermal-based technologies, but they need pre-treatment of the RO concentrate to reduce the concentration of scale forming ions to limit the formation of scales on the surface of the membranes. Thermal-based technologies are combined with those that are membrane-based, to achieve complete ZLD, but their higher energy consumption and capital costs results in considerable treatment costs [168]. Some other efficient emerging technologies allow for considerable brine volume reductions such as ED [115], forward osmosis [146, 155, 239], membrane distillation [155] that facilitates recovery of salts, nutrients and valuable compounds from RO concentrates [96, 111, 199]. The cost of concentrate disposal depends on the characteristics of concentrate, level of treatment before disposal, disposal method and brine volume [7, 25].

2.7.3 Economic Assessment of PV-RO Systems

Economic analysis is essential for successful commercialization of any technology. In case of PV-RO system, per unit water production cost is affected by many factors including recovery ratio, SEC, cost of equipment (membrane and solar system), hybridization configuration, interest rate, subsidy given by government, labour cost etc.

Seawater desalination processes are very expensive compared to the brackish rivers or groundwater, since, they require large amount of energy to achieve separation of dissolved salts [86]. It is estimated that, near about ten thousand tons of oil per year is required to produce 1000 m^3/d of fresh water from RO water treatment [1, 117]. The reported cost of a PV - seawater RO desalination system ranges from 7.95 to 29 US\$/m^3 [244] with capacity of 120 to 12 m^3/day, since, for a PV - brackish water RO system, the cost ranges from 6.5 to 9.1 US\$/m^3 with same capacity.

Effective integration of membrane desalination processes can reduce the water cost and electric energy consumption. Several works have been investigated with the combination of RO and other membrane (MF/UF/NF). These hybrid systems have demonstrated several benefits including lowering in SEC, increase in RO membrane life, efficiency, productivity and overall cost reduction [156, 201, 202, 214].

Chapter 3.
Materials and Methods

3.1 System Configuration and Operational Procedure

3.1.1 Experimental Setup

A laboratory scale hybrid membrane unit (Permionics membrane Pvt. Ltd., Vadodara, India) was designed and procured to perform various membrane experiments in isolation and hybrid modes. A 1.5 kWp grid connected PV system consisting of eleven multi-crystalline silicon PV modules (make: Moserbaer, India, model: MBPV BCAP BC) was employed in combination with grid connected solar inverter (make: AnHui EHE new energy Tech. Co., Ltd., version: TL-EU-UME-V3.0) capable to supply loads of up to 3 kWp, metering devices and distribution system (Figure 3.1). The technical specifications for PV system are provided in Table 3.1. The general layout of laboratory membrane unit along with PV and data acquisition system has been shown in Figure 3.1. The actual photographs of membrane filtration unit and PV panels are presented in Figure 3.2. A small scale membrane unit consists of a feed tank and high pressure pump along with the membrane module which comprises of spiral wound NF and RO membranes (5 cm diameter and 30.5 cm length). The feed and permeate flow rate was determined by a flow rotameter. Feed flow rate was kept constant during experiments by pumping feed water while passing along a feed bypass valve. The system pressure was adjusted by using a concentrate valve (pressure regulator) and monitored by a pressure gauge. Minimum and maximum applied pressure used in RO experiments were within the prescribed limits recommended by the membrane manufacturers (Table 3.2). Permeate and concentrate streams were recycled in the feed tank for continuous evaluation of the system. Automatic temperature control unit was used to regulate feed water temperature as well as to avoid the heat generated by high pressure pump.

Prior to a long term shutdown and for scheduled routine maintenance, cleaning procedures were carried out to minimize the plugging of the feed line with dislodged inorganic foulants. The cleaning was conducted by recirculating 0.5% HCl solutions (pH 2-3) through the membranes for about 10-15 min without applying pressure followed by permeate water flushing to neutralize the acid.

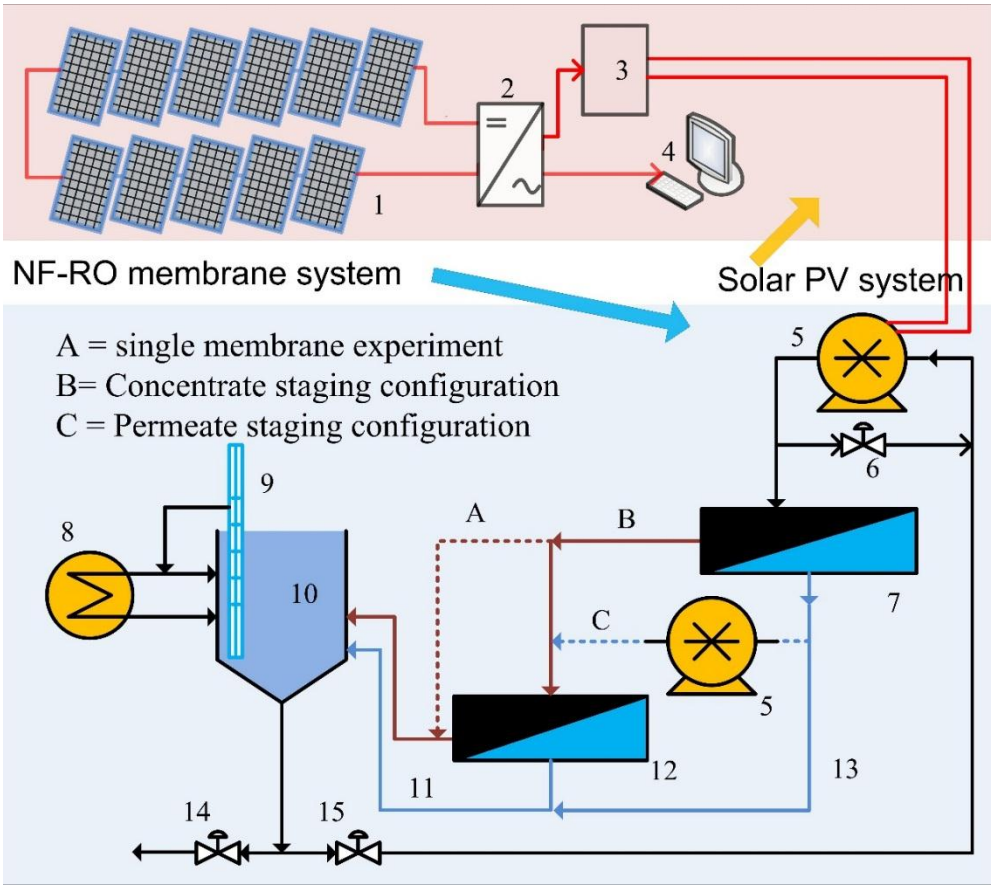

1 = PV modules, 2 = DC-AC inverter, 3 = AC distribution board, 4 = Data logging system, 5 = high pressure pump, 6 = bypass valve, 7 = NF module, 8 = temperature controller, 9 = temperature probe, 10 = feed water tank, 11 = concentrate stream, 12 = RO module, 13 = permeate stream, 14 & 15 = valve.

Figure 3.1. Different schemes of single and hybrid PV-NF/RO membrane experimental setup.

Figure 3.2. Experimental setup with membrane filtration unit and PV system.

Table 3.1. Technical specifications of 1.5 kWp PV modules and solar inverter.

Specification	**Value**
Number of modules	11
Module specification	
Max. Power (Watts)	139.04
Voltage at Pmpp, V_{mp} (Volts)	17.86
Current at Pmpp, I_{mp} (Amps)	7.79
Open Circuit Voltage, V_{oc} (Volts)	22.30
Short Circuit Current, I_{sc}, Amps	8.39
Maximum system voltage, Volts	1000
Solar Inverter specification	
Model	N3KTL
PV side	
Max PV Power (Wp)	3300
Input short circuit current (Amps)	25
MPPT voltage (Volts DC)	125~420
PV start voltage (Volts)	150
MPPT voltage range (%)	99.99
Grid Side	
Rated output power (Wp)	3000
Max output current (Amps)	15
Power factor	>0.99
Max. efficiency (%)	96.9
Output voltage (Volts)	180~260
Permitted grid frequency range (Hz)	47~51.5
Standby power consumption (W)	5

3.1.2 Experimental Procedure

Optimization experiments were carried out to maximize water recovery and TDS rejection and to minimize SEC of small scale brackish water RO process [116] using pH, feed temperature, feed pressure and concentration of feed solution as input parameters.

Three hybrid membrane experiments were conducted to examine the concentrate and permeate staging configurations. In the first and second experiments, concentrate of NF membrane was fed in RO and NF membrane respectively. In the third experiment, permeate collected from the NF membrane was used as feed in RO membrane. Around 20 ml of permeate and concentrate from both the membranes were collected on hourly basis. The temperature, pH and TDS of collected samples along with permeate and concentrate flowrate were measured.

The concentrations of anions and cations in these samples were also measured using Ion Chromatograph (Make: Metrohm Ltd., Switzerland). The TDS of feed and permeate water was measured using a conductivity meter (make: HACH Co., model: HQ40D). To determine the TDS

from this meter, EC/TDS conversion factor (0.7) was used that resembles the actual EC/TDS ratio in the groundwater in this region as estimated from field experiments. The percentage rejection of salt was determined by using equation (3.1):

$$\text{Salt rejection} = \left(1 - \frac{C_p}{C_f}\right) \times 100\ (\%) \tag{3.1}$$

Where, C_f = feed concentration (mg/l), C_p = permeate concentration (mg/l). The percentage recovery of feed water was measured by using equation (3.2):

$$\text{Water recovery} = \left(\frac{Q_p}{Q_f}\right) \times 100\ (\%) \tag{3.2}$$

Where, Q_p = permeate flow rate (L/h), Q_f = feed flow rate (L/h). Also, SEC (kWh/m^3) was calculated by using equation (3.3):

$$\text{SEC} = \left(\frac{I \times V}{Q_p}\right) \text{kWh/m}^3 \tag{3.3}$$

Where I = current (Amperes), V = voltage (Volts) of AC power used to operate motor.

3.2 Membranes

3.2.1 Availability of Thin Film Composite Membranes

Six TFC RO and NF (MWCO 100, 250 and 400 Da) membranes from four leading manufacturing companies (CSM, Dow, Vontron and Permionics) in spiral wound configuration were used to perform laboratory scale experiments. Operating specifications of these membranes used for limiting the range of input parameters for each membrane are given in Table 3.2. Prior to testing, the membranes were soaked in MilliQ water for several hours, followed by thorough rinsing with MilliQ water.

3.2.2 Membrane Characterization

Membranes were characterized by AFM, FTIR and contact angle measurement. Before measurement, all membrane samples were extensively rinsed and immersed in MilliQ water fo.r 12 hours to ensure the absence of any preservative solution and dried at room temperature.

FTIR was performed using a fourier transform infrared spectrometer (make: Thermo Fisher Scientific Inc.). Membrane was tightly pressed with potassium bromide in a circular disk. FTIR spectra were obtained for every membrane type, with each spectrum collected from 600 to 4000 cm^{-1}. Each spectrum was corrected for penetration depth and background subtraction using OMNIC 8.0 software (Thermo Fisher Scientific Inc.).

Surface morphology and roughness of membranes were analysed by AFM [141]. It was conducted on a scanning probe microscope (make: NT-MDT NTEGRA). Tapping mode of scanning was used to analyse surface roughness of membranes.

The sessile drop method was employed to measure the hydrophilicity of three RO membranes. A water drop (3 ml) was placed on flat RO surface using a microsyringe fitted with stainless steel needle. The contact angle between liquid drop and RO surface was measured by video image, recorded by a monochrome interline video camera (make: Easydrop, KRUSS). Average value of the three consecutive measurements were taken for calculation.

Table 3.2. Different operating parameters and specification of RO and NF membranes used in experiments.

Membrane make	**Model**	**Avg. permeate flow (LPH)**	**Max. operating pressure (MPa)**	**Area (m^2)**	**Max. operating temp. (^oC)**	**pH range**	**Max. feed flow (LPH)**
RO membranes							
CSM RO	(RE 1812 80)	12	0.88	0.38	45	2-11	450
DOW RO	(TW30 1812 75)	12	2.09	0.38	45	2-11	450
Vontron RO	(ULP 1812 75)	12	2.09	0.46	45	3-10	450
NF membranes							
Permionics NF (MWCO-100, 250, 400 Da)	HPA100, HPA250, HPA400	36	1.37	0.3	45	2-11	540

3.3 Formulation of Synthetic Groundwater

3.3.1 Analysis of Sampled Groundwater

Laboratory scale membrane experiments are many times not feasible with actual brackish groundwater due to its inadequate availability and fluctuating quality [45, 157, 194].

In view of this, researchers generally perform RO experiments after preparing synthetic water by dissolving known amount of salts in de-mineralized water to make approximate ionic concentration of desired element (s) that may or may not correlate with the ionic concentration of actual groundwater. For example, Bohdziewicz et al. [45] determined nitrate separation properties of RO membrane by testing them with a solution of NaCl of 5 g/dm^3 concentration in pure water and tap water in which nitrate concentration was increased up to the value of 100 mg/dm^3 by adding KNO_3. Kamizono [118] employed a procedure for synthesis of one liter of groundwater by dissolving a fixed amount of $CaS0_4.2H_2O$, Na_2CO_3 and $MgCO_3$ in deionized water. Rahardianto et al. [194] prepared synthetic solution by dissolving inorganic salts such as $CaCl_2$, $MgSO_4$, NaCl, $NaSO_4$, and $NaHCO_3$.

In present study, synthetic water was formulated in the laboratory on the basis of major ionic elements of actual groundwater and further used for performing different membrane experiments. Ground water samples were collected from Timarpur (sample I), Dhansa (sample II) and Nangli Sakrawati Ind. Area, Najaf Garh (sample III). All these areas are well understood to display problem of brackish groundwater in New Delhi (India). The various drinking water quality parameters of these water samples are analysed and presented in Table 3.3.

The average value of the samples was taken into consideration. As shown in Table 3.3, the ground water samples were contaminated in terms of dissolved constituents mainly calcium, magnesium, chloride and sulphate. Hence, the use of RO treatment plant is very much suitable for treating this type of water and for making it suitable for drinking and other household, industrial use.

The first step after the water analysis was an assessment of the quality of the data, which was accomplished by calculating the balance of positive and negative ions. Water fulfills the principle of electro-neutrality and is therefore always uncharged. The level of error in the data was calculated using the following formula [23]:

$$\text{Error of ion balance} = \frac{\sum cations - \sum anions}{\sum cations + \sum anions} \times 100 \quad (3.1)$$

An error of up to ±3% is tolerable, while every water sample with a calculated error outside this range should be measured again. The error of ion balance for the measured water samples were within this range (0.68%, 2.26% and 0.67% for sample I, sample II and sample III, respectively). This indicates that the resultant data quality is sufficient for chemical modelling or for drawing simple conclusions about water quality.

3.3.2 Synthetic Water Formulation and Validation

For the formation of synthetic groundwater, a mathematical matrix based computation was employed for estimating the desired quantity of different required salt compounds [4]. The total dissolved solids value (4456 mg/l) of the sample I was found very near to be in the highest range of the the brackish water (2000-5000 mg/l). Therefore, elemental concentration from sample I (Timarpur, Delhi) was further considered for calculation and formulation of synthetic water. The concentration of each compound was achieved by multiplying the concentration of the desired element with the inverse of a square array of matrix that consists of a number of atoms and charge of each element or ion of a compound (Table 3.4). Table 3.5 presents the estimated concentration of different salt compounds.

Based on this formulation, synthetic water was prepared in the laboratory using analytical grade chemicals (make: Merck, India).

Furthermore, to validate the accuracy of this formulation, concentrations of elements of the synthetic groundwater were analysed experimentally and compared with that of actual ground water as shown in Table 3.6. The two results displayed a net correlation of 0.9982.

Table 3.3. Physical and chemical characteristics of actual groundwater used for synthetic groundwater formulation.

Parameter	**Unit**	**Method of test**	**DL***	**PL***	**Sample I**	**Sample II**	**Sample III**
pH	-	Potentiometric	6.5 to 8.5	NR	7.45	7.3	7.44
Temperature	(^oC)	Conductivity thermometer	-	-	27.7	27.7	28
Electrical conductivity	µS/cm	Conductivity Cell Potentiometric	-	-	6180	3910	16170
Turbidity	NTU	Turbidimeter	5	10	1.56	0.44	1.43
Alkalinity (as $CaCO_3$)	mg/L	Titrimetric	200	600	34	62	24
Total Hardness (as $CaCO_3$)	mg/L	Titrimetric	300	600	**1480**	**720**	**4000**
Total dissolve solids	mg/L	Gravimetric	500	2000	**4456**	**2404**	**12450**
Total suspended solids	mg/L	Gravimetric	-	-	192	76	22
Total solids	mg/L	Gravimetric	-	-	4648	2480	12472
Sodium (as Na)	mg/L	IC	-	-	745.7	415.75	1975
Potassium (as K)	mg/L	IC	-	-	ND	12.61	ND
Calcium (as Ca)	mg/L	IC	75	200	**452.55**	140.95	**941.6**
Magnesium (as Mg)	mg/L	IC	30	100	**156.5**	75.95	**621.6**
Fluoride (as F)	mg/L	IC	1	1.5	0.5	1.49	1.35
Chloride (as Cl)	mg/L	IC	250	1000	**1951.95**	753.2	**5593**
Nitrate (as NO_3)	mg/L	IC	45	NR	**47**	**57.75**	**126.3**
Sulphate (as SO_4)	mg/L	IC	200	400	**538.72**	385.39	**676.45**
Iron (as Fe)	mg/L	ICP-MS	0.3	1	0.62	0.23	0.88
Copper (as Cu)	mg/L	ICP-MS	0.05	1.5	0.01	ND	ND
Manganese (as Mn)	mg/L	ICP-MS	0.1	0.3	ND	0.03	0.06
Mercury (as Hg)	mg/L	ICP-MS	0.001	NR	ND	ND	ND
Arsenic (as As)	mg/L	ICP-MS	0.01	0.05	0.01	ND	0.02
Lead (as Pb)	mg/L	ICP-MS	0.01	NR	0.01	ND	ND
Chromium (as Cr)	mg/L	ICP-MS	0.05	NR	ND	0.01	ND
Cadmium (as Cd)	mg/L	ICP-MS	0.003	NR	ND	ND	ND
Selenium (as Se)	mg/L	ICP-MS	0.01	NR	0.02	0.01	0.09
Aluminium (as Al)	mg/L	ICP-MS	0.03	0.2	ND	ND	ND
Boron (as B)	mg/L	ICP-MS	0.3	1.5	0.01	0.03	0.02
Zinc (as Zn)	mg/L	ICP-MS	5	15	0.01	0.01	0.01

DL = desirable limit, PL = permissible limit, *As per IS:10500, ND = Not determined, NR = No relaxation, ICP-MS = Inductive Coupled Plasma-Mass spectrometry, IC = Ion Chromatography.

Table 3.4. Elements contributed by chemical components along with square array of matrix.

Element	Atomic Weight	Concentration (mg/L)	Molarity (mol/L)	NaCl	$CaCl_2$	$MgCl_2$	$NaNO_3$	Na_2SO_4	NaHCO	Charge
Chloride	35.45	1951	0.06	1	2	2	0	0	0	-1
Sodium	22.98	746	0.03	1	0	0	1	2	1	1
Sulphate	96.06	539	0.01	0	0	0	0	1	0	-2
Calcium	40.08	452	0.01	0	1	0	0	0	0	2
Magnesium	24.31	157	0.01	0	0	1	0	0	0	2
Bicarbonate	61.02	15	0.00	0	0	0	0	0	1	-1
Nitrate	62.00	47	0.00	0	0	0	1	0	0	1

Table 3.5. Final concentration of compounds taken for synthetic water formulation.

Compounds	Amount (g/L)
NaCl	1.1687
$CaCl_2$	1.2411
$MgCl_2.6H_2O$	1.2931
$NaNO_3$	0.0603
Na_2SO_4	0.8108
$NaHCO_3$	0.0247

Table 3.6. Comparison of actual and synthetic groundwater composition.

Parameter	Actual groundwater concentration (mg/L)	Synthetic water concentration (mg/L)	Difference (%)
TDS (Gravimetric)	4456	4762	-6.8
TDS (Calculated by ions)	3907	3835	1.8
Sodium	746	714	4.3
Calcium	452	498	-10.2*
Magnesium	157	140	10.8*
Chloride	1951	1890	3.1
Nitrate	47	48	-2.1
Sulphate	539	545	-1.3

* Difference in Calcium and Magnesium ion concentrations can be due to using hydrated salts of these ions. Since anhydrous form is hygroscopic (readily absorbs water from air) and difficult to weigh accurately, therefore, hydrated salts are often selected when preparing solutions.

3.4 Experiment Design, Model Fitting and Statistical Analysis

In the present study we have optimized the performance of a laboratory-scale RO plant by simultaneously maximizing water recovery and salt rejection along with minimizing energy demands. Synthetic groundwater was used for all the experiments. Due to the appreciable contribution of RSM in creditable enhancement in precision and accuracy of evaluated optimized values of process variables, it is usually employed for experimental design [198]. The advantages of RSM include reduction in number of experiments and minimization of experimental cost and time consumption [84, 260]. In the present study, optimization was performed employing RSM using CCD. Furthermore, experiments to validate these RO results were conducted employing the optimized process variables values derived from RSM prediction. Although RSM is a good modelling tool, assumption of homogeneous parameter values [222], restricted predictive capability, requirement of prior specification and a limited number of polynomial fitting functions make its use limited to quadratic approximations only [55]. Emergence of stronger modelling tools with better predictive power like ANN offers an alternative to polynomial regression method and overcomes the drawbacks of RSM. Few previous investigations highlighted the relevance of ANN models to evaluate the predictions recommended by RSM [41, 175, 224]. It is assumed that ANN needs comparatively lesser data if the input data are statistically well distributed [251]. Since RSM proposes the surface plots offering a better approach to envisage relations between independent and dependent variables, both the RSM and ANN methods have been applied for modelling using the same experimental data. Finally, the validation of optimized process conditions suggested by the RSM was also carried out by the generated ANN model in MATLAB.

3.4.1 Predictive Modelling Using Response Surface Methodology

To determine both linear and quadratic models, CCD based statistical experimental design was used [55, 112, 198]. It combines two level full factorial (cubic) designs with additional axial (star) points and a set of centre points at the centre of the experimental region. The centre points were repeated to improve the precision of experiments [39, 84]. During RS modelling, input variables (x_1, x_2,...,x_n) in coded scale level vary from the minimum level (-1) up to the maximum level (+1). To determine a critical point (maximum, minimum, or saddle), a

second-order model containing quadratic terms is often used and can be presented in a general form as:

$$y = \beta_0 + \sum_{i=1}^{n} \beta_i x_i + \sum_{i=1}^{n} \beta_{ii} x_i^2 + \sum_{i<j}^{n} \beta_{ij} x_i x_j + \varepsilon \quad (3.2)$$

where y denotes the predicted response, x_i refers to the coded levels of input variables, β_0, β_i, β_{ii} and β_{ij} are the regression coefficients (constant term, linear, quadratic and interaction parameters), n is the number of variables and ε is the experimental error, which is assumed to be random with zero mean [39]. In RSM model solution, homogeneity was assumed for all factors that were continuously monitored and regulated. To the mark that these were assumptions, additional error (ε) was introduced [222]. Design-Expert software, (Stat-Ease Inc., version 7) was used for graphical analysis and model fitting.

In this study, the mutual effect and the relative significance of four input factors on the performance of membrane process was investigated employing RSM with CCD [129]. Experiments were carried out for different ranges of concentration, temperature, pH and pressure of feed water. A total of 30 experiments were proposed by the design expert software, comprising 16 factorial experiments, 8 axial experiments and 6 replicate experiments at the central point that can be calculated from the equation (3.3):

$$N = 2^n + 2n + n_c = 2^4 + (2 \times 4) + 6 = 30 \quad (3.3)$$

where N is the total number of experiments required, n is the number of numeric factors and n_c is replicate number at the central point. Experiments were carried out for various ranges of concentration, temperature, pH and pressure of feed water for NF and RO membranes (Table 3.7).

Furthermore, multi-parameter nonlinear regression models were developed as actual and coded factors [167]. The responses considered in this study are water recovery, TDS rejection and SEC. Usually, it is assumed that the responses are correlated within runs but are independent otherwise.

The diagnostic statistical study of the CCD model was undertaken to examine outliers using experimental and predicted values [39, 69]. Analysis of variance (ANOVA) was used to develop a predictive model considering water recovery, TDS rejection and SEC. Lack of fit and coefficient of determination (R^2) were used to test the goodness of fit of the model [167].

Table 3.7. Range of input variables taken in different NF and RO membranes experiments.

Actual input variables	**Coded symbol**	**Coded level**				
		- α	**-1**	**0**	**+1**	**+ α**
Temperature (ºC)						
• CSM RO, Dow RO	A	20	24	28	32	36
• Vontron RO, NF100, NF250, NF400		15	20	25	30	35
Pressure (MPa)						
• CSM RO	B	0.49	0.59	0.69	0.78	0.88
• Dow RO		0.59	0.88	1.18	1.47	1.77
• Vontron RO		0.29	0.59	0.88	1.18	1.47
• NF100		0.29	0.49	0.69	0.88	1.08
• NF250		0.20	0.49	0.78	1.08	1.37
• NF400		0.29	0.39	0.49	0.59	0.69
Concentration (mg/L)						
• CSM RO, Dow RO, Vontron RO, NF100, NF250, NF400	C	500	1500	2500	3500	4500
pH						
• CSM RO, Dow RO, Vontron RO, NF100, NF250, NF400	D	5	6	7	8	9

Three dimensional surface plots for response surfaces (RS) were generated from the model equation. Numerical optimization was carried out by assigning a desired goal along with higher and lower limits for each response. Finally, an overall desirability function of goal achievement was created, ranging from 0 to 1 i.e. least to the highest probability. After optimization of membranes by the RSM software, validation experiments were performed employing the optimal values of the input parameters and the results verified against the predicted values of the RSM.

3.4.2 Predictive Modelling Using Artificial Neural Network

ANN modelling has earlier been used by few researchers for performance prediction of RO plants [128, 145, 169, 195, 257]. ANN comprises of highly interconnected processing elements called neurons, which operate with summing junction and transfer function [39]. In contrast to RSM, ANN modelling consists of input (factors), target (experimental response) and output (predicted response). The artificial neurons are arranged in a group of layers consisting of input layer (representing independent variables), output layer (representing dependent variables) and hidden layers that associate inputs with output [55, 84]. Each neuron from one layer is linked with each neuron in the next layer. The pattern of interconnection among the neurons is represented in Figure 3.3.

The number of neurons belonging to input and output layers is set by the number of input and output processes. On the contrary, the number of neurons in hidden layers is based on trial and error. In this study, the number of neurons giving minimum average error was selected for the network [55, 251]. The connections between neurons consist of weights (w) and biases (b) with neurons referring information. Purelin, logsig and tansig transfer functions are commonly used to solve the linear and nonlinear regression problems [41, 129]. The commonly used neural network architecture for solving nonlinear regression problems is multilayer feed-forward neural network. Back propagation (BP) method is the most common training algorithm for the feed-forward neural network [224].

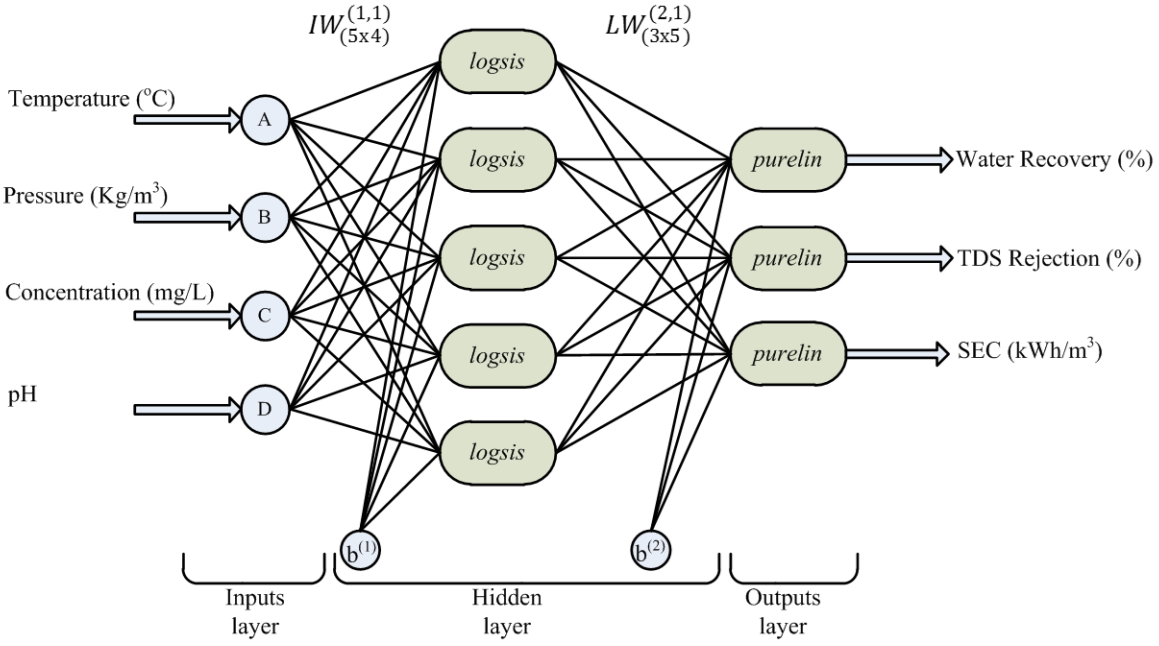

Figure 3.3. Architecture of ANN model for the prediction of RO outputs.

Data generated from experimental design by RSM have been used as relevant inputs, as well as output, for ANN training [219]. According to BP algorithm, the weights and biases are iteratively updated in the direction in which the performance function (mean squared error) decreases. The training phase is completed when the mean square error is minimized across all training experiments. Once ANN has been trained, it has a good predictive capability and ability to accurately describe the RS even without any knowledge of the physical and chemical background of the modelled system [39, 94].

In the present study, MATLAB neural network tool was used to train the ANN model by using the RSM data. Five neurons were used for the hidden layer. Input to the hidden layer and hidden to output mapping were done using log sigmoid (logsis) and linear (purelin) transfer functions, respectively [129]. Figure 3.3 shows the architecture of the present ANN model. In this figure, $IW^{(1,1)}$ indicates the input weight matrix of size (5×4). $LW^{(2,1)}$ denotes the layer weight matrix, where the superscripts indicate the source and destination connections, respectively. All neurons from the network have the bias $b^{(l)}$ where the superscript *l* indicates the layer index.

The experimental results given by the CCD method were used to develop ANN model intended to recognize the non-linear relationships present between the water recovery, salt rejection and SEC, i.e. the ANNs output and the operating variables, viz. the feed concentration, pressure, temperature and pH, i.e. ANNs inputs.

The network was trained using Bayesian regulation based function 'TRAINBR' in error BP framework [41]. Finally, the validation of RSM predictions was carried out by the generated ANN model.

3.5 Photovoltaic Assisted Hybrid Membrane Experiments

3.5.1 NF-RO Hybrid Membrane Experiments

In many hybrid configurations, NF –RO integrated membranes were used for various purposes [15, 68, 188, 221, 231, 254]. However, all of these were in permeate staging configuration. To increase the recovery and minimize the SEC of overall system, the concentrate staging configuration have generally been used [16, 19, 174, 192]. In this study, laboratory scale experiments were carried out on RO–NF membranes in concentrate (NF-C-RO) and permeate (NF-P-RO) staging configuration. RO and NF membranes used in these experiments showed the best performance on optimized input parameters estimated using RSM experiments. First hybrid

configuration (NF-C-RO) consisted of placing high flux NF membrane in first stage and low flux RO membrane in the second stage to achieve a good hydraulic balance. Generally, it is preferred to use low operating pressure membrane in the second stage in concentrate stage configuration to overcome the osmotic pressure at the end of second stage [192]. The reject from first stage is used as feed water in the subsequent stage to increase water recovery [16]. In the second hybrid configuration (NF-P-RO), permeate of first stage was pumped as a feed water in the second stage.

3.5.2 Integration of NF-RO Systems With Photovoltaic System

Solar irradiance, the energy incident upon the earth's atmosphere, is collected via PV system and converted to electrical energy. To collect the solar irradiance data over Roorkee region, 1.5 kW grid connected PV system was installed over the rooftop of the department of hydrology, IIT Roorkee. Data from PV system (DC/AC current, voltage and energy) were recorded and stored from June 2013 to February 2014.

3.6 Prediction of Fouling Potential

Inorganic fouling/scaling of membranes may have adverse effects on the performance of the membrane system. Proper assessment of the membrane feed water scaling potential is necessary to avoid scaling. Reverse osmosis inorganic fouling assessment (ROIFA) software is able to calculate inorganic fouling load of feed water [75]. With this software, it is further possible to calculate the optimum design and possible treatment options. The same was employed in this study.

3.7 Economic Assessment of Photovoltaic Assisted Membrane Systems

Economic analysis of any device or process is essential for subsequent commercialization. The cost analysis among the PV-hybrid, PV-RO and PV-NF systems implies three modes of comparisons for the product water cost. The principal objective of the economic assessment was to estimate the water production cost for these systems. Water production costs include the following items [85]:

• Capital cost: It presents a constant value, dependent on the capital cost and depreciation factor. The capital cost are recognized at present market rates and are subjected to distribution for annual expenditure to arrive at production costs at Indian conditions.

• Annual operation and maintenance cost: It presents a variable value, dependent on the operational (manpower) and maintenance cost, consumption and cost of chemicals used for pre- and post-treatment of water (especially in NF and RO systems) and the membranes replacement rate in a NF and RO systems.

Installation of PV system decreases the operational cost of a desalination system compared to on-grid systems, whereas on the other hand it increases the capital cost. The decreased operational cost comes from removing all the expenditure on electricity (normally the highest component of operational expense for an on-grid RO system). The increased capital cost comes from the panels, supporting control system, inverters, and batteries.

Per unit water production cost is affected by various factors including recovery ratio, SEC, cost of equipment (membrane and solar system), hybridization configuration, interest rate, subsidy given by government, labour cost etc.

Chapter 4.
Membrane Characterization and Optimization of Input Process Parameters

4.1 General

This chapter presents the details and findings of characterization of six commercially available small scale RO and NF membranes and also the optimization experiments using CCD of RSM. Physical aspects of characterizing NF and RO membranes from various manufacturers brand have been investigated. Physical surface characteristics including surface roughness, occurrence of functional groups and hydrophobicity/hydrophilicity properties were determined by AFM, FTIR and contact angle measurement, respectively [225]. A correlation between surface properties and membrane filtration results was obtained.

Due to the appreciable contribution of response surface methodology (RSM) in creditable enhancement in precision and accuracy of evaluated optimized values of process variables, it is usually employed for experimental design. Synthetic water nearly close to actual groundwater was used for the laboratory scale experiments. Optimization experiments were carried out to maximize water recovery, TDS rejection and to minimize SEC of small scale brackish water membrane process using different range of pH, feed temperature, feed pressure and concentration of feed solution as the input parameters. Experiments employing optimized input conditions validated the developed RSM model. Removal efficiency of major ions was observed in validation experiments. Since RSM proposes the surface plots offering a better approach to envisage relations between independent and dependent variables, and ANN offer a stronger modelling tool with good predictive power, both the RSM and ANN methods were applied for modelling using same experimental data. ANN model was developed and used to validate the RSM predicted optimized process conditions.

4.2 Membrane Characterization

4.2.1 AFM Analysis

Surface characterization was carried out by different measurement techniques. Surface roughness of three RO membranes as measured by AFM analysis is shown in Figure 4.1. The in-plane x and y scales are 10 µm x 10 µm (1 µm/div), while the z axis varied with respect to surface roughness. Figure 4.1 reveals that the RMS (Rq) roughness value of the RO membranes varies from below 35 µm to nearly 55 µm.

The CSM RO membrane was found to be the smoothest, with an RMS (Rq) value of 33.99 µm. Total surface area of the membrane increases with surface roughness which leads to the accumulation of foulants at the ridge-valley structure of the surface. The AFM technique has already proved earlier that rough surfaces are more vulnerable to fouling which causes decline in flux and salt rejection [253].

4.2.2 FTIR Analysis

In order to authenticate functional groups on the membrane surfaces, FTIR analysis graphs are obtained for each virgin membranes and shown in Figure 4.2. These figures represents FTIR spectra of wave number ranged between 500 and 4000 cm^{-1}. In general, all the membranes had very similar spectra peaks at low wave numbers (650–2000 cm^{-1}). Both polyamide and polysulfone layers could be detected due to the greater penetration depth (>300 nm) in this wave number range.

Tang et al. [238] studied the higher range FTIR spectra, noticed the peaks of the coated membranes between 2300 and 4000 cm^{-1}, and found that the coated layer is aliphatic with a significant amount of OH groups. All the virgin polyamide membranes showed a broad band centered around 3400 cm^{-1} and several smaller peaks around 3000 cm^{-1}. At these wave numbers, FTIR is much more surface sensitive with a penetration depth around 200 nm or lower [238]. The peaks around 2900–3000 cm^{-1} can be assigned to aliphatic (C–H) stretching vibrations, consistent with a coating material abundant in aliphatic carbons [229]. On the other hand the broad band around 3400 cm^{-1} may be attributed to a complex band due to the overlapping of stretching vibration of free hydrogen bonded N–H stretching modes and carboxylic groups (-COOH) of polyamide layer, and additional groups (such as -OH groups) [223] from the coating

layer. IR spectra of all RO and NF membranes were found very similar to poly (aryl) ether (Figure 4.2).

The FTIR spectrum is directed with vibrational bands in the region of 1500 to 1580 cm^{-1}, which describes the presence of polysulfonyl group in the porous polysulfone layer [143]. The main vibrational bands related to the thin polyamide layer are the amide I (C-O) near 1740 cm^{-1}, amide II (N-H) near 1580 cm^{-1} and C-C ring vibrations of polyamide at 1745, 1490, and 1404 cm^{-1} [89, 211].

Such results provide some insight into the chemical nature of the coating material, i.e., the coating material is mostly aliphatic with great abundance of OH groups. Therefore, it can be predicted that all RO and NF membranes contained thin polyamide layer with polysulfone support.

4.2.3 Contact Angle Measurement

Membrane hydrophilic-hydrophobic properties are based on contact angle between the liquid-gas tangent and membrane-liquid boundary [241]. Usually membrane materials having large contact angle are prone to adsorption of various solutes.

Earlier, it had been shown that RO membrane fouling, improved flux during operation and the surface roughness are strongly correlated to each other, as hydrophilic RO membranes with smoother surfaces are less prone to adsorption of various solutes (inorganic fouling) compared to the relatively more hydrophobic and rough membranes [77]. The smaller contact angle (higher hydrophilicity) and smoother surface of CSM membrane among RO membranes and NF250 among NF membranes (Figure 4.3) might be the reason of its better performance.

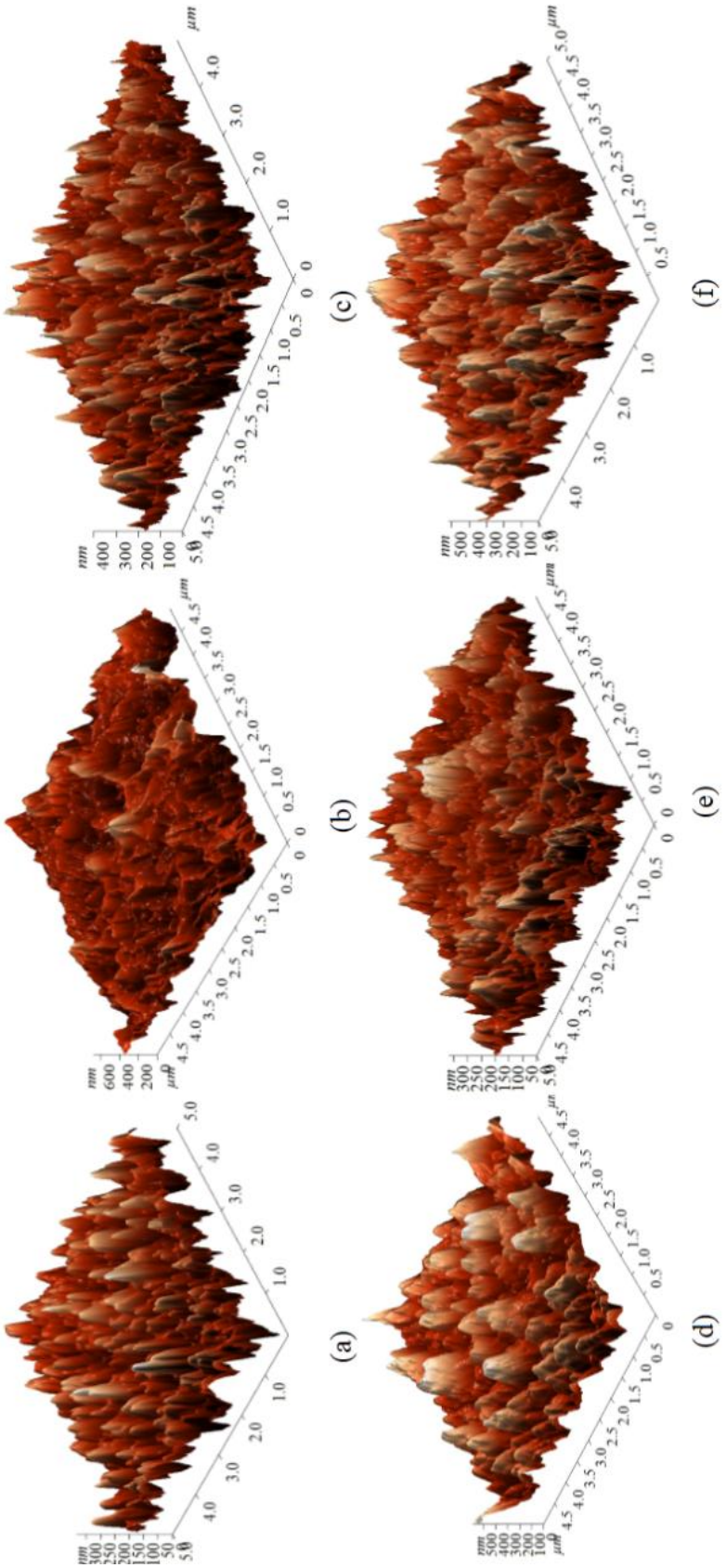

(a) CSM, (b) Dow, (c) Vontron, (d) NF100, (e) NF250, (f) NF400

Figure 4.1. AFM image showing surface roughness of different RO and NF membranes.

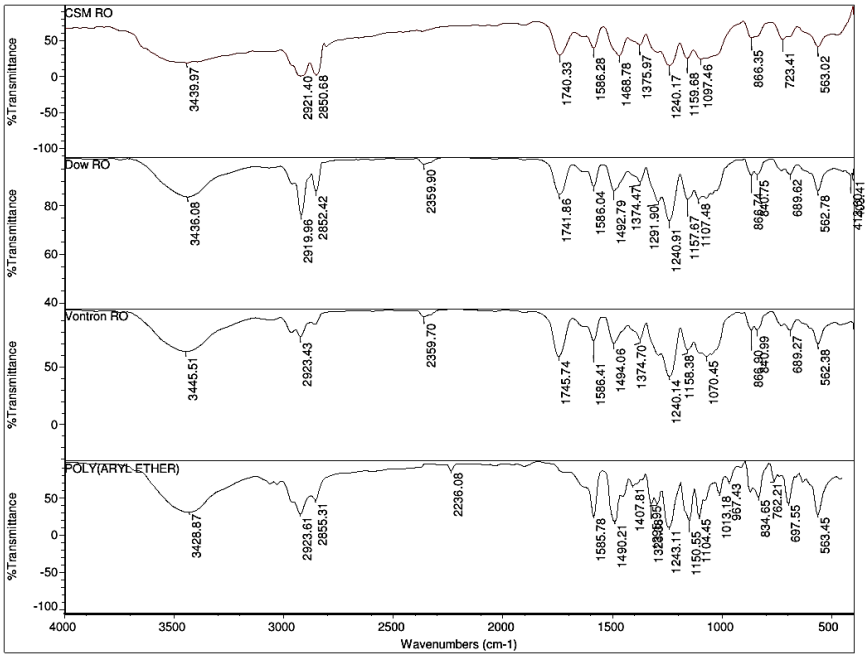

(a)

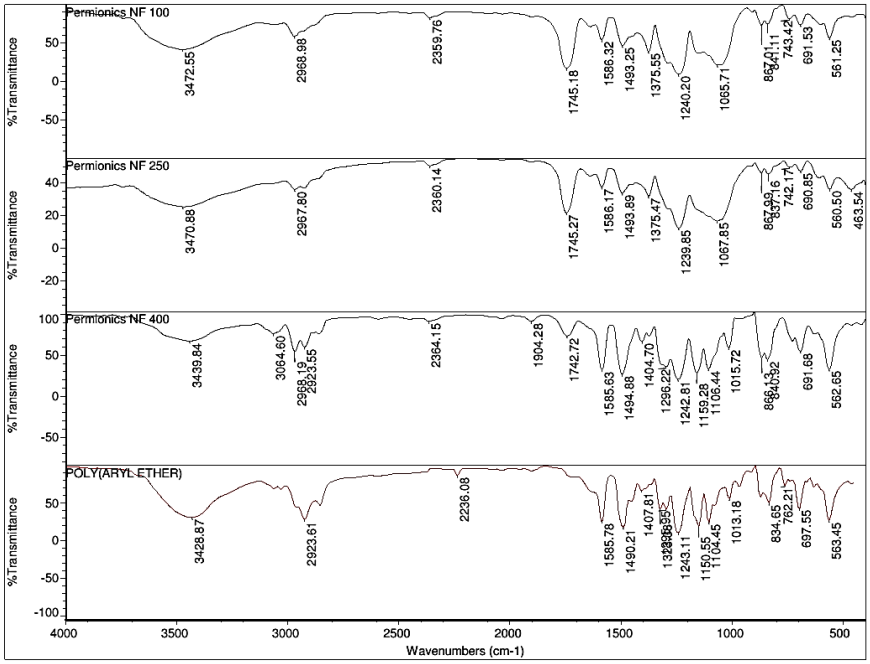

(b)

Figure 4.2. FTIR spectra different (a) RO and (b) NF membranes matched with the spectra of poly (aryl ether).

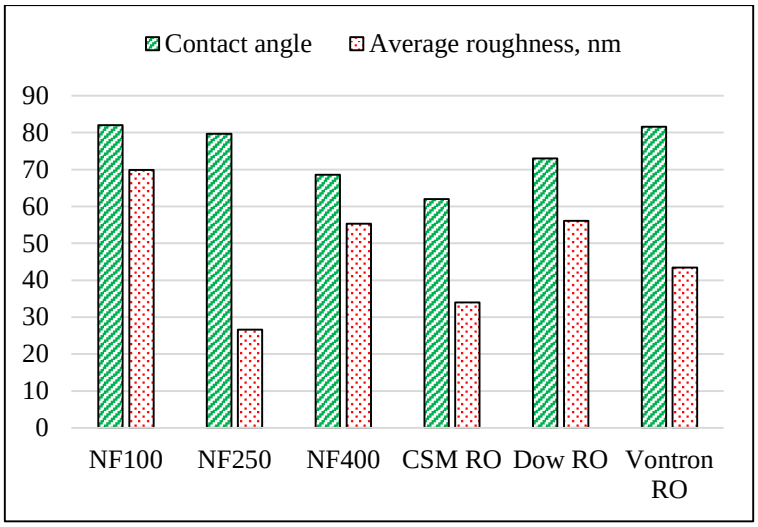

Figure 4.3.Comparison between contact angle and average roughness of different RO and NF membranes.

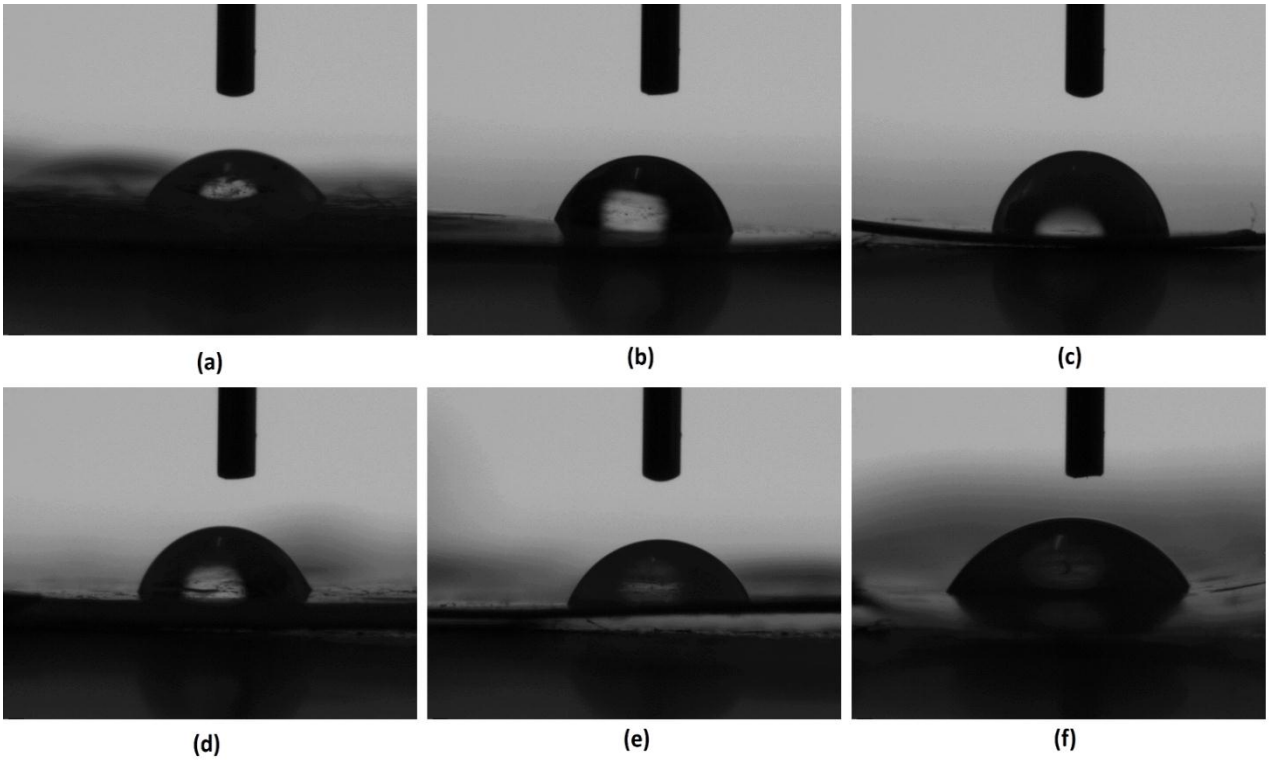

(a) CSM, (b) Dow, (c) Vontron, (d) NF100, (e) NF250, (f) NF400

Figure 4.4. Contact angle measurement of different membranes using sessile drop method

4.3 Response Surface Modelling and ANOVA Analysis

In the present study, RSM method using CCD was employed to investigate the mutual effect of four input factors on the performance of membrane process. A total of 30 experiments were employed as derived by the Design Expert software (Stat-Ease, Inc, Minneapolis), comprising 16 factorial experiments, 8 axial experiments and 6 replicate experiments at the central point. Experiments were carried out for different ranges of concentration, temperature, pH and pressure of feed water. Detail of the entire experimental design for the treatment of brackish water with RO (CSM, Dow and Vontron) and NF (NF100, NF250 and NF400) membranes, comprising actual values of input factors and output responses are given in Table 4.1 to Table 4.6.

Linear, interactive and quadratic models were fitted to the experimental data to obtain the regression equations. ANOVA was used to analyze experimental data in RSM and experimental response models were derived. These response models could be used to find optimal values of the operating variables.

4.3.1 Optimization of Water Recovery

4.3.1.1 Effect of Process Parameters on Water Recovery

Graphical presentation of the data and analysis from RSM were compared in the form of RS plots. The comparative RS plots for water recovery as a function of different variables are shown in Figure 4.5 and Figure 4.6. At low and high value of temperature, water recovery increased with increase in pressure from 0.59 MPa to 0.79 MPa for CSM membrane (Figure 4.5a), 0.88 MPa to 1.47 MPa for Dow membrane (Figure 4.5b) and 0.59 MPa to 1.18 MPa for Vontron membrane (Figure 4.5c).

Similar trend was observed with increase in pressure from 0.49 MPa to 0.88 MPa for NF100 membrane, 0.49 MPa to 1.08 MPa for NF250 membrane and 0.39 MPa to 0.59 MPa for NF400 membrane (Figure 4.6a to c). The water recovery increases apparently because higher pressure allows enhanced flow of water through the membranes [133, 213].

Effect of feed water concentration and pH on water recovery were not significant for CSM membrane (Figure 4.5d). However, at low and high pH, water recovery decreased with concentration from 1500 mg/l to 3500 mg/l for Dow and Vontron RO membranes (Figure 4.5e

to f) and also for all three NF membranes (Figure 4.6d to f). Lower water recovery is apparently because of higher salt concentration, causing the negative effect of concentration polarization and decreasing membrane water flux [133]. On the other hand, the effect of pH and temperature on water recovery are not significant in these cases because of the low susceptibility of polysulphone membrane to conformational variations in response to changes in temperature and pH [24]. The response surface indicates a general trend that increasing feed pressure will enhance the water recovery. In contrast, water recovery decreases on increasing feed water concentrations.

4.3.1.2 Statistical Analysis and Fitting of Second-Order Polynomial Equation

ANOVA results for water recovery of RO and NF membranes are given in Table 4.7 to Table 4.12. Based on ANOVA analysis, all the factors followed second-order effects, yielding a quadratic model for water recovery of different RO and NF membranes. Value of "Prob > F" less than 0.0001 indicates that the model displays high statistical significance and less than 0.05 indicates significance only.

RO Membranes

Table 4.7, Table 4.8 and Table 4.9 show ANOVA results for water recovery of CSM, Dow and Vontron RO membranes respectively. Respective F-values of 26.48, 24.08 and 212.80 imply that the quadratic model is significant. The large P values (> 0.05) for lack of fit showed that the F-statistic was insignificant for all RO membranes, implying significant model correlation between the variables and process responses.

For the CSM RO membrane, ANOVA response for water recovery obtained from the response surface quadratic model (Table 4.7) shows that model term B is highly significant, whereas A, B^2, C^2 are significant terms. A high R^2 coefficient (close to unity) (Figure 4.7a) confirms a satisfactory fit of the quadratic model to the experimental data. The quadratic equation in terms of the coded factors for response on "water recovery" of CSM membrane is given as follows:

$$\text{Water recovery}_{csm} = 12.06 + 0.96(A) + 4.44(B) - 0.23(C) - 0.47(D) + 0.58(AB) + 0.21(AC) + 0.3(AD) - 0.12(BC) - 0.55(BD) + 0.61(CD) + 0.20(A^2) + 0.83(B^2) - 0.54(C^2) - 0.13(D^2) \quad (4.1)$$

where, A is the temperature (^oC), B is the pressure (MPa), C is the concentration (mg/l) and D is the pH.

Table 4.8 shows that the model terms B, C are highly significant, whereas A, AB, AC are significant terms. Note that R^2 value is about 0.9574, being close to unity, which represents an excellent fit (Figure 4.7b). The quadratic equation in terms of the coded factors for response on "water recovery" of Dow membrane is given as follows:

$$\text{Water recovery}_{Dow} = 9.65 + 0.99(A) + 2.75(B) - 1.77(C) - 0.34(D) + 0.55(AB) - 0.51(AC) + 2.57E\text{-}003(AD) - 0.27(BC) + 0.070(BD) + 0.038(CD) + 0.019(A^2) + 0.087(B^2) + 0.014(C^2) - 0.34(D^2) \quad (4.2)$$

For the Vontron RO membrane, ANOVA response for water recovery obtained from the response surface quadratic model (Table 4.9) shows that the model terms A, B, C are highly significant, whereas AB, AC, BC and CD are significant terms. The R^2 value of 0.9949 (99.49%) represents a excellent fit of of the regression model for water recovery of Vontron membrane (Figure 4.7c). The quadratic equation in terms of coded factors for for reponse on "water recovery" of Vontron membrane, is given as follows:

$$\text{Water recovery}_{Vontron} = 6.9 + 0.81(A) + 3.17(B) - 0.7(C) - 0.037(D) + 0.40(AB) - 0.37(AC) - 0.11(AD) - 0.16(BC) - 0.15(BD) - 0.3(CD) + 0.022(A^2) + 5.36E\text{-}004(B^2) - 1.48E\text{-}003(C^2) - 0.1(D^2) \quad (4.3)$$

NF Membranes

For the NF100 membrane, ANOVA response for water recovery obtained from the response surface quadratic model (Table 4.10) shows that the model terms A, C, D are highly significant, whereas B, CD, B^2 and D^2 are significant terms.

Table 4.11 and Table 4.12 show F-value of 217.93, 53.09 and 39.37 respectively, implying that the quadratic model is significant. Further, data given in these tables demonstrate that all the models are significant at the 5% confidence level since P-values are less than 0.05. The closeness of the R^2 value to unity (0.9951) implies good accuracy of the response predicted by the model (Figure 4.8a). The final empirical model formulated in terms of the coded factors for response on "water recovery" of NF100 membrane is stated by following equation:

$$\text{Water recovery}_{NF100} = 7.12 - 1.19(A) - 0.17(B) + 0.7(C) + 3.35(D) - 0.044(AB) - 0.17(AC) - 0.16(AD) + 0.012(BC) + 0.023(BD) + 0.18(CD) - 0.048(A^2) - 0.13(B^2) + 0.017(C^2) + 0.28(D^2) \quad (4.4)$$

where, A is the concentration (mg/l), B is the pH, C is the temperature (^oC) and D is the pressure (MPa). Positive sign before the terms indicates synergistic effect, whereas antagonistic effect is indicated by negative sign before the terms. Table 4.11 shows that the model terms A, C, D are highly significant, whereas B^2 and D^2 are significant terms. R^2 value is about 0.9802, being close to unity, which represents an excellent fit of regression model (Figure 4.8b). The quadratic equation in terms of the coded factors for reponse on "water recovery" of NF250 membrane is given as follows:

$$\text{Water recovery}_{NF250} = 11.93 - 0.96(A) + 0.12(B) + 1.28(C) + 4.44(D) - 0.39(AB) - 0.17(AC) + 0.040(AD) - 0.16(BC) + 0.15(BD) + 0.29(CD) + 0.12(A^2) - 0.41(B^2) + 0.13(C^2) - 0.42(D^2) \quad (4.5)$$

For the NF400 membrane, ANOVA response for water recovery obtained from the response surface quadratic model (Table 4.12) shows model terms A, C, D are highly significant, whereas A^2 are significant terms. A high R^2 value (0.9735) represents a good fit of the regression model for water recovery of NF400 membrane (Figure 4.8c). The quadratic equation in terms of the coded factors for response of "water recovery" of NF400 membrane is given as follows:

$$\text{Water recovery}_{NF400} = 10.22 - 0.98(A) + 0.041(B) + 0.97(C) + 2.67(D) - 0.22(AB) + 0.015(AC) - 0.095(AD) - 0.33(BC) + 0.10(BD) + 0.20(CD) - 0.42(A^2) - 0.047(B^2) + 0.14(C^2) + 0.15(D^2) \quad (4.6)$$

Table 4.1. Experimental inputs and responses of CSM RO membrane.

Run	A	B	C	D	Recovery (%)		Rejection (%)		SEC (kWh/m^3)	
					Exp.	Pred.	Exp.	Pred.	Exp.	Pred.
1	24	0.59	1500	6	9.09	8.76	91.62	91.52	28.16	28.50
2	32	0.59	1500	6	6.98	8.48	90.22	89.94	28.00	26.91
3	24	0.79	1500	6	18.92	17.84	90.99	90.57	17.60	18.99
4	32	0.79	1500	6	20	19.87	89.19	87.86	17.60	16.57
5	24	0.59	3500	6	6.98	6.90	86.60	86.62	38.72	36.70
6	32	0.59	3500	6	8.84	7.47	85.14	84.47	29.94	31.90
7	24	0.79	3500	6	14.63	15.49	83.52	83.15	26.40	26.00
8	32	0.79	3500	6	17.83	18.38	78.33	79.86	22.47	20.37
9	24	0.59	1500	8	8.16	7.09	92.02	91.21	29.04	30.81
10	32	0.59	1500	8	9.09	8.02	92.08	92.38	29.04	28.63
11	24	0.79	1500	8	12.79	13.95	90.11	90.70	28.00	25.23
12	32	0.79	1500	8	17.65	17.20	90.03	90.72	20.53	22.22
13	24	0.59	3500	8	7.75	7.67	85.67	86.93	35.62	35.84
14	32	0.59	3500	8	8.92	9.46	86.39	87.52	32.17	30.45
15	24	0.79	3500	8	16.08	14.05	82.90	83.89	28.31	29.07
16	32	0.79	3500	8	18.03	18.15	83.31	83.34	24.00	22.85
17	20	0.69	2500	7	10	10.96	89.16	88.91	29.92	29.70
18	36	0.69	2500	7	15	14.78	87.16	86.78	20.53	21.89
19	28	0.49	2500	7	5.88	6.49	89.61	89.51	37.55	37.45
20	28	0.88	2500	7	24.14	24.26	84.92	84.38	19.11	20.34
21	28	0.69	500	7	10.01	10.37	93.53	94.53	20.53	20.02
22	28	0.69	4500	7	9.09	9.46	83.90	82.25	27.20	28.85
23	28	0.69	2500	5	12.82	12.49	84.27	85.40	25.34	26.24
24	28	0.69	2500	9	9.52	10.59	90.34	88.58	30.80	31.04
25	28	0.69	2500	7	12.2	12.06	90.12	89.90	24.64	26.15
26	28	0.69	2500	7	12.73	12.06	92.00	89.90	25.14	26.15
27	28	0.69	2500	7	13.13	12.06	88.25	89.90	23.69	26.15
28	28	0.69	2500	7	11.28	12.06	88.93	89.90	28.00	26.15
29	28	0.69	2500	7	10.53	12.06	89.96	89.90	30.80	26.15
30	28	0.69	2500	7	12.5	12.06	90.15	89.90	24.64	26.15

A = Temperature, B = Feed Pressure, C = Feed Concentration, D = pH; Exp. = Experimental, Pred. = Predicted

Table 4.2. Experimental inputs and responses of Dow RO membrane.

Run	A	B	C	D	Recovery (%)		Rejection (%)		SEC (kWh/m^3)	
					Exp.	Pred.	Exp.	Pred.	Exp.	Pred.
1	24	0.88	1500	6	8.26	7.68	89.90	89.45	29.30	29.58
2	32	0.88	1500	6	10.39	9.57	89.80	89.03	23.40	24.75
3	24	1.47	1500	6	12.59	12.48	84.40	82.54	24.40	24.48
4	32	1.47	1500	6	16.11	16.57	85.50	82.43	19.30	19.56
5	24	0.88	3500	6	5.08	5.62	82.70	81.06	42.40	42.92
6	32	0.88	3500	6	5.50	5.49	83.60	83.31	38.90	38.10
7	24	1.47	3500	6	8.59	9.34	73.10	72.75	31.20	31.51
8	32	1.47	3500	6	11.22	11.41	76.40	75.31	25.50	26.59
9	24	0.88	1500	8	7.52	6.78	91.10	91.33	34.00	33.21
10	32	0.88	1500	8	8.81	8.69	90.70	88.85	27.30	27.52
11	24	1.47	1500	8	11.22	11.86	87.00	85.18	26.10	27.41
12	32	1.47	1500	8	17.06	15.96	82.30	83.01	21.90	21.60
13	24	0.88	3500	8	4.71	4.87	86.10	86.99	45.80	46.03
14	32	0.88	3500	8	5.20	4.75	86.20	87.19	40.10	40.33
15	24	1.47	3500	8	8.62	8.88	79.60	79.45	35.00	33.91
16	32	1.47	3500	8	9.75	10.95	81.70	79.95	27.80	28.11
17	20	1.18	2500	7	8.17	7.74	82.80	83.84	32.10	32.16
18	36	1.18	2500	7	11.35	11.71	81.90	83.93	22.30	21.54
19	28	0.59	2500	7	3.45	4.50	87.30	87.26	46.90	46.74
20	28	1.77	2500	7	16.61	15.50	70.00	73.11	30.00	29.42
21	28	1.18	500	7	12.02	13.24	87.80	90.78	20.90	20.15
22	28	1.18	4500	7	7.46	6.17	79.20	79.33	40.00	40.00
23	28	1.18	2500	5	9.14	8.97	78.80	82.07	27.50	26.32
24	28	1.18	2500	9	7.51	7.62	88.80	88.59	31.10	31.48
25	28	1.18	2500	7	10.07	9.65	77.60	80.91	25.50	25.17
26	28	1.18	2500	7	8.99	9.65	82.10	80.91	25.50	25.17
27	28	1.18	2500	7	10.07	9.65	77.60	80.91	25.50	25.17
28	28	1.18	2500	7	8.99	9.65	82.10	80.91	25.50	25.17
29	28	1.18	2500	7	9.88	9.65	83.10	80.91	24.40	25.17
30	28	1.18	2500	7	9.88	9.65	83.10	80.91	24.40	25.17

A = Temperature, B = Feed Pressure, C = Feed Concentration, D = pH; Exp. = Experimental, Pred. = Predicted

Table 4.3. Experimental inputs and responses of Vontron RO membrane.

Run	A	B	C	D	Recovery (%)		Rejection (%)		SEC (kWh/m^3)	
					Exp.	Pred.	Exp.	Pred.	Exp.	Pred.
1	20	0.58	1500	6	3.12	2.89	67.11	68.20	55.00	54.97
2	30	0.58	1500	6	4.23	4.68	82.59	83.50	43.21	43.79
3	20	1.17	1500	6	8.88	9.04	79.07	79.30	26.79	25.23
4	30	1.17	1500	6	12.39	12.42	85.58	86.53	21.11	20.76
5	20	0.58	3500	6	2.91	3.14	70.00	69.21	67.22	66.37
6	30	0.58	3500	6	3.52	3.46	80.75	79.25	53.78	53.47
7	20	1.17	3500	6	8.93	8.67	80.15	80.40	29.18	30.33
8	30	1.17	3500	6	10.63	10.58	80.99	82.37	24.87	24.14
9	20	0.58	1500	8	3.89	3.96	72.62	72.34	50.00	51.53
10	30	0.58	1500	8	5.00	5.28	86.21	85.11	41.72	40.28
11	20	1.17	1500	8	9.42	9.50	79.20	79.85	26.79	26.81
12	30	1.17	1500	8	12.64	12.42	82.64	84.54	20.64	22.28
13	20	0.58	3500	8	2.99	2.99	79.25	77.45	63.68	63.73
14	30	0.58	3500	8	3.00	2.85	84.08	84.95	48.40	50.76
15	20	1.17	3500	8	8.34	7.91	84.85	85.04	32.50	32.71
16	30	1.17	3500	8	9.12	9.37	86.42	84.47	26.73	26.46
17	15	0.88	2500	7	5.16	5.37	72.42	72.77	44.25	44.25
18	35	0.88	2500	7	8.86	8.61	88.11	87.50	27.30	26.82
19	25	0.29	2500	7	0.85	0.57	61.26	62.69	80.00	79.31
20	25	1.47	2500	7	13.00	13.24	75.00	73.32	25.06	25.26
21	25	0.88	500	7	8.59	8.30	85.31	83.26	27.30	27.37
22	25	0.88	4500	7	5.24	5.50	82.41	84.21	43.50	42.95
23	25	0.88	2500	5	6.68	6.57	86.77	85.63	34.68	35.99
24	25	0.88	2500	9	6.34	6.42	90.99	91.88	36.67	34.87
25	25	0.88	2500	7	6.80	6.90	85.95	85.29	35.16	34.63
26	25	0.88	2500	7	6.98	6.90	84.72	85.29	34.22	34.63
27	25	0.88	2500	7	7.24	6.90	85.00	85.29	32.91	34.63
28	25	0.88	2500	7	6.89	6.90	83.91	85.29	34.68	34.63
29	25	0.88	2500	7	6.80	6.90	85.73	85.29	35.16	34.63
30	25	0.88	2500	7	6.72	6.90	86.43	85.29	35.65	34.63

A = Temperature, B = Feed Pressure, C = Feed Concentration, D = pH; Exp. = Experimental, Pred. = Predicted

Table 4.4. Experimental inputs and responses of NF100 membrane.

Run	A	B	C	D	Recovery (%)		Rejection (%)		SEC (kWh/m^3)	
					Exp.	Pred.	Exp.	Pred.	Exp.	Pred.
1	1500	6	20	0.49	4.31	4.40	76.62	75.11	39.11	38.89
2	3500	6	20	0.49	2.99	2.75	65.00	64.81	58.67	58.30
3	1500	8	20	0.49	4.31	4.08	72.06	71.52	40.33	40.39
4	3500	8	20	0.49	2.10	2.25	64.81	64.73	60.00	60.18
5	1500	6	30	0.49	5.59	5.75	75.05	74.50	30.63	30.64
6	3500	6	30	0.49	3.26	3.43	65.60	65.16	51.01	51.13
7	1500	8	30	0.49	5.28	5.48	74.71	74.84	31.03	32.03
8	3500	8	30	0.49	3.05	2.99	69.11	69.02	53.33	52.89
9	1500	6	20	0.88	10.71	10.99	70.64	70.00	20.70	20.33
10	3500	6	20	0.88	9.01	8.72	68.45	68.82	25.93	24.80
11	1500	8	20	0.88	11.03	10.77	67.25	68.19	21.29	21.06
12	3500	8	20	0.88	8.26	8.32	70.71	70.52	26.74	25.91
13	1500	6	30	0.88	13.32	13.07	70.00	70.59	15.62	15.33
14	3500	6	30	0.88	9.69	10.13	70.58	70.38	21.75	20.87
15	1500	8	30	0.88	12.44	12.89	73.26	72.72	16.40	15.95
16	3500	8	30	0.88	9.96	9.78	74.00	76.02	21.75	21.86
17	500	7	25	0.69	9.47	9.31	75.25	76.19	21.04	20.82
18	4500	7	25	0.69	4.51	4.54	69.91	69.19	45.00	46.15
19	2500	5	25	0.69	7.05	6.92	71.84	73.01	27.40	28.50
20	2500	9	25	0.69	6.25	6.25	76.00	75.06	31.17	31.00
21	2500	7	15	0.69	5.50	5.78	69.00	69.81	30.00	30.98
22	2500	7	35	0.69	9.00	8.59	75.27	74.69	18.75	18.69
23	2500	7	25	0.29	1.62	1.56	60.29	61.82	70.00	69.36
24	2500	7	25	1.08	15.00	14.94	65.00	63.70	18.21	19.78
25	2500	7	25	0.69	7.26	7.12	73.14	72.43	27.30	27.79
26	2500	7	25	0.69	6.98	7.12	72.66	72.43	27.70	27.79
27	2500	7	25	0.69	7.16	7.12	72.96	72.43	27.70	27.79
28	2500	7	25	0.69	6.69	7.12	70.96	72.43	28.99	27.79
29	2500	7	25	0.69	7.26	7.12	71.74	72.43	27.30	27.79
30	2500	7	25	0.69	7.36	7.12	73.14	72.43	27.70	27.79

A = Feed Concentration, B = pH, C = Temperature, D = Feed Pressure; Exp. = Experimental, Pred. = Predicted

Table 4.5. Experimental inputs and responses of NF250 membrane.

Run	A	B	C	D	Recovery (%)		Rejection (%)		SEC (kWh/m^3)	
					Exp.	Pred.	Exp.	Pred.	Exp.	Pred.
1	1500	6	20	0.49	6.05	6.21	67.68	67.02	25.00	25.39
2	3500	6	20	0.49	4.95	5.34	46.02	44.66	36.67	36.38
3	1500	8	20	0.49	7.11	7.27	69.20	68.15	23.01	23.57
4	3500	8	20	0.49	4.52	4.82	46.09	46.64	35.00	35.50
5	1500	6	30	0.49	8.82	8.86	67.36	65.16	17.62	17.86
6	3500	6	30	0.49	6.20	7.31	41.78	41.75	28.14	28.40
7	1500	8	30	0.49	8.99	9.27	67.96	65.56	16.84	17.34
8	3500	8	30	0.49	6.52	6.14	42.61	42.99	28.14	28.81
9	1500	6	20	1.08	14.00	14.14	73.12	71.16	14.07	13.54
10	3500	6	20	1.08	13.79	13.42	51.01	52.89	17.42	17.61
11	1500	8	20	1.08	16.99	15.80	71.81	71.32	12.33	12.76
12	3500	8	20	1.08	13.79	13.52	53.28	53.89	17.88	17.77
13	1500	6	30	1.08	18.34	17.95	71.43	70.37	9.79	9.98
14	3500	6	30	1.08	16.94	16.55	51.58	51.05	14.02	13.59
15	1500	8	30	1.08	19.58	18.96	70.02	69.79	10.07	10.49
16	3500	8	30	1.08	16.25	15.99	51.17	51.31	14.74	15.04
17	500	7	25	0.78	13.79	14.34	75.00	78.97	10.00	9.32
18	4500	7	25	0.78	10.71	10.49	40.00	38.13	25.00	24.86
19	2500	5	25	0.78	10.56	10.06	53.73	55.64	21.04	21.45
20	2500	9	25	0.78	9.73	10.56	56.86	57.04	22.32	21.09
21	2500	7	15	0.78	9.69	9.87	62.01	62.20	21.75	21.59
22	2500	7	35	0.78	14.85	14.99	55.87	57.77	12.00	11.34
23	2500	7	25	0.20	2.54	1.35	50.00	52.32	40.00	38.99
24	2500	7	25	1.37	17.61	19.12	65.00	64.78	13.19	13.37
25	2500	7	25	0.78	12.68	11.93	58.47	58.94	17.11	17.45
26	2500	7	25	0.78	11.53	11.93	60.38	58.94	16.89	17.45
27	2500	7	25	0.78	12.53	11.93	57.66	58.94	17.34	17.45
28	2500	7	25	0.78	11.20	11.93	59.83	58.94	17.95	17.45
29	2500	7	25	0.78	11.41	11.93	59.49	58.94	17.58	17.45
30	2500	7	25	0.78	12.23	11.93	57.82	58.94	17.82	17.45

A = Feed Concentration, B = pH, C = Temperature, D = Feed Pressure; Exp. = Experimental, Pred. = Predicted

Table 4.6. Experimental inputs and responses of NF400 membrane.

Run	A	B	C	D	Recovery (%)		Rejection (%)		SEC (kWh/m^3)	
					Exp.	Pred.	Exp.	Pred.	Exp.	Pred.
1	1500	6	20	0.39	6.56	7.02	57.25	55.74	23.68	23.18
2	3500	6	20	0.39	5.20	5.67	38.04	38.61	31.29	29.80
3	1500	8	20	0.39	8.33	8.00	52.82	53.46	20.95	21.27
4	3500	8	20	0.39	5.93	5.77	37.32	38.40	27.94	28.73
5	1500	6	30	0.39	9.50	9.18	50.10	50.00	16.76	17.08
6	3500	6	30	0.39	8.05	7.89	35.13	35.07	21.73	22.45
7	1500	8	30	0.39	9.26	8.83	49.70	48.85	17.25	17.78
8	3500	8	30	0.39	6.52	6.66	35.01	35.99	25.23	23.98
9	1500	6	20	0.59	11.63	11.93	57.89	56.68	15.32	15.92
10	3500	6	20	0.59	10.15	10.19	42.11	42.48	18.91	18.81
11	1500	8	20	0.59	13.54	13.32	56.35	55.93	14.93	14.64
12	3500	8	20	0.59	9.96	10.71	43.94	43.80	19.33	18.36
13	1500	6	30	0.59	15.13	14.91	52.69	51.13	12.34	11.98
14	3500	6	30	0.59	12.47	13.23	40.00	39.13	14.58	13.62
15	1500	8	30	0.59	15.00	14.97	52.32	51.52	12.47	13.31
16	3500	8	30	0.59	13.25	12.41	40.56	41.59	14.84	15.77
17	500	7	25	0.49	10.10	10.51	62.00	64.55	16.07	15.24
18	4500	7	25	0.49	7.07	6.60	39.32	37.48	23.27	24.32
19	2500	5	25	0.49	10.58	9.95	44.27	46.11	17.04	17.81
20	2500	9	25	0.49	9.54	10.11	47.40	46.28	18.62	18.06
21	2500	7	15	0.49	9.46	8.83	49.15	49.10	21.73	22.43
22	2500	7	35	0.49	12.11	12.70	40.39	41.15	14.24	13.75
23	2500	7	25	0.29	5.29	5.48	39.72	38.99	28.42	28.59
24	2500	7	25	0.69	16.39	16.14	44.08	45.52	13.10	13.13
25	2500	7	25	0.49	9.93	10.22	45.67	45.58	17.79	17.11
26	2500	7	25	0.49	10.58	10.22	45.96	45.58	16.58	17.11
27	2500	7	25	0.49	9.57	10.22	44.70	45.58	18.06	17.11
28	2500	7	25	0.49	10.97	10.22	48.19	45.58	15.92	17.11
29	2500	7	25	0.49	9.95	10.22	45.30	45.58	17.29	17.11
30	2500	7	25	0.49	10.32	10.22	43.68	45.58	17.04	17.11

A = Feed Concentration, B = pH, C = Temperature, D = Feed Pressure; Exp. = Experimental, Pred. = Predicted

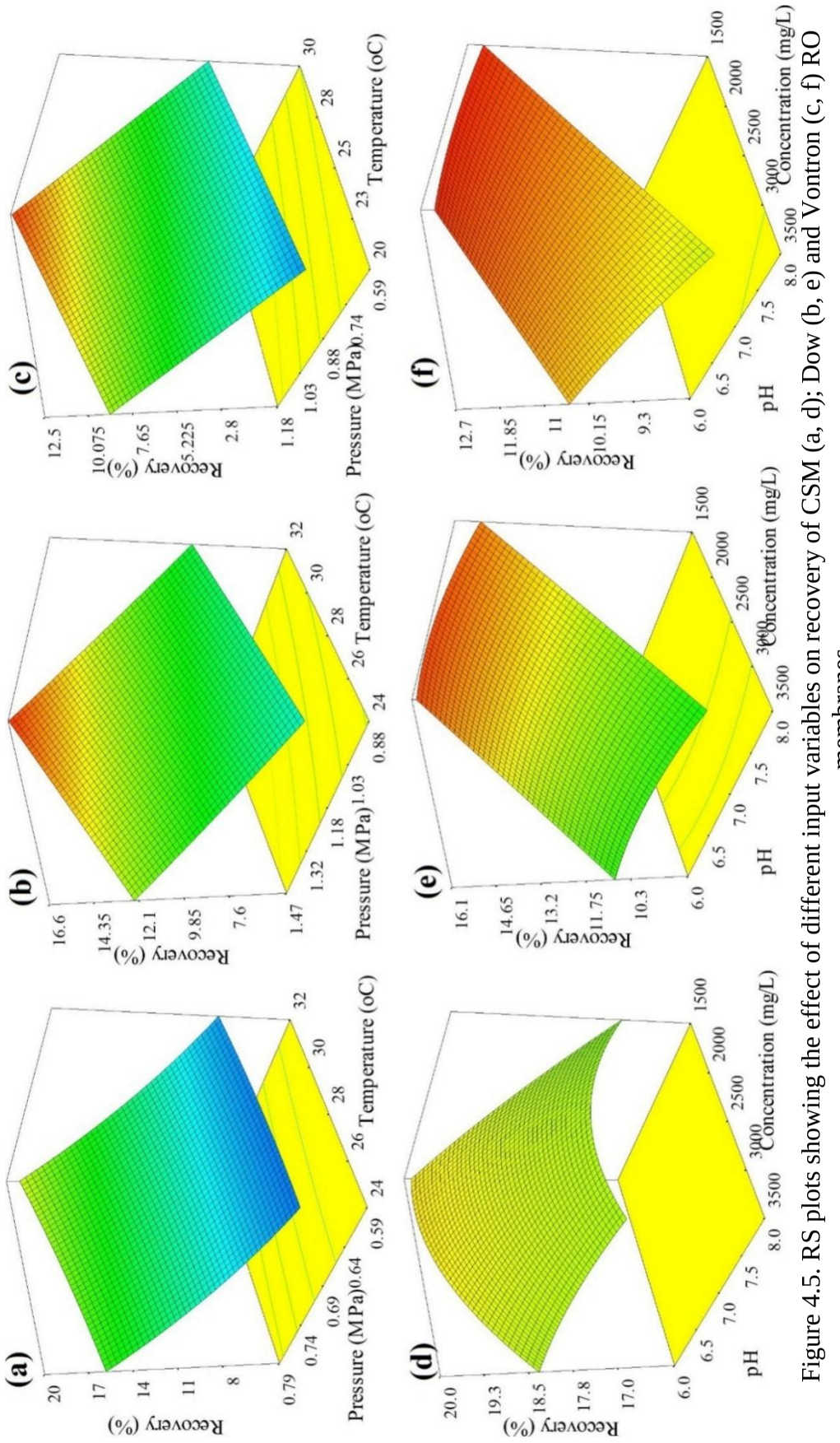

Figure 4.5. RS plots showing the effect of different input variables on recovery of CSM (a, d); Dow (b, e) and Vontron (c, f) RO membranes.

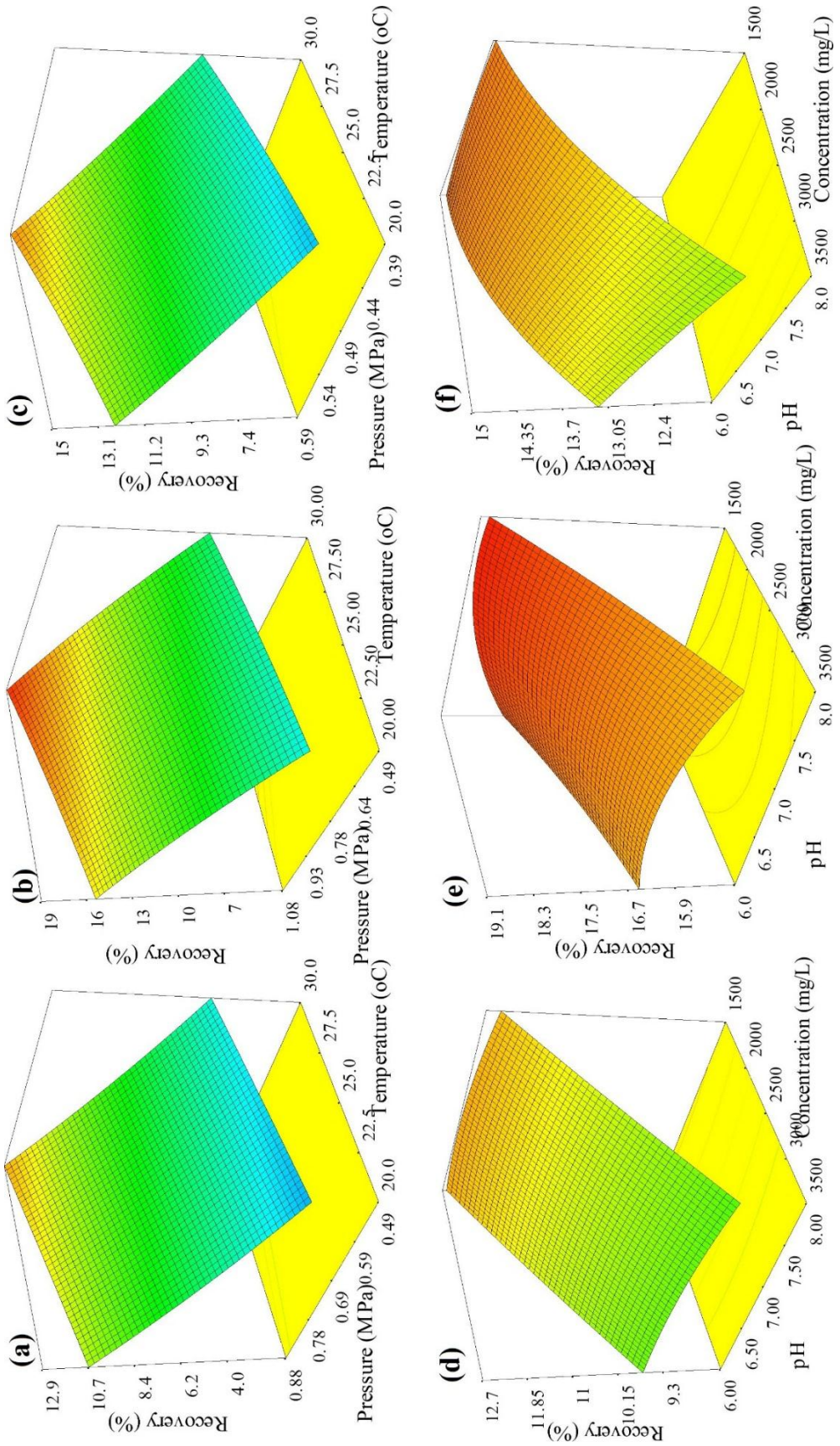

Figure 4.6. RS plots showing the effect of different input variables on recovery of NF100 (a, d); NF250 (b, e) and NF400 (c, f) membranes.

Table 4.7. ANOVA for RS quadratic model for water recovery of CSM RO membrane.

Source	Sum of Squares	DF	Mean Square	F Value	P > F	Remark
Model	553.6266	14	39.5447	26.4869	< 0.0001	Highly significant
A-Temperature	21.8967	1	21.8967	14.6663	0.0016	Significant
B-Pressure	473.8165	1	473.8160	317.360	< 0.0001	Highly significant
C-Concentration	1.2437	1	1.2437	0.8330	0.3758	
D-pH	5.4001	1	5.4001	3.6170	0.0766	
AB	5.3258	1	5.3258	3.5672	0.0784	
AC	0.7320	1	0.7320	0.4903	0.4945	
AD	1.4862	1	1.4862	0.9955	0.3342	
BC	0.2359	1	0.2359	0.1580	0.6965	
BD	4.9032	1	4.9032	3.2841	0.0900	
CD	6.0003	1	6.0003	4.0190	0.0634	
A^2	1.1146	1	1.1146	0.7465	0.4012	
B^2	18.8555	1	18.8555	12.6293	0.0029	Significant
C^2	7.8595	1	7.8595	5.2643	0.0366	Significant
D^2	0.4662	1	0.4662	0.3122	0.5845	
Residual	22.3948	15	1.4929			
Lack of Fit	17.6326	10	1.7632	1.851309	0.2576	Not significant
Pure Error	4.7622	5	0.9524			
Cor Total	576.0214	29				

DF: Degree of freedom

Table 4.8. ANOVA for RS quadratic model for water recovery of Dow RO membrane.

Source	Sum of Squares	DF	Mean Square	F Value	P > F	Remark
Model	296.9527	14	21.2109	24.0834	< 0.0001	Highly significant
A-Temperature	23.6483	1	23.6483	26.8510	0.0001	Significant
B-Pressure	181.578	1	181.578	206.1691	< 0.0001	Highly significant
C-Concentration	75.0153	1	75.0153	85.1746	< 0.0001	Highly significant
D-pH	2.7489	1	2.7489	3.1212	0.0976	
AB	4.8037	1	4.8037	5.4543	0.0338	Significant
AC	4.1106	1	4.1106	4.6673	0.0473	Significant
AD	0.0001	1	0.0001	0.0001	0.9914	
BC	1.1581	1	1.1581	1.3149	0.2695	
BD	0.0792	1	0.0792	0.0900	0.7682	
CD	0.0229	1	0.0229	0.0260	0.8740	
A^2	0.0101	1	0.0101	0.0115	0.9158	
B^2	0.2059	1	0.2059	0.2338	0.6356	
C^2	0.0055	1	0.0055	0.0062	0.9378	
D^2	3.1560	1	3.1560	3.5834	0.0778	
Residual	13.2108	15	0.8807			
Lack of Fit	11.8829	10	1.1882	4.4741	0.0560	Not significant
Pure Error	1.3278	5	0.2655			
Cor Total	310.1635	29				

DF: Degree of freedom

Table 4.9. ANOVA for RS quadratic model for water recovery of Vontron RO membrane.

Source	Sum of Squares	DF	Mean Square	F Value	P > F	Remark
Model	275.6002	14	19.6857	212.8065	< 0.0001	Highly significant
A-Temperature	15.7686	1	15.7686	170.4618	< 0.0001	Highly significant
B-Pressure	240.5521	1	240.5521	2600.414	< 0.0001	Highly significant
C-Concentration	11.8145	1	11.8145	127.7176	< 0.0001	Highly significant
D-pH	0.0333	1	0.0333	0.3608	0.5570	
AB	2.5290	1	2.5290	27.3390	0.0001	Significant
AC	2.1370	1	2.1370	23.1015	0.0002	Significant
AD	0.2087	1	0.2087	2.2570	0.1538	
BC	0.3874	1	0.3874	4.1888	0.0586	Significant
BD	0.3628	1	0.3628	3.9226	0.0663	
CD	1.4775	1	1.4775	15.9726	0.0012	Significant
A^2	0.0129	1	0.0129	0.1400	0.7135	
B^2	7.91E-06	1	7.91E-06	8.55E-05	0.9927	
C^2	6.07E-05	1	6.07E-05	0.0006	0.9799	
D^2	0.2870	1	0.2870	3.1032	0.0985	
Residual	1.3875	15	0.092505			
Lack of Fit	1.2166	10	0.1216	3.5595	0.0869	Not significant
Pure Error	0.1709	5	0.0341			
Cor Total	276.9878	29				

DF: Degree of freedom

Table 4.10. ANOVA for RS quadratic model for water recovery of NF100 membrane.

Source	Sum of Squares	DF	Mean Square	F Value	P > F	Remark
Model	319.8451	14	22.8461	217.9386	< 0.0001	Highly significant
A-Concentration	34.0740	1	34.0740	325.0470	< 0.0001	Highly significant
B-pH	0.6834	1	0.6834	6.5190	0.0221	Significant
C-Temperature	11.8532	1	11.8532	113.0728	< 0.0001	Highly significant
D-Pressure	268.6720	1	268.6720	2562.9784	< 0.0001	Highly significant
AB	0.0304	1	0.0304	0.2904	0.5979	
AC	0.4438	1	0.4438	4.2336	0.0575	
AD	0.3881	1	0.3881	3.7023	0.0735	
BC	0.0022	1	0.0022	0.0214	0.8858	
BD	0.0087	1	0.0087	0.0829	0.7774	
CD	0.5310	1	0.5310	5.0653	0.0398	Significant
A^2	0.0635	1	0.0635	0.6061	0.4484	
B^2	0.4863	1	0.4863	4.6388	0.0479	Significant
C^2	0.0083	1	0.0083	0.0791	0.7824	
D^2	2.1875	1	2.1875	20.8672	0.0004	Significant
Residual	1.5724	15	0.1048			
Lack of Fit	1.2652	10	0.1265	2.0594	0.2201	Not significant
Pure Error	0.3072	5	0.0614			
Cor Total	321.4175	29				

DF: Degree of freedom

Table 4.11. ANOVA for RS quadratic model for water recovery of NF250 membrane.

Source	Sum of Squares	DF	Mean Square	F Value	P > F	Remark
Model	551.9345	14	39.4239	53.0952	< 0.0001	Highly significant
A-Concentration	22.1497	1	22.1497	29.8306	< 0.0001	Highly significant
B-pH	0.3724	1	0.3724	0.5015	0.4897	
C-Temperature	39.4248	1	39.4248	53.0963	< 0.0001	Highly significant
D-Pressure	474.0229	1	474.0229	638.4028	< 0.0001	Highly significant
AB	2.4561	1	2.4561	3.3078	0.0890	
AC	0.4667	1	0.4667	0.6286	0.4402	
AD	0.0255	1	0.0255	0.0344	0.8553	
BC	0.4228	1	0.4228	0.5695	0.4622	
BD	0.3681	1	0.3681	0.4957	0.4922	
CD	1.3408	1	1.3408	1.8058	0.1990	
A^2	0.4044	1	0.4044	0.5447	0.4719	
B^2	4.5107	1	4.5107	6.0749	0.0263	Significant
C^2	0.4289	1	0.4289	0.5776	0.4590	
D^2	4.9160	1	4.9160	6.6208	0.0212	Significant
Residual	11.1377	15	0.7425			
Lack of Fit	9.1748	10	0.9175	2.3371	0.1806	Not significant
Pure Error	1.9629	5	0.3926			
Cor Total	563.0722	29				

DF: Degree of freedom

Table 4.12. ANOVA for RS quadratic model for water recovery of NF400 membrane.

Source	Sum of Squares	DF	Mean Square	F Value	P > F	Remark
Model	226.2665	14	16.1619	39.3726	< 0.0001	Highly significant
A-Concentration	22.9497	1	22.9497	55.9087	< 0.0001	Highly significant
B-pH	0.0397	1	0.0397	0.0968	0.7600	
C-Temperature	22.4050	1	22.4050	54.5816	< 0.0001	Highly significant
D-Pressure	170.5646	1	170.5646	415.5193	< 0.0001	Highly significant
AB	0.7711	1	0.7711	1.8785	0.1907	
AC	0.0035	1	0.0035	0.0084	0.9281	
AD	0.1457	1	0.1457	0.3551	0.5601	
BC	1.7722	1	1.7722	4.3174	0.0553	
BD	0.1705	1	0.1705	0.4153	0.5290	
CD	0.6645	1	0.6645	1.6187	0.2226	
A^2	4.7406	1	4.7406	11.5487	0.0040	Significant
B^2	0.0611	1	0.0611	0.1489	0.7050	
C^2	0.5020	1	0.5020	1.2231	0.2862	
D^2	0.5967	1	0.5967	1.4538	0.2466	
Residual	6.1573	15	0.4105			
Lack of Fit	4.8665	10	0.4866	1.8851	0.2509	Not significant
Pure Error	1.2908	5	0.2582			
Cor Total	232.4238	29				

DF: Degree of freedom

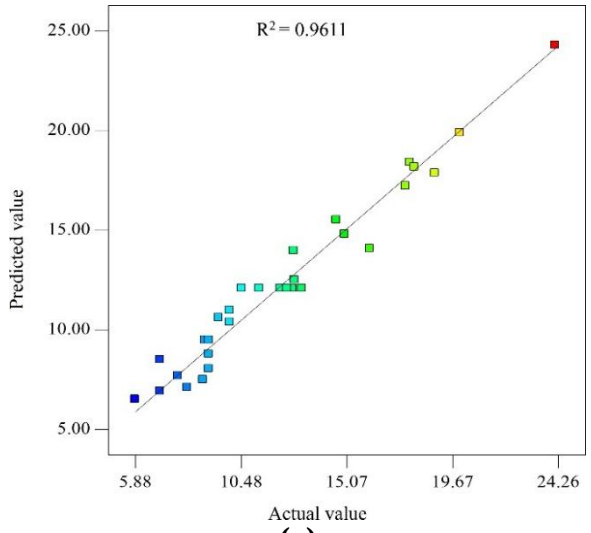

(a)

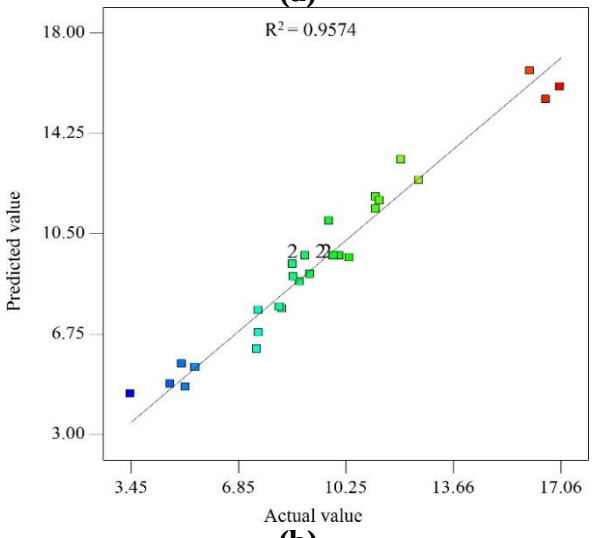

(b)

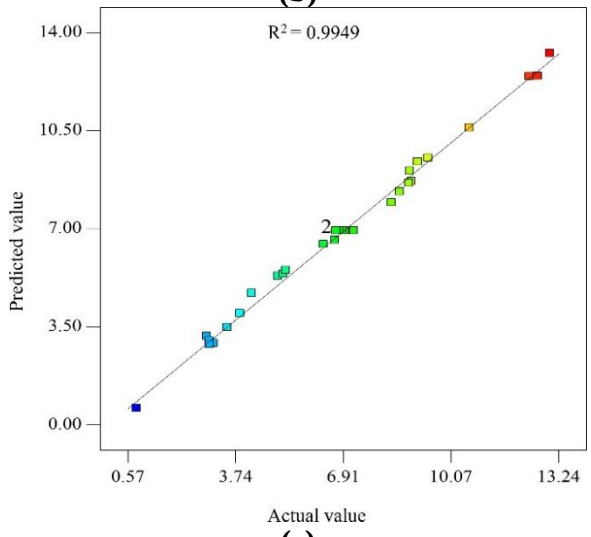

(c)

Figure 4.7. Correlation of actual and predicted values of water recovery for (a) CSM, (b) Dow and (c) Vontron RO membranes.

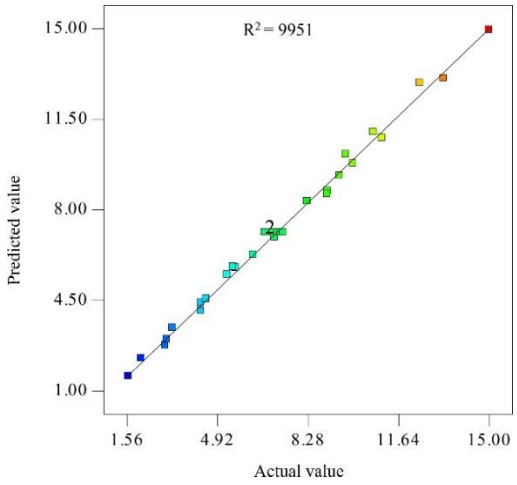

(a)

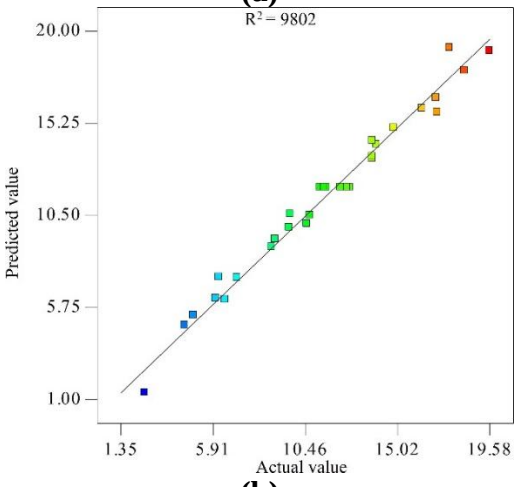

(b)

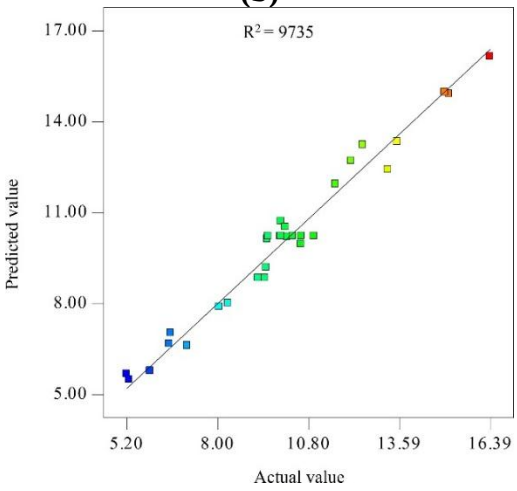

(c)

Figure 4.8. Correlation of actual and predicted values of water recovery for (a) NF100, (b) NF250and (c) NF400 NF membranes.

4.3.2 Optimization of Salt Rejection

4.3.2.1 Effect of Process Parameters on Salt Rejection

Three dimensional comparative RS plots for salt rejection as a function of different input variables are depicted in Figure 4.9 and Figure 4.10. At high and low values of temperature, salt rejection does not show any significant change with pressure for either CSM or Dow membranes (Figure 4.9a to b). However, it increased at low value of pressure (0.59 MPa) with temperature ranging from 20^{o}C to 30^{o}C for Vontron membrane (Figure 4.9c). This is because higher diffusion rate of solute through the membrane is possible as the solubility increases with temperature [26, 93].

Similarly, at high and low value of temperature, salt rejection increased with the pressure for Vontron membrane (from 0.59 MPa to 1.03 MPa) (Figure 4.9c) and NF100 membrane (from 0.49 to 0.78 MPa). However, from 0.78 MPa to 0.88 MPa salt rejection stabilizes for NF100 membrane (Figure 4.10a). Similar trend occurred with NF250 membrane (Figure 4.10b). At low and high value of temperature, salt rejection increased with pressure from 0.49 to 1.08 MPa because the rejection increases with increasing operating pressure, partly due to higher formation of concentration polarization at the membrane interface [248, 261]. However, at high and low values of temperature, effect of pressure on salt rejection is not significant for NF400 membrane (Figure 4.10c).

At high and low value of pH, salt rejection decreased with feed water concentration ranging from 1500 mg/l to 3500 mg/l for all three RO membranes, NF250 and NF400 membranes (Figure 4.9d to f and Figure 4.10e to f). This is because at high feed salinity, salt passage increases [37]. However, at high and low values of pH, the salt rejection does not show any significant changes with feed water concentration for NF100 membrane (Figure 4.10d).

This analysis shows that salt rejection in small scale RO and NF plants would be better at low feed concentration, low pH and high pressure. CSM (89.2%) and vontron (89.66%) among RO membranes and NF250 (70.64%) among NF membranes show the best performance for salt rejection (Table 4.25).

4.3.2.2 Statistical Analysis and Fitting of Second-Order Polynomial Equation

ANOVA results for salt rejection of RO and NF membranes are given in Table 4.13 to Table 4.18. Based on ANOVA analysis, all the factors followed second-order effects, yielding a quadratic model for salt rejection of different RO and NF membranes.

RO Membranes

In Table 4.13, Table 4.14 and Table 4.15 ANOVA result show F-values of 13.14, 7.16 and 34.17 for salt rejection of CSM, Dow and Vontron RO membranes respectively, implying that the quadratic model is significant. The large P values (> 0.05) for lack of fit showed that the F-statistic are insignificant for all RO membranes, implying significant model correlation between the variables and process responses.

For the CSM RO membrane, ANOVA response for salt rejection obtained from the response surface quadratic model (Table 4.13) shows that the model term C is highly significant, whereas B, D, AD, B^2 and D^2 are significant terms. Note that R^2 value is about 0.9246, being close to unity, which represents an excellent fit (Figure 4.11a). Through multiple regression analysis on the experimental data, predicted response for the salt rejection of CSM RO membranes could be expressed by the following second-order polynomial equation in term of coded values:

$$\text{Salt rejection}_{csm} = 89.90 - 0.53(A) - 1.28(B) - 3.07(C) + 0.79(D) - 0.29(AB) - 0.14(AC) + 0.69(AD) - 0.63(BC) + 0.11(BD) + 0.15(CD) - 0.51(A2) - 0.74(B2) - 0.38(C2) - 0.73(D2) \quad (4.7)$$

where, A is the temperature (^oC) pH, B is the pressure (MPa), C is the concentration (mg/l) and D is the pH.

For the Dow RO membrane, ANOVA response for salt rejection obtained from the response surface quadratic model (Table 4.14) shows that model terms B, C are highly significant, whereas D, C^2 and D^2 are significant terms. A high R^2 coefficient (close to unity) (Figure 4.11b) confirms a satisfactory fit of the quadratic model to the experimental data. The quadratic equation in terms of the coded factors for response on "salt rejection" of Dow membrane is given as follows:

$$\text{Salt rejection}_{\text{Dow}} = 80.91 + 0.022(A) - 3.54(B) - 2.86(C) + 1.63(D) + 0.077(AB) + 0.67(AC) - 0.51(AD) - 0.35(BC) + 0.19(BD) + 1.01(CD) + 0.74(A^2) - 0.18(B^2) + 1.04(C^2) + 1.11(D^2) \quad (4.8)$$

For the Vontron RO membrane, ANOVA response for salt rejection obtained from the response surface quadratic model (Table 4.15) shows that the model terms A, B, B^2 are highly significant, whereas D, AB, AC, BD, CD, A^2 and D^2 are significant terms. The R^2 value of 0.9696 (close to unity) confirms a satisfactory fit of the quadratic model to the experimental data (Figure 4.11c). The quadratic equation in terms of the coded factors for response on "salt rejection" of Vontron membrane is given as follows:

$$\text{Salt rejection}_{\text{Vontron}} = 85.29 + 3.68(A) + 2.66(B) + 0.24(C) + 1.56(D) - 2.02(AB) - 1.31(AC) - 0.64(AD) + 0.023(BC) - 0.90(BD) + 1.02(CD) - 1.29(A^2) - 4.32(B^2) - 0.39(C^2) + 0.87(D^2) \quad (4.9)$$

NF Membranes

ANOVA results for salt rejection of NF100, NF250 and NF400 membranes given in Table 4.16, Table 4.17 and Table 4.18 show F-value of 20.34, 48.31 and 34.98 respectively, implying that the quadratic model is significant. Further, data given in these tables demonstrate that all the models are significant at the 5% confidence level since P-values are less than 0.05.

For the NF100 membrane, ANOVA response for salt rejection obtained from the response surface quadratic model (Table 4.16) shows that the model terms A, AD, D^2 are highly significant, whereas C, AB and BC are significant terms. The closer the R^2 value to unity represents a satisfactory fit of the regression model for salt rejeciton of NF100 membrane (Figure 4.12a). The final empirical model formulated in terms of the coded factors for response on "salt rejection" of NF100 membrane is stated by following equation:

$$\text{Salt rejection}_{\text{NF100}} = 72.43 - 1.75(A) + 0.51(B) + 1.22(C) + 0.47(D) + 0.88(AB) + 0.24(AC) + 2.28(AD) + 0.98(BC) + 0.45(BD) + 0.30(CD) + 0.064(A^2) + 0.40(B^2) - 0.047(C^2) - 2.42(D^2) \quad (4.10)$$

where, A is the concentration (mg/l), B is the pH, C is the temperature (^oC) and D is the pressure (MPa). Positive sign before the terms indicates synergistic effect, whereas antagonistic effect is indicated by negative sign before the terms.

For the NF250 membrane, ANOVA response for salt rejection obtained from the response surface quadratic model (Table 4.17) shows that the model terms A, D are highly significant, whereas C is significant terms. Note that R^2 value is about 0.9783, being close to unity, represents a good fit of the regression model for salt rejection of NF250 membrane (Figure 4.12b). The quadratic equation in terms of coded factors for response on "salt rejection" of NF250 membrane is given as follows:

$$\text{Salt rejection}_{NF250} = 58.94 - 10.21(A) + 0.35(B) - 1.11(C) + 3.11(D) + 0.21(AB) - 0.26(AC) + 1.02(AD) - 0.18(BC) - 0.24(BD) + 0.27(CD) - 0.098(A^2) - 0.65(B^2) + 0.26(C^2) - 0.098(D^2) \quad (4.11)$$

Table 4.8 shows that the model terms A, C are highly significant, whereas D and A^2 are significant terms. A high R^2 value (0.9703) reflects the good fit of the regression model for salt rejection of NF400 membrane (Figure 4.12c). The quadratic equation in terms of the coded factors for response on "salt rejection" of NF400 membrane is given as follows:

$$\text{Salt rejection}_{NF400} = 45.58 - 6.77(A) + 0.044(B) - 1.99(C) + 1.63(D) + 0.52(AB) + 0.55(AC) + 0.73(AD) + 0.28(BC) + 0.38(BD) + 0.047(CD) + 1.36(A^2) + 0.15(B^2) - 0.11(C^2) - 0.83(D^2) \quad (4.12)$$

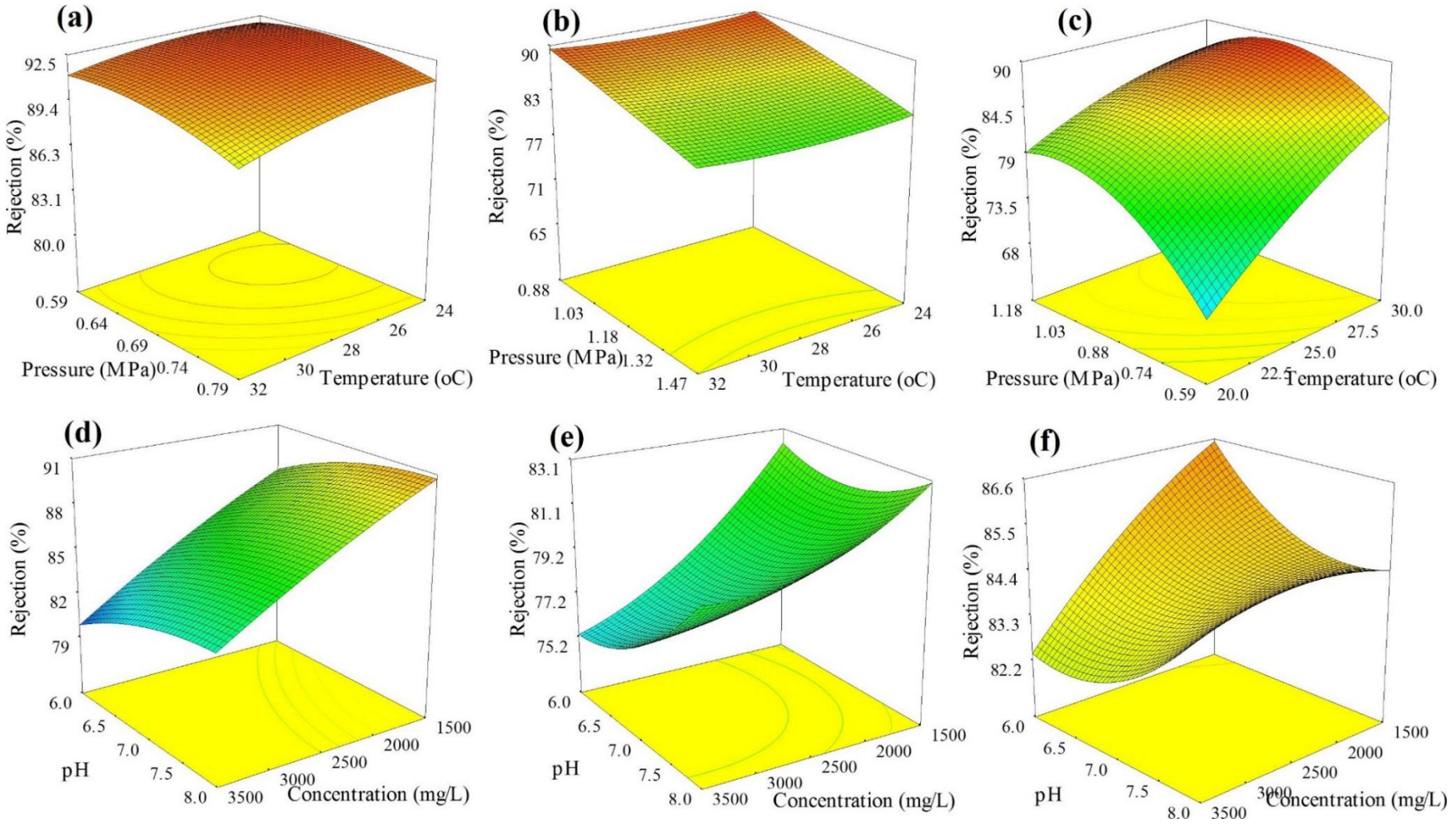

Figure 4.9. RS plots showing the effect of different input variables on salt rejection of CSM (a, d); Dow (b, e) and Vontron (c, f) RO membranes.

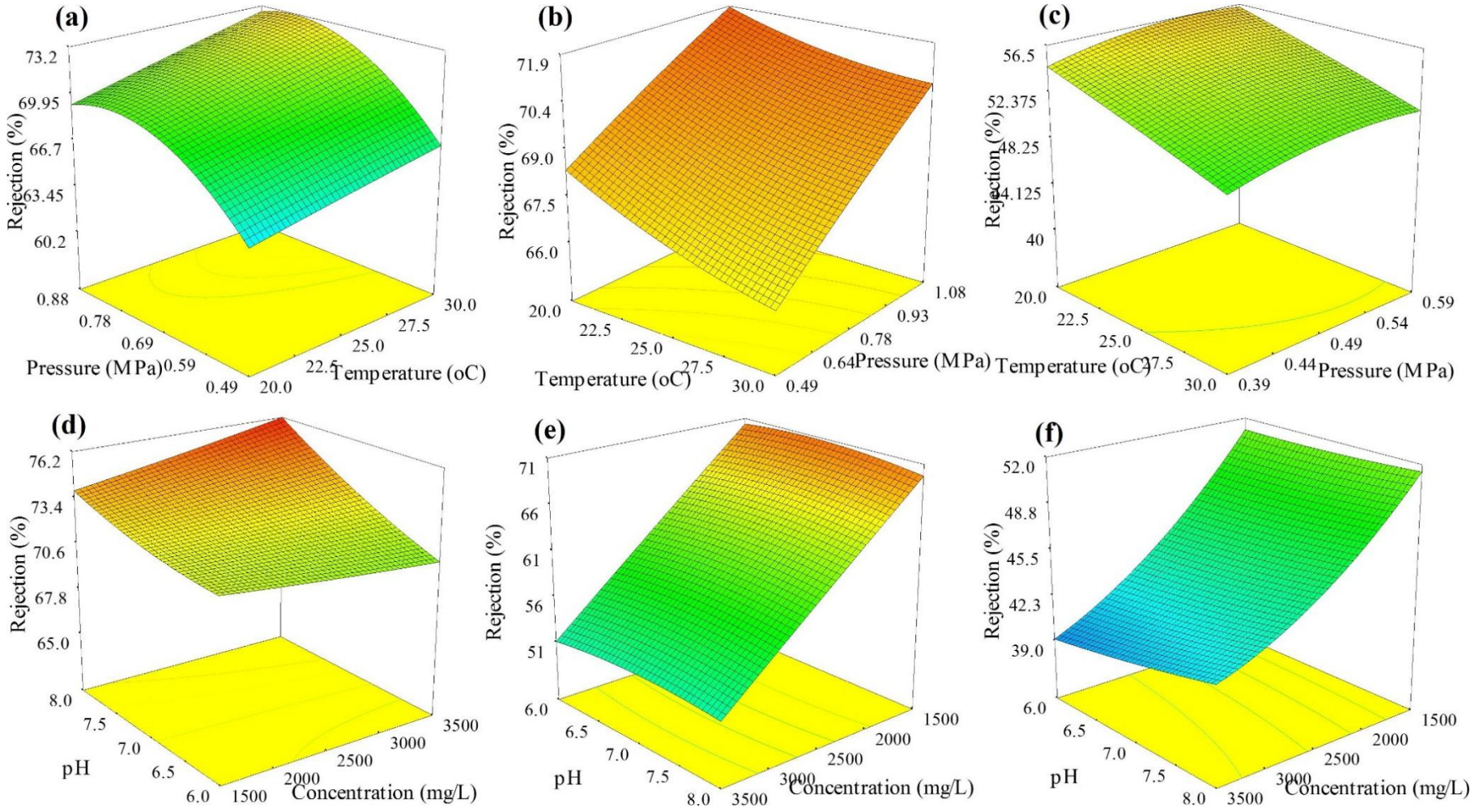

Figure 4.10. RS plots showing the effect of different input variables on salt rejection of NF100 (a, d); NF250 (b, e) and NF400 (c, f) membranes.

Table 4.13. ANOVA for RS quadratic model for salt rejection of CSM RO membrane.

Source	Sum of Squares	DF	Mean Square	F Value	P > F	
Model	333.2824	14	23.8058	13.1467	< 0.0001	Highly significant
A-Temperature	6.7890	1	6.7890	3.7492	0.0719	
B-Pressure	39.4060	1	39.4060	21.7618	0.0003	Significant
C-Concentration	226.1904	1	226.1904	124.9128	< 0.0001	Highly significant
D-pH	15.1108	1	15.1108	8.3448	0.0112	Significant
AB	1.3098	1	1.3098	0.7233	0.4084	
AC	0.3338	1	0.3338	0.1843	0.6737	
AD	7.5219	1	7.5219	4.1539	0.0596	Significant
BC	6.3922	1	6.3922	3.5300	0.0798	
BD	0.1885	1	0.1885	0.1041	0.7514	
CD	0.3774	1	0.3774	0.2084	0.6545	
A^2	7.2725	1	7.2725	4.0162	0.0635	
B^2	14.9837	1	14.9837	8.2746	0.0115	Significant
C^2	3.8928	1	3.8928	2.1498	0.1632	
D^2	14.5359	1	14.5359	8.0274	0.0126	Significant
Residual	27.1617	15	1.8107			
Lack of Fit	18.9688	10	1.8968	1.1576	0.4628	Not significant
Pure Error	8.1929	5	1.6385			
Cor Total	360.4442	29				

DF: Degree of freedom

Table 4.14. ANOVA for RS quadratic model for salt rejection of Dow RO membrane.

Source	Sum of Squares	DF	Mean Square	F Value	P > F	
Model	659.8309	14	47.1307	7.1681	0.0003	Significant
A-Temperature	0.0111	1	0.0111	0.0016	0.9677	
B-Pressure	300.1831	1	300.1831	45.6551	< 0.0001	Highly significant
C-Concentration	196.6018	1	196.6018	29.9013	< 0.0001	Highly significant
D-pH	63.7694	1	63.7694	9.6987	0.0071	Significant
AB	0.0939	1	0.0939	0.0142	0.9064	
AC	7.1221	1	7.1221	1.0832	0.3145	
AD	4.2146	1	4.2146	0.6410	0.4358	
BC	1.9471	1	1.9471	0.2961	0.5943	
BD	0.5736	1	0.5736	0.0872	0.7718	
CD	16.4817	1	16.4817	2.5067	0.1342	
A^2	15.1794	1	15.1794	2.3086	0.1494	
B^2	0.8908	1	0.8908	0.1354	0.7180	
C^2	29.4346	1	29.4346	4.4767	0.0515	Significant
D^2	33.5800	1	33.5800	5.1072	0.0391	Significant
Residual	98.6251	15	6.5750			
Lack of Fit	63.9939	10	6.3993	0.9239	0.5740	Not significant
Pure Error	34.6311	5	6.926236			
Cor Total	758.456	29				

DF: Degree of freedom

Table 4.15. ANOVA for RS quadratic model for salt rejection of Vontron RO membrane.

Source	Sum of Squares	DF	Mean Square	F Value	P > F	
Model	1279.251	14	91.37509	34.17517	< 0.0001	Highly significant
A-Temperature	325.6021	1	325.6021	121.7784	< 0.0001	Highly significant
B-Pressure	169.3597	1	169.3597	63.34217	< 0.0001	Highly significant
C-Concentration	1.333458	1	1.333458	0.498726	0.4909	
D-pH	58.48193	1	58.48193	21.87281	0.0003	Significant
AB	65.19805	1	65.19805	24.3847	0.0002	Significant
AC	27.66428	1	27.66428	10.34671	0.0058	Significant
AD	6.453872	1	6.453872	2.413811	0.1411	
BC	0.008369	1	0.008369	0.00313	0.9561	
BD	12.97519	1	12.97519	4.852849	0.0437	Significant
CD	16.80406	1	16.80406	6.284881	0.0242	Significant
A^2	45.54172	1	45.54172	17.03305	0.0009	Significant
B^2	512.3103	1	512.3103	191.609	< 0.0001	Highly significant
C^2	4.150518	1	4.150518	1.552334	0.2319	
D^2	20.5844	1	20.5844	7.698765	0.0142	Significant
Residual	40.10591	15	2.673727			
Lack of Fit	35.87492	10	3.587492	4.239548	0.0622	Not significant
Pure Error	4.230985	5	0.846197			
Cor Total	1319.357	29				

DF: Degree of freedom

Table 4.16. ANOVA for RS quadratic model for salt rejection of NF100 membrane.

Source	Sum of Squares	DF	Mean Square	F Value	P > F	
Model	417.3784	14	29.8127	20.3468	< 0.0001	Highly significant
A-Concentration	73.5755	1	73.5755	50.2143	< 0.0001	Highly significant
B-pH	6.2929	1	6.2929	4.2948	0.0559	
C-Temperature	35.7819	1	35.7819	24.4207	0.0002	Significant
D-Pressure	5.3431	1	5.3431	3.6466	0.0755	
AB	12.3260	1	12.3260	8.4123	0.0110	Significant
AC	0.9424	1	0.9424	0.6432	0.4351	
AD	83.3104	1	83.3104	56.8582	< 0.0001	Highly significant
BC	15.4686	1	15.4686	10.5571	0.0054	Significant
BD	3.1734	1	3.1734	2.1658	0.1618	
CD	1.4539	1	1.4539	0.9923	0.3350	
A^2	0.1138	1	0.1138	0.0776	0.7843	
B^2	4.3957	1	4.3957	3.0000	0.1038	
C^2	0.0600	1	0.0600	0.0409	0.8424	
D^2	160.4464	1	160.4464	109.5025	< 0.0001	Highly significant
Residual	21.9785	15	1.4652			
Lack of Fit	18.0149	10	1.8015	2.2725	0.1889	Not significant
Pure Error	3.9636	5	0.7927			
Cor Total	439.3568	29				

DF: Degree of freedom

Table 4.17. ANOVA for RS quadratic model for salt rejection of NF250 membrane.

Source	Sum of Squares	DF	Mean Square	F Value	P > F	
Model	2802.9184	14	200.2085	48.3192	< 0.0001	Highly significant
A-Concentration	2501.4830	1	2501.4830	603.7186	< 0.0001	Highly significant
B-pH	2.9409	1	2.9409	0.7098	0.4128	
C-Temperature	29.4535	1	29.4535	7.1084	0.0176	Significant
D-Pressure	232.6702	1	232.6702	56.1536	< 0.0001	Highly significant
AB	0.7078	1	0.7078	0.1708	0.6852	
AC	1.1115	1	1.1115	0.2682	0.6121	
AD	16.7183	1	16.7183	4.0349	0.0629	
BC	0.5382	1	0.5382	0.1299	0.7236	
BD	0.9472	1	0.9472	0.2286	0.6395	
CD	1.1382	1	1.1382	0.2747	0.6079	
A^2	0.2630	1	0.2630	0.0635	0.8045	
B^2	11.5689	1	11.5689	2.7921	0.1155	
C^2	1.8766	1	1.8766	0.4529	0.5112	
D^2	0.2630	1	0.2630	0.0635	0.8045	
Residual	62.1519	15	4.1435			
Lack of Fit	55.8780	10	5.5878	4.4533	0.0565	Not significant
Pure Error	6.2738	5	1.2548			
Cor Total	2865.0702	29				

DF: Degree of freedom

Table 4.18. ANOVA for RS quadratic model for salt rejection of NF400 membrane.

Source	Sum of Squares	DF	Mean Square	F Value	P > F	
Model	1360.4031	14	97.1717	34.9805	< 0.0001	Highly significant
A-Concentration	1098.6400	1	1098.6400	395.4953	< 0.0001	Highly significant
B-pH	0.0466	1	0.0466	0.0168	0.8986	
C-Temperature	94.9501	1	94.9501	34.1807	< 0.0001	Highly significant
D-Pressure	64.0845	1	64.0845	23.0696	0.0002	Significant
AB	4.3010	1	4.3010	1.5483	0.2325	
AC	4.8218	1	4.8218	1.7358	0.2074	
AD	8.5619	1	8.5619	3.0822	0.0995	
BC	1.2863	1	1.2863	0.4631	0.5066	
BD	2.3549	1	2.3549	0.8477	0.3718	
CD	0.0358	1	0.0358	0.0129	0.9111	
A^2	50.6171	1	50.6171	18.2214	0.0007	Significant
B^2	0.6453	1	0.6453	0.2323	0.6368	
C^2	0.3561	1	0.3561	0.1282	0.7253	
D^2	18.9643	1	18.9643	6.8269	0.0196	
Residual	41.6683	15	2.7779			
Lack of Fit	30.2293	10	3.0229	1.3213	0.3997	Not significant
Pure Error	11.4390	5	2.2878			
Cor Total	1402.0714	29				

DF: Degree of freedom

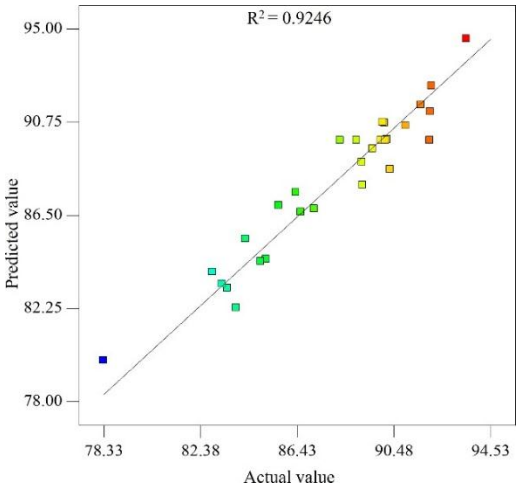

(a)

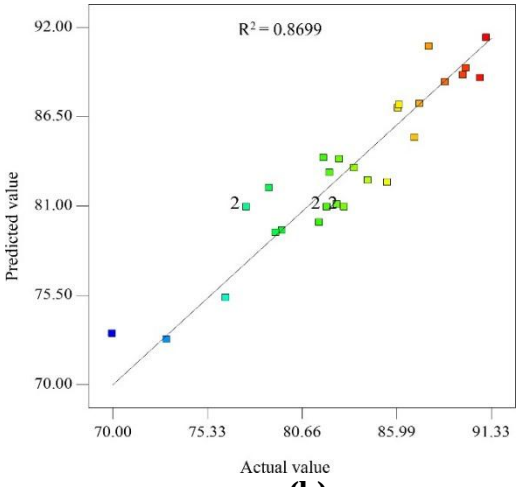

(b)

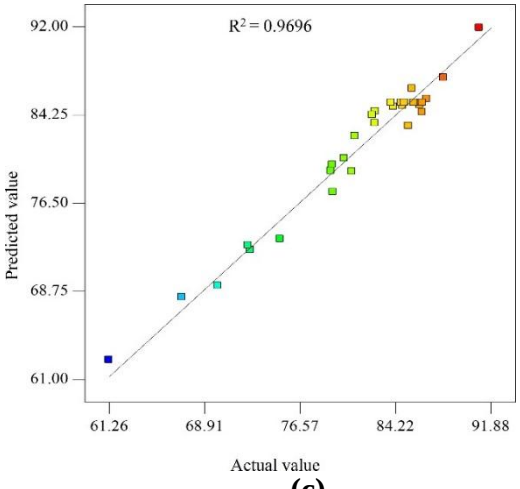

(c)

Figure 4.11. Correlation of actual and predicted values of rejection for (a) CSM, (b) Dow and (c) Vontron RO membranes.

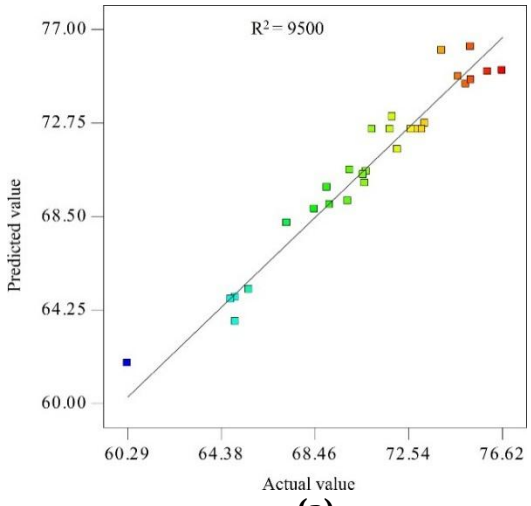

(a)

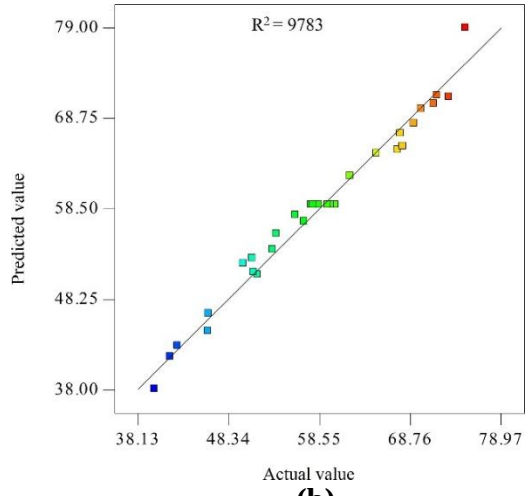

(b)

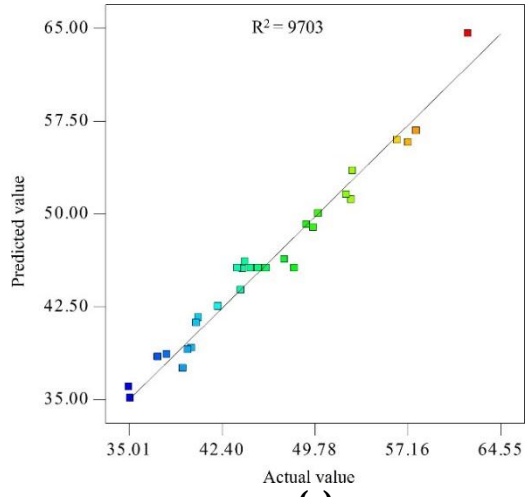

(c)

Figure 4.12. Correlation of actual and predicted values of rejection for (a) NF100, (b) NF250and (c) NF400 NF membranes.

4.3.3 Optimization of Specific Energy Comsumption

4.3.3.1 Effect of Process Parameters on Specific Energy Comsumption

The RS plots in Figure 4.13 and Figure 4.14 illustrate the effect of temperature, pressure, pH and concentration on SEC for all RO and NF membranes.

At low and high temperature of feed water, SEC decreased with increasing pressure from 0.59 MPa to 0.79 MPa for CSM membrane, from 0.88 MPa to 1.32 MPa for Dow membrane and from 0.59 MPa to 1.18 MPa for Vontron membrane (Figure 4.13a to c). Similar trend are observed with NF membranes (Figure 4.14a to c).

SEC decreased with increase in pressure from 0.49 MPa to 0.88 MPa for NF100 membrane, 0.49 MPa to 1.08 MPa for NF250 membrane and 0.39 MPa to 0.59 MPa for NF400 membrane. This is because the permeate flow rate and the recovery increases with applied pressure. Also, decrease in SEC compensates largely for the energy required to apply a higher desalination pressure [140].

At a low and high value of pH, SEC increased with concentration ranging from 1500 mg/l to 3500 mg/l for all RO and NF membranes (Figure 4.13d to f and Figure 4.14d to f). This trend was observed because the minimum value of required energy linearly increases as a function of the solution concentration [140].

It is considerable to note that high rejection of Vontron membrane as compared to the other membranes results in higher concentration polarization, higher osmotic pressure and consequently lower flux and directly impacts in higher SEC (Table 4.25) [204]. Based on this analysis, it may be predicted that small scale RO plants show a low SEC at higher pressure and lesser feed concentration.

4.3.3.2 Statistical Analysis and Fitting of Second-Order Polynomial Equation

ANOVA results for SEC of RO and NF membranes are given in Table 4.19 and Table 4.24. Based on ANOVA analysis, all the factors followed second-order effects, yielding a quadratic model for SEC of different RO and NF membranes.

RO Membranes

Table 4.19 and Table 4.20 and Table 4.21 ANOVA result showed F-values of 10.14, 132.56 and 215.77 for SEC of CSM, Dow and Vontron RO membranes respectively, implying that the quadratic model is significant. The large P values (> 0.05) for lack of fit showed that the F-statistic are insignificant for all RO membranes, implying significant model correlation between the variables and process responses. Table 4.19 shows that the model term B is highly significant, whereas C and D are significant terms. A high R^2 coefficient (close to unity) (Figure 4.15a) confirms a satisfactory fit of the quadratic model to the experimental data. Through multiple regression analysis on the experimental data, predicted response for the SEC of CSM RO membranes could be expressed by the following second-order polynomial equation in term of coded values:

$$SEC_{csm} = 26.15 - 1.95(A) - 4.28(B) + 2.21(C) + 1.20(D) - 0.21(AB) - 0.80(AC) - 0.15(AD) - 0.30(BC) + 0.98(BD) - 0.79(CD) - 0.089(A^2) + 0.69(B^2) - 0.43(C^2) + 0.62(D^2) \quad (4.13)$$

where A, B, C and D are the coded variables for temperature, pressure, concentration and pH, respectively. Table 4.20 shows that model terms A, B, C, D, BC, B^2, C^2, D^2 are highly significant, whereas A^2 is significant terms. Note that R^2 value is about 0.9919, being close to unity, represents an excellent fit of the regression model for SEC of Dow membrane (Figure 4.15b). The quadratic equation in terms of the coded factors for response on "SEC" of Dow membrane is given as follows:

$$SEC_{Dow} = 25.17 - 2.66(A) - 4.33(B) + 4.96(C) + 1.29(D) - 0.026(AB) - 1.663E - 004(AC) - 0.22(AD) - 1.58(BC) - 0.18(BD) - 0.13(CD) + 0.42(A^2) + 3.23(B^2) + 1.23(C^2) + 0.93(D^2) \quad (4.14)$$

For the Vontron RO membrane, ANOVA response for SEC obtained from the response surface quadratic model (Table 4.21) shows that the model terms A, B, C, B^2 are highly significant, whereas AB, BC and BD are significant terms. The R^2 value of 0.9950 (99.5%) represents an excellent fit of the regression model for SEC of Vontron membrane (Figure 4.15c).

The quadratic equation in terms of coded factors for response on "SEC" of Vontron membrane is given as follows:

$$SEC_{Vontron} = 34.63 - 4.36(A) - 13.51(B) + 3.90(C) - 0.28(D) + 1.68(AB) - 0.43(AC) - 0.016(AD) - 1.58(BC) + 1.26(BD) + 0.20(CD) + 0.23(A^2) + 4.41(B^2) + 0.13(C^2) + 0.20(D^2) \quad (4.15)$$

NF Membranes

ANOVA results for SEC of NF100, NF250 and NF400 membranes given in Table 4.22, Table 4.23 and Table 4.24 show F-value of 467.50, 258.68 and 43.18 respectively, implying that the quadratic model is significant. Further, data given in these tables demonstrates that all the models are significant at the 5% confidence level since P-values are less than 0.05.

For the NF100 membrane, ANOVA response for SEC obtained from the response surface quadratic model (Table 4.22) shows that the model terms A, C, D, AD, A^2, D^2 are highly significant, whereas B, CD, B^2 and C^2 are significant terms. The closeness of R^2 value to unity (0.9977) represents an excellent fit of the regression model for SEC of NF100 membrane (Figure 4.16a). The final empirical models formulated in terms of the coded factors for response on "SEC" of NF100 membrane is stated by following equation:

$$SEC_{NF100} = 27.79 + 6.33(A) + 0.62(B) - 3.07(C) - 12.40(D) + 0.092(AB) + 0.27(AC) - 3.73(AD) - 0.029(BC) - 0.19(BD) + 0.81(CD) + 1.42(A^2) + 0.49(B^2) - 0.74(C^2) + 4.20(D^2) \quad (4.16)$$

where, A is the concentration (mg/l), B is the pH, C is the temperature (^oC) and D is the pressure (MPa).

For the NF250 membrane, ANOVA response for SEC obtained from the response surface quadratic model (Table 4.23) shows that the model terms A, C, D, AD, CD, B^2 and D^2 are highly significant. R^2 value is about 0.9959, being close to unity, represents an excellent fit of the regression model for SEC of NF250 membrane (Figure 4.16b). The quadratic equation in terms of the coded factors for response on "SEC" of NF250 membrane is given as follows:

$$SEC_{NF250} = 17.45 + 3.89(A) - 0.09(B) - 2.56(C) - 6.41(D) + 0.24(AB) - 0.11(AC) - 1.73(AD) + 0.32(BC) + 0.26(BD) + 0.99(CD) - 0.09(A^2) + 0.95(B^2) - 0.25(C^2) + 2.18(D^2) \quad (4.17)$$

For the NF400 membrane, ANOVA response for SEC obtained from the response surface quadratic model (Table 4.24) shows the model terms A, C, D are highly significant, whereas AD, BC, A^2 and D^2 are significant terms. A high R^2 value (0.9758) reflects the goot fit of the regression model for SEC of NF400 membrane (Figure 4.16c). The quadratic equation in terms of the coded factors for SEC of NF400 membrane is given as follows:

$$SEC_{NF400} = 17.11 + 2.27(A) + 0.062(B) - 2.17(C) - 3.87(D) + 0.21(AB) - 0.31(AC) - 0.93(AD) + 0.65(BC) + 0.16(BD) + 0.54(CD) + 0.67(A^2) + 0.21(B^2) + 0.24(C^2) + 0.94(D^2) \quad (4.18)$$

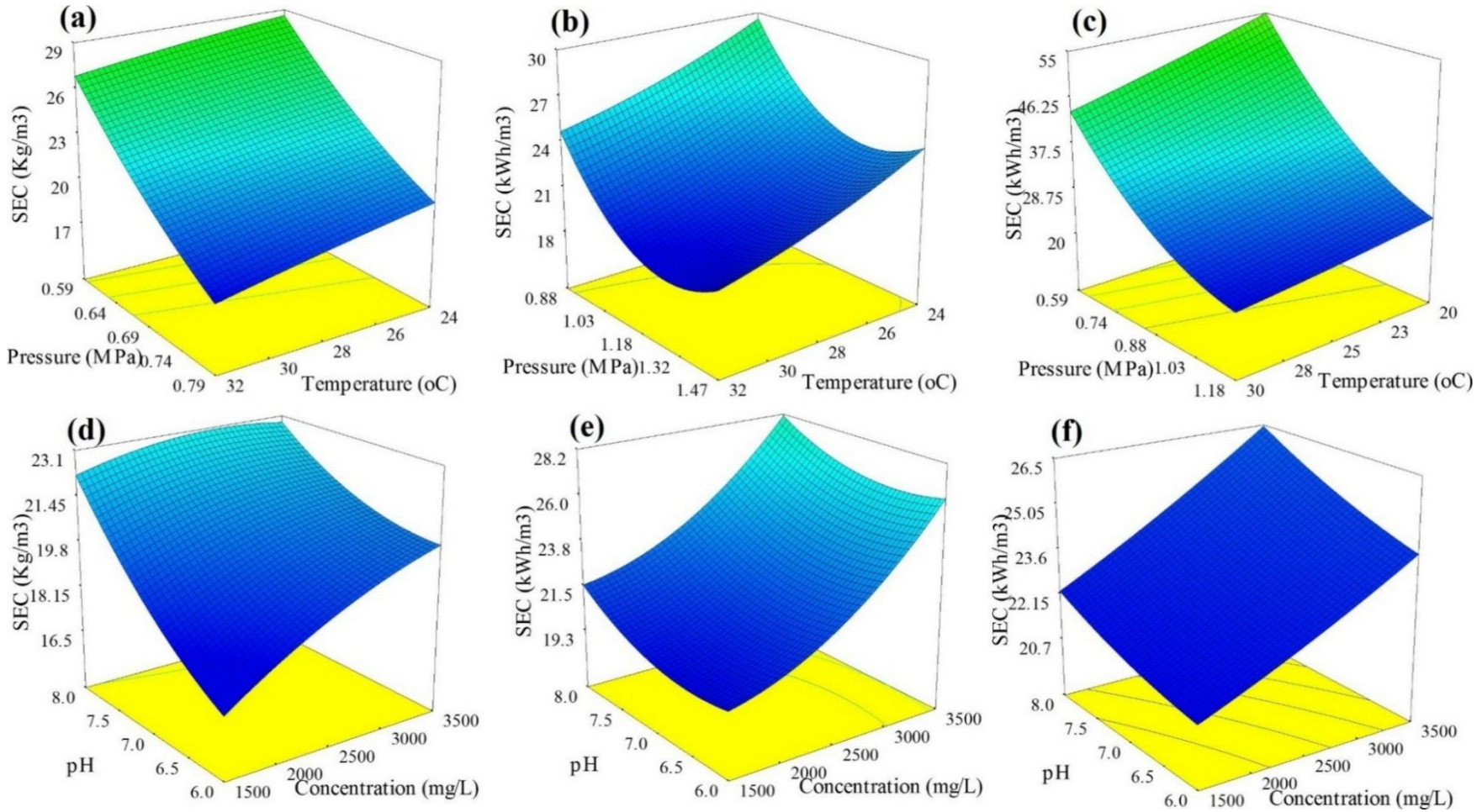

Figure 4.13. RS plots showing the effect of different input variables on SEC of CSM (a, d); Dow (b, e) and Vontron (c, f) RO membranes.

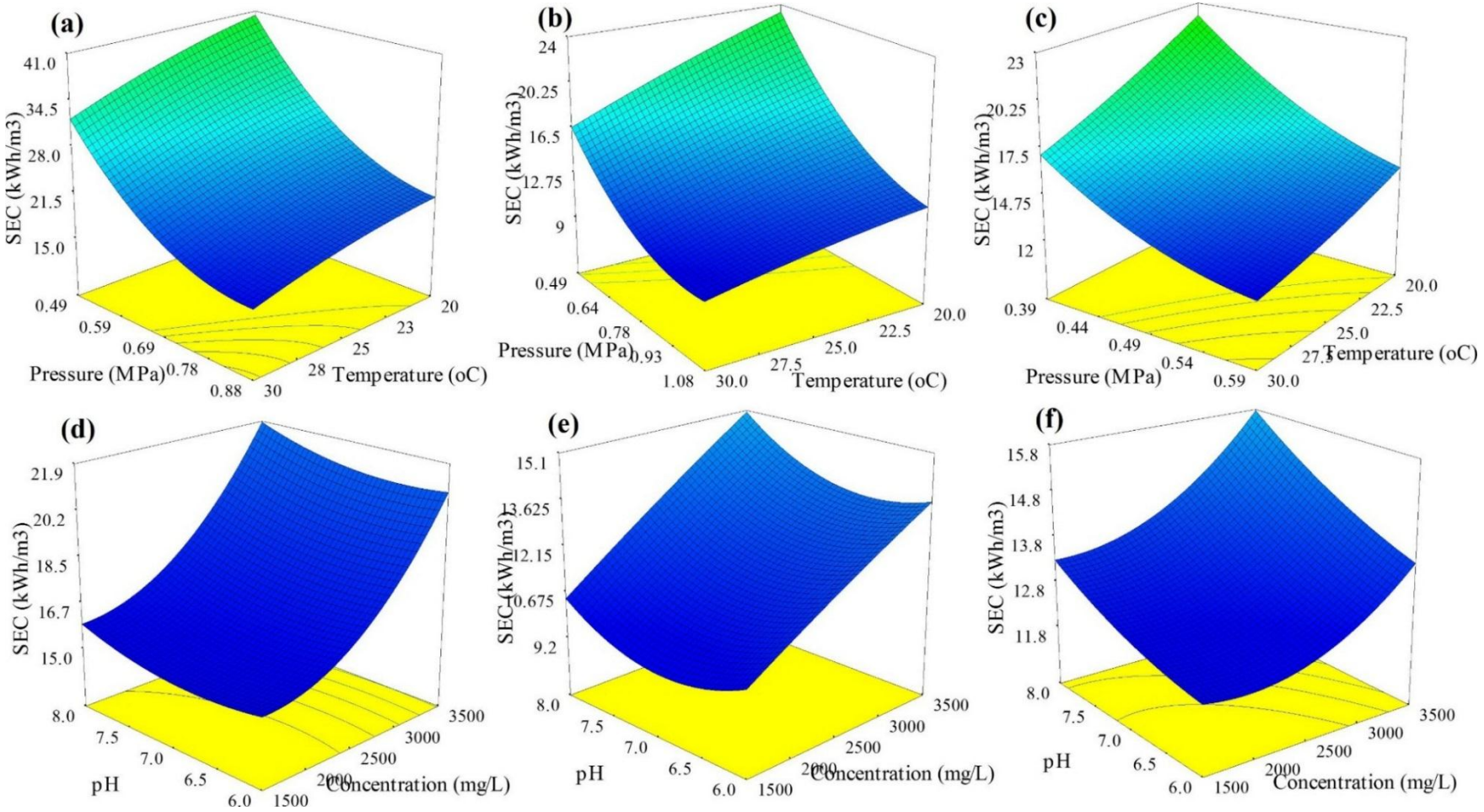

Figure 4.14. RS plots showing the effect of different input variables on SEC of NF100 (a, d); NF250 (b, e) and NF400 (c, f) membranes.

Table 4.19. ANOVA for RS quadratic model for SEC of CSM RO membrane.

Source	Sum of Squares	DF	Mean Square	F Value	P > F	
Model	751.8794	14	53.7056	10.1417	< 0.0001	Highly significant
A-Temperature	91.5481	1	91.5481	17.2879	0.0008	Significant
B-Pressure	439.0508	1	439.0508	82.9101	< 0.0001	Highly significant
C-Concentration	116.9991	1	116.9991	22.0940	0.0003	Significant
D-pH	34.4239	1	34.4239	6.5005	0.0222	Significant
AB	0.6900	1	0.6900	0.1303	0.7231	
AC	10.3155	1	10.3155	1.9479	0.1831	
AD	0.3460	1	0.3460	0.0653	0.8017	
BC	1.4169	1	1.4169	0.2675	0.6125	
BD	15.4554	1	15.4554	2.9185	0.1082	
CD	10.0416	1	10.0416	1.8962	0.1887	
A^2	0.2195	1	0.2195	0.0414	0.8414	
B^2	12.8991	1	12.8991	2.4358	0.1394	
C^2	5.0589	1	5.0589	0.9553	0.3439	
D^2	10.6071	1	10.6071	2.0030	0.1774	
Residual	79.4325	15	5.2955			
Lack of Fit	42.7727	10	4.2772	0.5833	0.7811	Not significant
Pure Error	36.6597	5	7.3319			
Cor Total	831.3119	29				

DF: Degree of freedom

Table 4.20. ANOVA for RS quadratic model for SEC of Dow RO membrane.

Source	Sum of Squares	DF	Mean Square	F Value	P > F	
Model	1598.153	14	114.1538	132.5644	< 0.0001	Highly significant
A-Temperature	169.285	1	169.285	196.5872	< 0.0001	Highly significant
B-Pressure	449.8844	1	449.8844	522.4415	< 0.0001	Highly significant
C-Concentration	590.7954	1	590.7954	686.0786	< 0.0001	Highly significant
D-pH	39.9412	1	39.9412	46.383	< 0.0001	Highly significant
AB	0.0104	1	0.0104	0.0121	0.9136	
AC	4.42E-07	1	4.42E-07	5.14E-07	0.9994	
AD	0.7668	1	0.7668	0.8904	0.3603	
BC	39.9026	1	39.9026	46.3380	< 0.0001	Highly significant
BD	0.5145	1	0.5145	0.5974	0.4515	
CD	0.2733	1	0.2733	0.3174	0.5815	
A^2	4.8208	1	4.8208	5.5984	0.0319	Significant
B^2	285.466	1	285.466	331.5059	< 0.0001	Highly significant
C^2	41.1781	1	41.1781	47.8193	< 0.0001	Highly significant
D^2	23.8653	1	23.8653	27.7143	< 0.0001	Highly significant
Residual	12.9167	15	0.8611			
Lack of Fit	11.3289	10	1.1328	3.5674	0.0865	Not significant
Pure Error	1.5878	5	0.3175			
Cor Total	1611.069	29				

DF: Degree of freedom

Table 4.21. ANOVA for RS quadratic model for SEC of Vontron RO membrane.

Source	Sum of Squares	DF	Mean Square	F Value	P > F	
Model	5865.027	14	418.9305	215.7788	< 0.0001	Highly significant
A-Temperature	455.95	1	455.95	234.8464	< 0.0001	Highly significant
B-Pressure	4381.738	1	4381.738	2256.905	< 0.0001	Highly significant
C-Concentration	364.1115	1	364.1115	187.5431	< 0.0001	Highly significant
D-pH	1.8902	1	1.8902	0.9735	0.3394	
AB	45.1195	1	45.1195	23.2397	0.0002	Significant
AC	2.9890	1	2.9890	1.5395	0.2337	
AD	0.0040	1	0.0040	0.0021	0.9640	
BC	39.7101	1	39.7101	20.4535	0.0004	Significant
BD	25.2821	1	25.2821	13.0220	0.0026	Significant
CD	0.6477	1	0.6477	0.3336	0.5721	
A^2	1.3980	1	1.3980	0.7201	0.4094	
B^2	534.156	1	534.156	275.1281	< 0.0001	Highly significant
C^2	0.4780	1	0.4780	0.2462	0.6269	
D^2	1.0967	1	1.0967	0.5648	0.4639	
Residual	29.1222	15	1.9414			
Lack of Fit	24.3826	10	2.4382	2.5722	0.1544	Not significant
Pure Error	4.7395	5	0.9479			
Cor Total	5894.149	29				

DF: Degree of freedom

Table 4.22. ANOVA for RS quadratic model for SEC of NF100 membrane.

Source	Sum of Squares	DF	Mean Square	F Value	P > F	
Model	5683.3812	14	405.9558	467.5015	< 0.0001	Highly significant
A-Concentration	962.5627	1	962.5627	1108.4938	< 0.0001	Highly significant
B-pH	9.3497	1	9.3497	10.7671	0.0050	Significant
C-Temperature	226.5701	1	226.5701	260.9197	< 0.0001	Highly significant
D-Pressure	3688.1955	1	3688.1955	4247.3514	< 0.0001	Highly significant
AB	0.1369	1	0.1369	0.1576	0.6970	
AC	1.1440	1	1.1440	1.3174	0.2690	
AD	223.1640	1	223.1640	256.9972	< 0.0001	Highly significant
BC	0.0138	1	0.0138	0.0159	0.9015	
BD	0.5965	1	0.5965	0.6869	0.4202	
CD	10.5221	1	10.5221	12.1173	0.0034	Significant
A^2	55.6704	1	55.6704	64.1104	< 0.0001	Highly significant
B^2	6.6022	1	6.6022	7.6032	0.0147	Significant
C^2	14.8889	1	14.8889	17.1461	0.0009	Significant
D^2	483.0489	1	483.0489	556.2824	< 0.0001	Highly significant
Residual	13.0253	15	0.8684			
Lack of Fit	11.0871	10	1.1087	2.8602	0.1288	Not significant
Pure Error	1.9381	5	0.3876			
Cor Total	5696.4065	29				

DF: Degree of freedom

Table 4.23. ANOVA for RS quadratic model for SEC of NF250 membrane.

Source	Sum of Squares	DF	Mean Square	F Value	P > F	
Model	1731.0939	14	123.6496	258.6836	< 0.0001	Highly significant
A-Concentration	362.4231	1	362.4231	758.2148	< 0.0001	Highly significant
B-pH	0.1965	1	0.1965	0.4111	0.5311	
C-Temperature	157.6000	1	157.6000	329.7104	< 0.0001	Highly significant
D-Pressure	984.5779	1	984.5779	2059.8067	< 0.0001	Highly significant
AB	0.8844	1	0.8844	1.8501	0.1939	
AC	0.2108	1	0.2108	0.4409	0.5167	
AD	47.9211	1	47.9211	100.2543	< 0.0001	Highly significant
BC	1.6664	1	1.6664	3.4863	0.0815	
BD	1.0784	1	1.0784	2.2560	0.1539	
CD	15.7319	1	15.7319	32.9122	< 0.0001	Highly significant
A^2	0.2214	1	0.2214	0.4632	0.5065	
B^2	25.0046	1	25.0046	52.3115	< 0.0001	Highly significant
C^2	1.6588	1	1.6588	3.4702	0.0822	
D^2	130.7761	1	130.7761	273.5928	< 0.0001	Highly significant
Residual	7.1699	15	0.4780			
Lack of Fit	6.3198	10	0.6320	3.7172	0.0801	Not significant
Pure Error	0.8501	5	0.1700			
Cor Total	1738.2639	29				

DF: Degree of freedom

Table 4.24. ANOVA for RS quadratic model for SEC of NF400 membrane.

Source	Sum of Squares	DF	Mean Square	F Value	P > F	
Model	655.8965	14	46.8497	43.1846	< 0.0001	Highly significant
A-Concentration	123.8942	1	123.8942	114.2018	< 0.0001	Highly significant
B-pH	0.0916	1	0.0916	0.0844	0.7754	
C-Temperature	113.1669	1	113.1669	104.3137	< 0.0001	Highly significant
D-Pressure	358.5660	1	358.5660	330.5150	< 0.0001	Highly significant
AB	0.6941	1	0.6941	0.6398	0.4363	
AC	1.5772	1	1.5772	1.4538	0.2466	
AD	13.9445	1	13.9445	12.8536	0.0027	Significant
BC	6.7943	1	6.7943	6.2628	0.0244	Significant
BD	0.3914	1	0.3914	0.3608	0.5571	
CD	4.6561	1	4.6561	4.2919	0.0560	
A^2	12.1879	1	12.1879	11.2344	0.0044	Significant
B^2	1.1641	1	1.1641	1.0731	0.3167	
C^2	1.6366	1	1.6366	1.5086	0.2383	
D^2	24.1225	1	24.1225	22.2354	0.0003	Significant
Residual	16.2731	15	1.0849			
Lack of Fit	13.1682	10	1.3168	2.1206	0.2104	Not significant
Pure Error	3.1048	5	0.6210			
Cor Total	672.1695	29				

DF: Degree of freedom

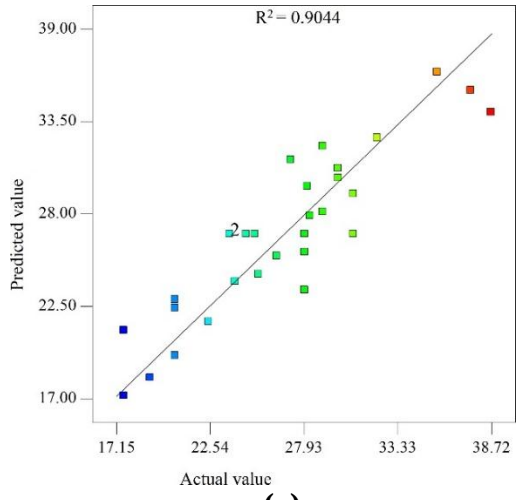

(a)

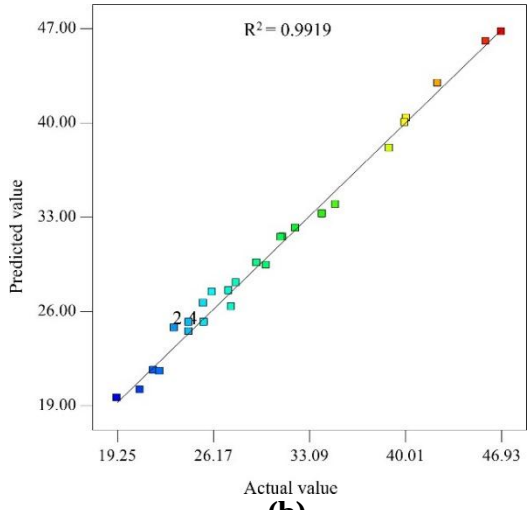

(b)

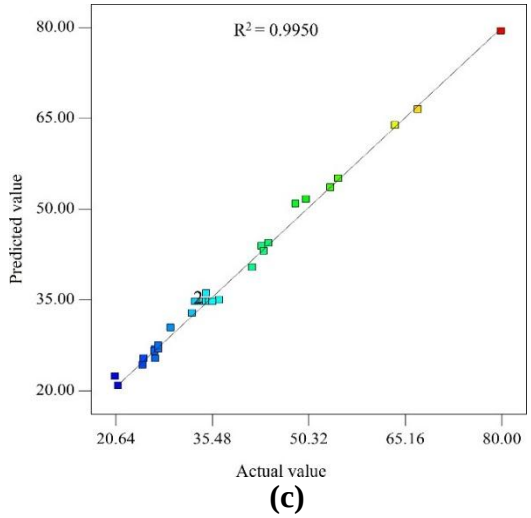

(c)

Figure 4.15. Correlation of actual and predicted values of SEC for (a) CSM, (b) Dow and (c) Vontron RO membranes.

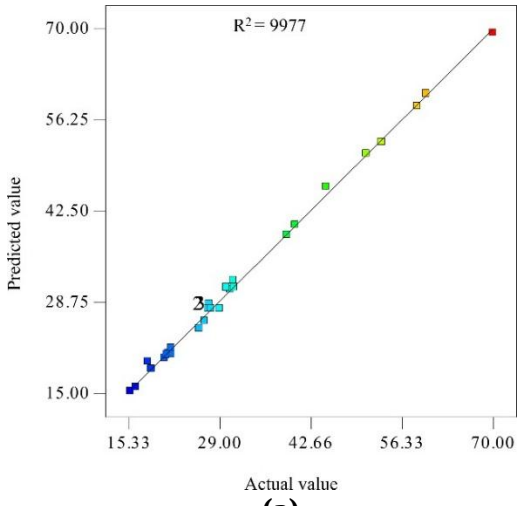

(a)

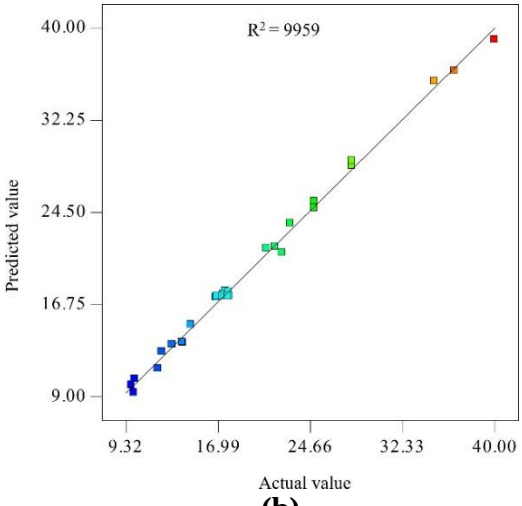

(b)

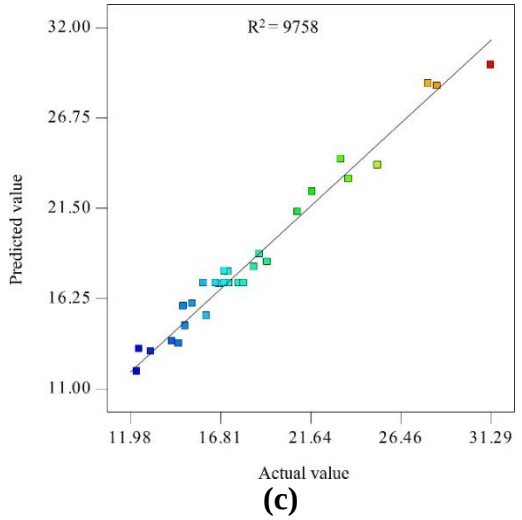

(c)

Figure 4.16. Correlation of actual and predicted values of SEC for (a) NF100, (b) NF250and (c) NF400 NF membranes.

4.4 Multiple Response Optimization

Membrane optimization was carried out by the RSM through regression analysis to achieve maximum recovery, highest salt rejection and lowest SEC. The optimized values of input parameters is presented in Table 4.25.

Table 4.25. Multiple response optimization and experimental validation of RSM/ ANN predictions.

Parameters	**RO membrane**			**NF membrane**		
	CSM	**Dow**	**Vontron**	**NF100**	**NF250**	**NF400**
Optimized input parameters						
Temperature (^oC)	31.92	32	30	30	30	29.58
Pressure (MPa)	0.79	1.43	1.178	0.86	1.08	0.59
Conc. (mg/L)	1500	1500	1500.8	1500.1	1505	1501.1
pH	6.53	6.14	6.73	8	7.15	6
RSM predictions						
Recovery (%)	19.25	16.1	12.75	12.35	18.98	14.76
Rejection (%)	89.2	82.53	89.66	73.43	70.64	51.38
SEC (KWh/m3)	17.6	18.99	19.02	13.22	9.35	12.11
ANN predictions						
Recovery (%)	19.51	16.16	12.48	12.28	18.59	14.86
Rejection (%)	88.92	82.95	88.44	73.12	71.4	51.46
SEC (KWh/m3)	16.60	18.8	18.79	13.39	9.43	11.63
Validation experiment at optimized conditions						
Recovery (%)	19.69	16.87	13.54	12.16	18.37	15.3
Rejection (%)	89.98	83.64	90.77	74.72	71.04	53.74
SEC (KWh/m3)	16.53	20.2	20.12	13.16	9.07	11.56

Model predictions validated by confirmation runs at these optimal process conditions are in agreement with the predicted responses. Less than 6% error for each response showed the reliability of CCD optimization process. These results demonstrate an improvement in the

performance of individual RO and NF membranes employing optimized input parameters (Table 4.25).

It can be predicted by the above analysis that CSM membrane (among RO membranes) showed the best performance at 31.92^{o}C temperature, 0.79 MPa pressure, 1500 mg/l feed salt concentration and 6.53 pH (very near to the actual i.e. 6.7) with 19.25% water recovery, 89.2% salt rejection and 17.6 kWh/m^3 of SEC (Table 4.25). Also, NF250 showed the best performance (among NF membranes) at 30^{o}C temperature, 1.08 MPa pressure, 1500 mg/l feed salt concentration and pH 7.15 with 18.98% water recovery, 70.64% salt rejection and 9.35 kWh/m^3 of SEC (Figure 4.17).

Removal efficiency of major ions of validation experiments was studied (Figure 4.18). For divalent ions (Ca^{2+}< Mg^{2+}<SO_4^{2+}), it was found to be higher as compared to monovalent ions (NO_3^-<Na^+< Cl^-) through RO and NF membranes. However, the overall removal efficiency of ions was generally higher in RO membranes than the NF membranes.

4.5 Artificial Neural Network Predictions

The optimal topology of ANN model involves a feedforward neural network with one input layer (four neurons), one hidden layer (with five neurons) and one output layer (including three neurons). Table 4.26 shows the weights and biases associated with a neural network after training. The training of the selected network architecture was terminated after 55 iterations when the mean square error got minimized to 0.0046.

Furthermore, ANN model was used to validate the RSM predicted optimized process conditions. Feed water temperature (31.92^{o}C), pressure (0.79 MPa), salt concentration (1500 mg/L) and pH (6.53) were used as input parameters for the ANN model. ANN predicted 19.51% and 18.59% of water recovery, 88.92% and 71.4% of TDS rejection and 16.60 kWh/m^3 9.43 kWh/m^3 of SEC for CSM and NF250 membranes respectively, at optimal process conditions (Table 4.25). A comparison of the predicted values between ANN and RSM reveals that the values predicted by both RSM and ANN model are much closer to experimental values. It also confirms that ANN has good potential to precisely predict RS even without having information about any physical and chemical background of the system [39]

Table 4.26. Optimal values of network weights and biases for ANN model.

Input Weight matrix (from input 1to hidden layer 1)	$IW^{(1,1)}$ = [-0.11971.9471 -1.0935 -0.3870; 0.0563 0.2663 -0.2294-2.8351; 1.9193 -0.2076 0.5675 -0.6581; 1.0336 -0.99841.06361.8266; -1.5332 2.2767 -0.56631.1217]
Bias to layer 1	$b^{(1)}$ = [-0.4559; 1.5344; 0.9288; -0.6384; 1.0518]
Layer Weight matrix (from Hidden layer 1to output layer 2)	$LW^{(2,1)}$ = [-0.6133-1.4310 0.1758 0.5653 0.8812; -1.3445 1.0168 -0.9082-1.0261 1.2008; 1.1128 -1.2573 1.5338 -2.2471 -1.4109]
Bias to output layer 2	$b^{(2)}$ = [0.1127; 0.2326; 1.1376]

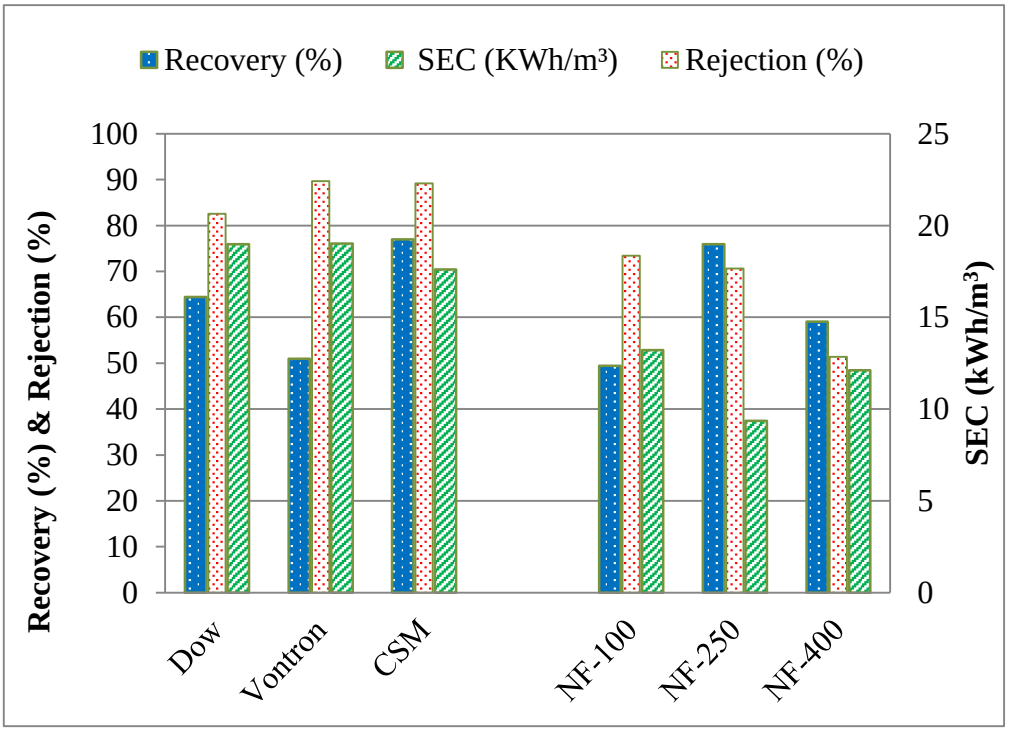

Figure 4.17. Graph showing the recovery, rejection and SEC of different RO and NF membranes.

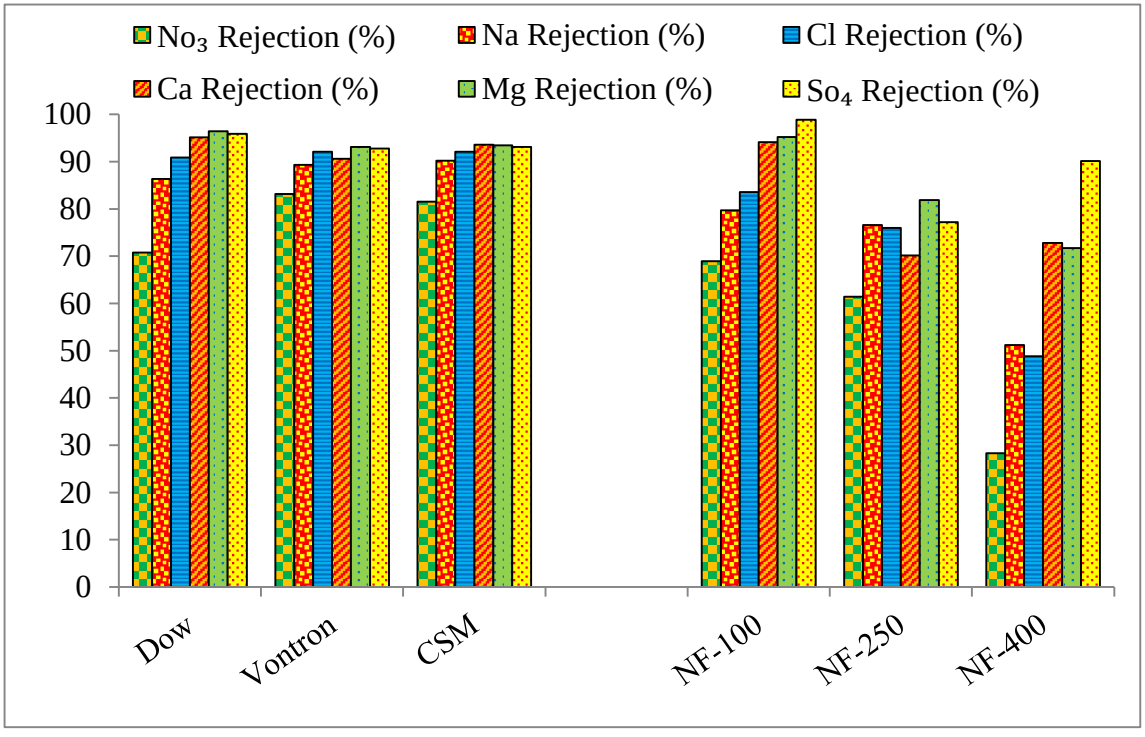

Figure 4.18. Graph showing the anions and cations rejection of different RO and NF membranes.

Chapter 5.
RO - NF Hybrid Experiments with PV System

5.1 NF-RO Hybrid Membrane Experiments

After RSM optimization, best RO and NF membranes were selected to perform validation runs followed by NF-RO hybrid experiments. According to the operating conditions of feed, concentrate and permeate flow streams (Table 5.1), the membrane performance data in isolation and hybrid configurations were analysed and shown in Figure 5.3. The hybrid configuration was operated on a closed-loop basis, with the concentrate and permeate recirculating back to the feed water supply tank (Figure 5.1and Figure 5.2). Close-loop operation was necessary for continuous evaluation of the system. The recirculating test unit was allowed to operate for at least 75 minutes prior to sample collection.

Table 5.1. Comparison of operating conditions of various membrane experiments in single and hybrid configurations.

Flow streams	**Operating conditions**	**Single RO**	**Single NF**	**NF-C-RO**			**NF-P-RO**	
				Stage 1	**Stage 2**	**Final**	**Stage 1**	**Stage 2**
Feed	Flow (LPH)	175	477	435	348.3		442.6	172.5
	Pressure (MPa)	0.78	1.08	1.08	1.03		1.08	0.78
	TDS (mg/L)	1500	1500	1500	1760.6		1500	450
Concentrate	Flow (LPH)	200	390	348.4	279.3		353.1	142.2
	Pressure (MPa)	0.71	1.03	1.03	0.69		0.98	1.03
	TDS (mg/L)	2020	1752	1760.6	2164.1		1766.2	549.3
Permeate	Flow (LPH)	34	87.6	86.6	69.1	155.7	89.5	30.3
	TDS (mg/L)	167	450	452.2	159.5	322.4	450.0	41.7

5.1.1 NF-C-RO Configuration

The schematic design of NF-Concentrate-RO (NF-C-RO) configuration is shown in Figure 5.1. The stream numbers in the figure are: 1 is raw feed water, 2 is NF feed water, 3 is NF concentrate/ RO feed, 4 is NF/system concentrate, 5 is RO permeate, 6 is NF permeate and 7 is final/system permeate. Overall, the system recovery of 35.79% was observed for NF-C-RO configuration (Figure 5.3). It is higher than the single NF (~19%), single RO (~19%) and hybrid NF-Permeate-RO (NF-P-RO) configuration i.e. ~7% (Figure 5.2 and Table 5.1). Salt rejection of 78.51% was observed for NF-C-RO configuration, which was still higher than individual NF system (~71%) and lower than the individual RO (~89%) and hybrid NF-P-RO systems (~97). Further, 5.02 kWh/m^3 SEC was found for the same NF-C-RO configuration which was the lowest in all membrane configurations (~17, ~9 and ~57 kWh/m^3 for single RO, single NF and NF-P-RO, respectively). In order to meet the recovery and SEC, one has to sacrifice the rejection as shown in the case of NF-C-RO (Figure 5.3). However, in this configuration, the final permeate TDS (322 mg/L) is well within the permissible level of Indian drinking water standards i.e. IS:10500 (Table 5.1).

5.1.2 NF-P-RO Configuration

In the NF-P-RO configuration the membrane of second-stage (RO) was exposed only to the higher quality feed water of first-stage (NF permeate) as shown in Figure 5.2. The first-stage (NF) operated at an overall recovery of approximately 20% and a rejection of ~70%. The second-stage RO membrane operated at a slightly lesser recovery of ~17% and higher salt rejection of ~91%. In the case of overall system performace of NF-P-RO configuration, lower water recovery (6.85%) and higher SEC (57.29 kWh/m^3) may be due to the use of another high pressure pump for pressurization of permeate of first-stage as a feed water for second-stage. The final permeate TDS level (~42 mg/L) is much lower than the permissible level of Indian drinking water standards i.e. IS:10500 (Table 5.1).

Membrane fouling and inorganic scaling is a major challenge for the concentrate staging configuration [19]. Therefore, prediction of inorganic fouling potential of feed as well as concentrate water is necessary to find out appropriate treatment option for avoiding inorganic fouling on membrane surface.

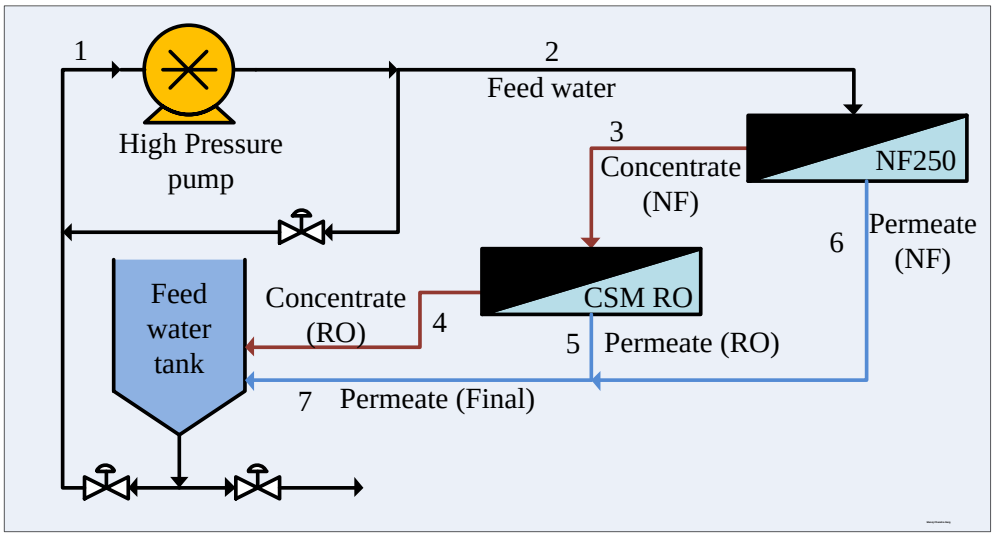

Figure 5.1. NF-RO hybrid configuration in NF-concentrate-RO mode (NF-C-RO).

Where:

	1	2	3	4	5	6	7
Flow (LPH)	0	435	348.36	279.29	69.07	86.64	155.71
Pressure (MPa)	0	1.08	1.03	0.687	0	0	0
TDS (ppm)	1500	1500	1760.58	2164.07	159.51	452.18	322.35

Figure 5.2. NF-RO hybrid configuration in NF-permeate-RO mode (NF-P-RO).

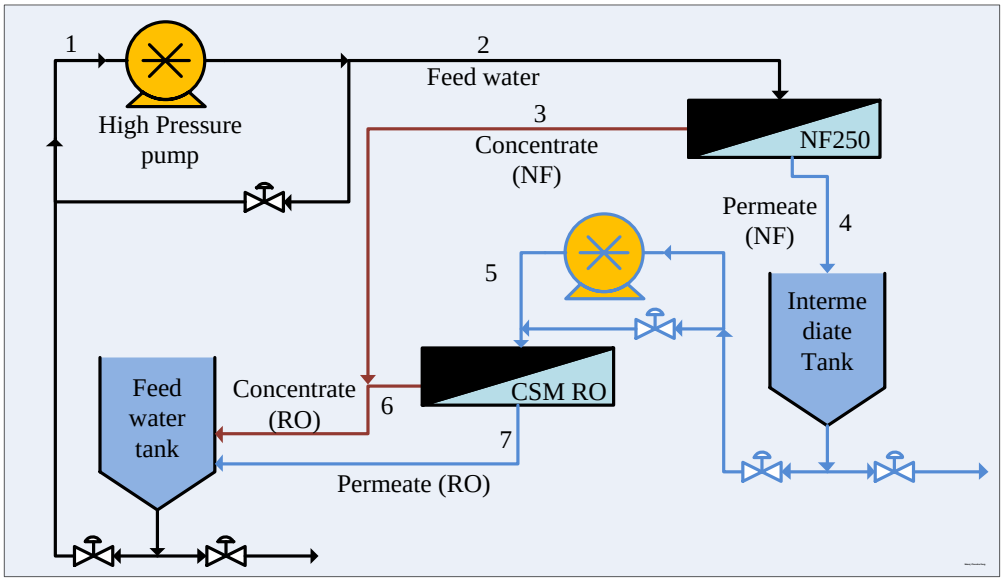

Where:

	1	2	3	4	5	6	7
Flow (LPH)	0	442.63	353.11	89.52	172.50	142.16	30.34
Pressure (MPa)	0	1.08	0.981	0	0.785	1.03	0
TDS (ppm)	1500	1500	1766.19	450.04	460	549.25	41.72

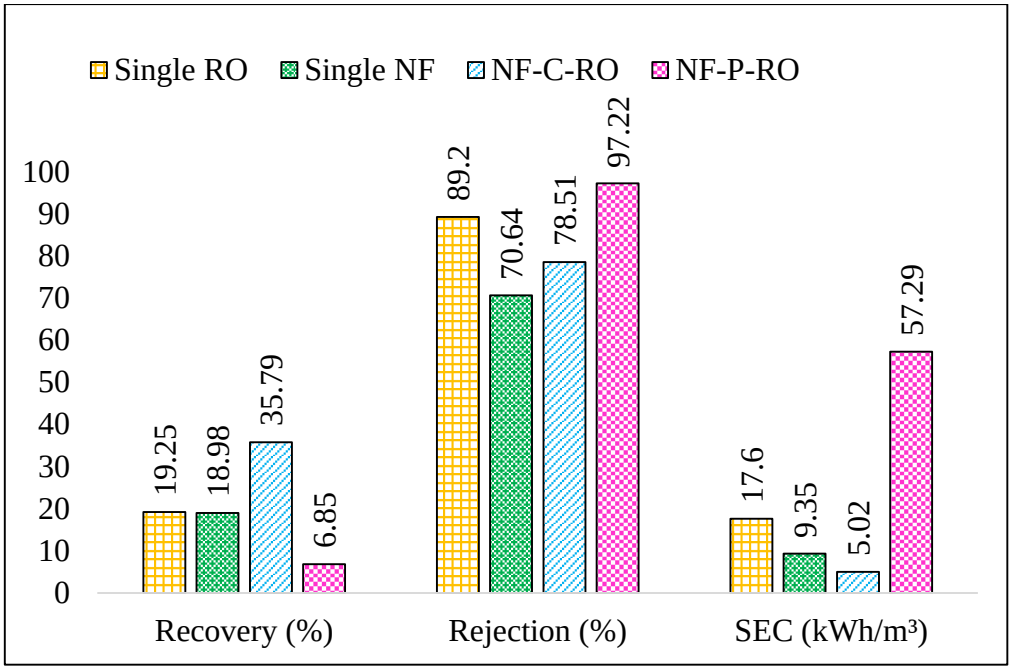

Figure 5.3. Graph showing the recovery, rejection and SEC of single and hybrid membrane treatment schemes.

5.2 Inorganic Fouling Assessment

Chemical analysis of feed and concentrate water displayed low salinity i.e. 1500 mg/L and 1760 mg/L respectively. On applying the ROIFA-4A model on the water chemical composition it was found that the total inorganic fouling flux value of NF concentrate water was higher than the NF feed water, but in both cases this range of inorganic fouling was almost negligible with respect to the guideline limit (8.00E+17 Molecules/0.1cc.sec) (Table 5.2) [73].

Table 5.2. Inorganic fouling flux measurement criterion

Inorganic Fouling Flux Range (Molecules / 0.1cc.sec)		**Fouling Potential Guidelines**	**Remarks**
From	**To**		
0.00E+00	8.00E+17	No Fouling	No treatment is required
8.00E+17	9.00E+17	Low Fouling	Short flushing is essential
9.00E+17	1.00E+18	Medium Fouling	Antiscalant + Chemical Cleaning
1.00E+18	1.50E+18	High Fouling	Antisc. + Short Chemical Cleaning.
1.50E+18	2.00E+18	Very High Fouling	Antiscalant action is questionable
>2.00E+18	-----	Excessive Fouling	Scale Blockage is a must

Source: El-Manharawy and Hafez [75]

Prediction of the chemical nature of scale was possible through ROIFA software by means of guidelines given by El-Manharawy and Hafez [73]. In both cases, the expected scaling chemical nature was mainly sulphate type with lesser amount of carbonate. The relative percentage of carbonate (45.53% and 46.18%) and sulphate (53.82% and 54.47%) were approximately similar in feed and concentrate water (Table 5.3). As per the guideline [73], no treatment is required from 0 to 100% saturation factor. The molar ratio (SO_4/alk) of the investigated feed and concentrate water reached 5.48 and 5.62 respectively, strongly indicating low sulphate scaling potential on membrane surface at higher recovery [74]. It meant that at this level of fouling potential of feed and concentrate water, the hybrid membrane plant could run safely without the risk of inorganic fouling and did not need any antiscalant.

Table 5.3. ROIFA software results showing fouling potential analysis of different hybrid membrane schemes.

Hybrid Scheme	**Total Inorganic Fouling Flux (Molecules / 0.1cc.sec)**	**Carbonates (%)**	**Sulfates (%)**	**Molar Ratio (SO_4 / Alk)**
NF feed	8.8973E+16	45.53	53.82	5.48
NF concentrate	1.10291E+17	46.18	54.47	5.62

5.2.1 FE-SEM Analysis

The surface of membrane covered with the layer of deposits could be more clearly observed after magnification of its surface. The surface of virgin and inorganically fouled membrane was compared by Field Emission Scanning Electron Microscopy (FE-SEM) analysis as shown in Figure 5.4 and Figure 5.5. Differences between the surface morphologies of various NF and RO membranes were clearly observed in SEM images.

The virgin membrane appeared clean and had fairly smooth surface in SEM images (Figure 5.4a and Figure 5.5a), while the inorganically fouled membrane surface comprised of embedded amorphous particulate matter (Figure 5.4b, c and Figure 5.5b, c).

The SEM analysis could be predominantly used to identify the amorphous deposits. Different size of the particles existed, although, no crystalline structures were apparent except calcium carbonate ($CaCO_3$).

Surface morphology and structure were studied by scanning electron microscope-energy dispersive using X-Ray (SEM-EDX). Also, fouling elements on the membrane surface were

determined by the EDX elemental analysis. EDX analysis of the virgin membrane validated the existence of C (72.04%) O (20.62%) and S (11%) as shown in Figure 5.4a and Figure 5.5a. Occurrence of sulphur on the virgin membrane was likely due to the presence of the polysulfone support layer of the membrane [178].

The chemical analysis by SEM-EDX demonstrated that Ca, Mg, Cl, O, C and S were the major elements of the inorganic deposits (Figure 5.4b, c and Figure 5.5b, c). Occurrence of calcium and its complexation with sulphate apparently resulted in an inorganic fouling deposition on the membrane surface [253]. The next highest cation, Mg was involved in the inorganic fouling process. The SEM-EDX analysis of inorganically fouled membranes signified that substantial quantity of deposits contained inorganic material and minerals.

Prior to a long term shutdown and for scheduled routine maintenance, cleaning procedures were carried out to minimize the plugging of the feed line with dislodged inorganic foulant. The cleaning was conducted by recirculating 0.5% HCl solutions (pH 2-3) through the membranes for about 10-15 minutes without applying pressure followed by permeate water flushing to neutralize the acid. After cleaning, the membrane surfaces appeared clean and smooth in SEM images (Figure 5.4d and Figure 5.5d).

5.2.2 X-Ray Diffraction Analysis

For every possible compound, initial search was performed using X-Ray diffraction analysis (XRD) data base. The XRD patterns of all inorganically fouled membranes were almost similar. The broad peaks of 2θ in the range 15-30^{o} assigned to the amorphous pattern of the polyamide membranes [182] as shown in Figure 5.6 and Figure 5.7.

Calcite ($CaCO_3$) was observed as a common element of the crystalline phase deposits observed on all membrane surfaces (Figure 5.6 and Figure 5.7). The chemical composition of deposition was also approved by EDX analysis (Figure 5.4 and Figure 5.5).

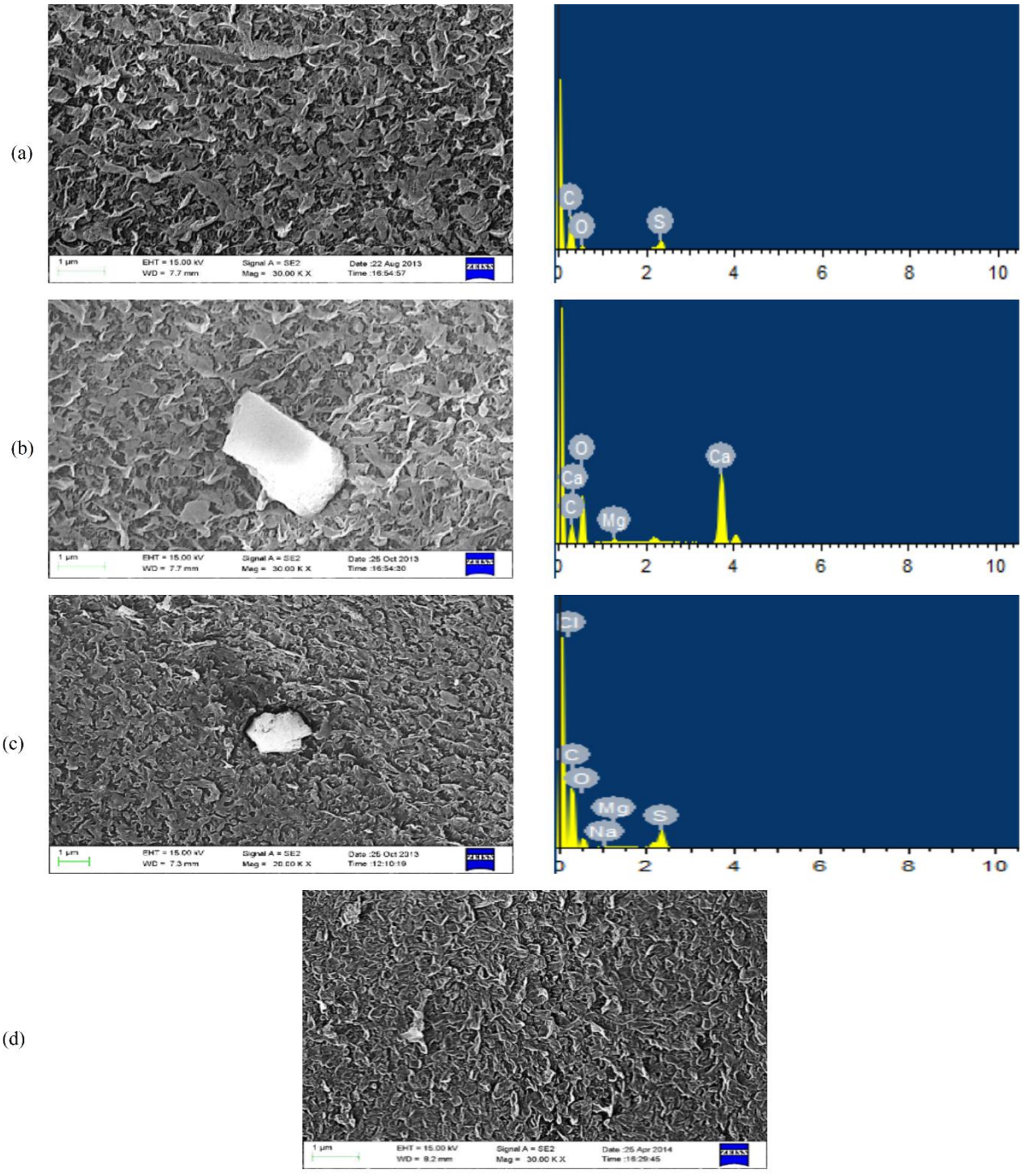

Figure 5.4. SEM micrograph and EDX spectra of NF250 membrane (a) before experiments (b) and (c) after few months of experiments and (d) after chemical cleaning.

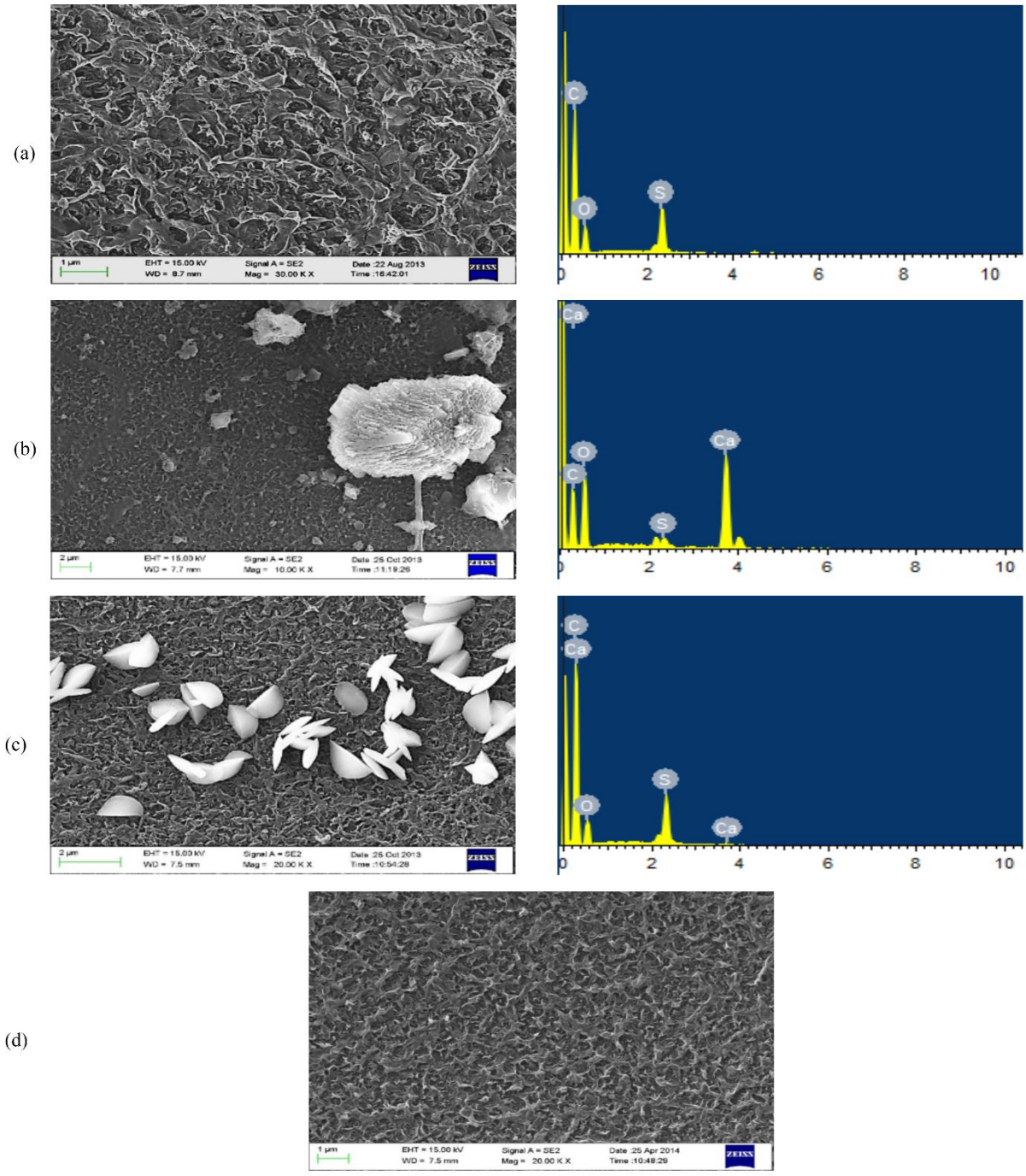

Figure 5.5. SEM micrograph and EDX spectra of CSM RO membrane (a) before experiments, (b) and (c) after few months of experiments and (d) after chemical cleaning.

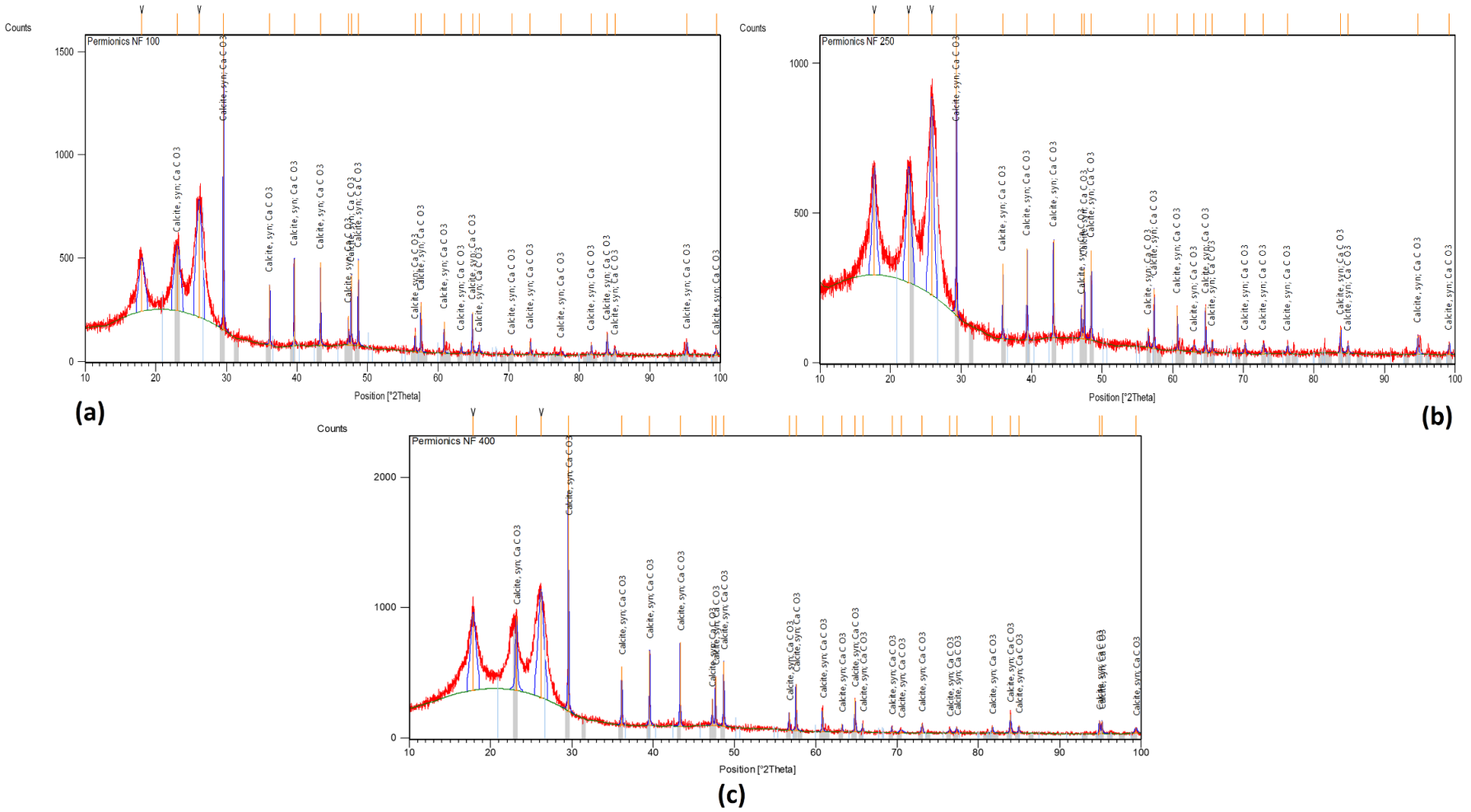

Figure 5.6. X-Ray diffractogram of deposit formed on the different NF250 membrane surfaces, (a) NF100, (b) NF250 and (c) NF400.

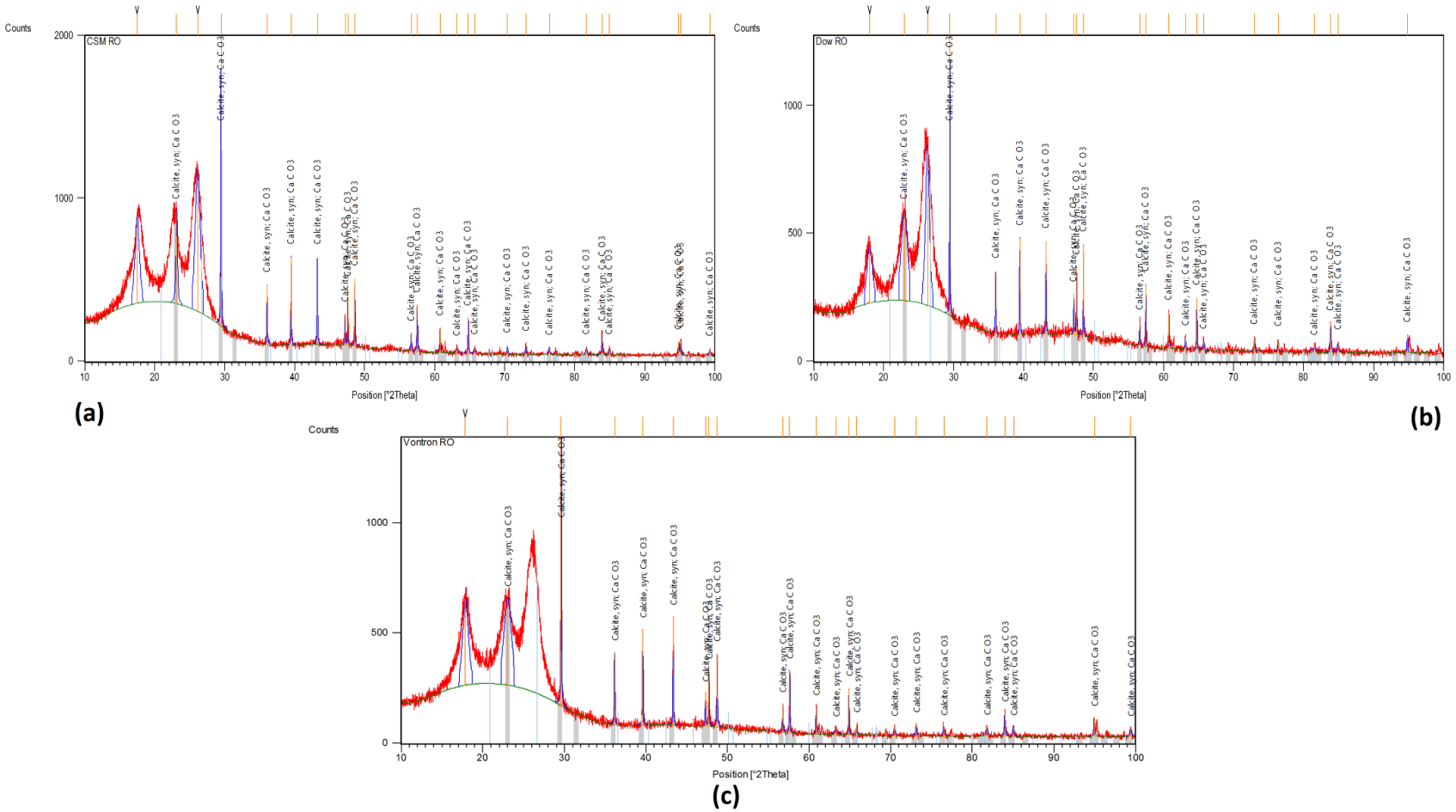

Figure 5.7. X-Ray diffractogram of deposit formed on the different CSM RO membrane surfaces (a) CSM, (b) Dow and (c) Vontron.

5.3 Photovoltaic System and its Integration with Membrane Systems

The study presents a generalized methodology to evaluate the feasibility of PV systems for brackish water NF-RO hybrid water treatment system for small, remote communities.

5.3.1 Solar Radiation Over Roorkee Town

The national aeronautics and space administration (NASA) surface meteorology and solar energy (SSE), a renewable energy resource web site, provides information regarding solar irradiance at any chosen location. It was used to collect data for location at Roorkee (29.8749° N, 77.8899° E), Uttrakhand, India.

SSE provided one year data of daily solar radiation on horizontal surface over Roorkee town. Daily solar radiation on tilted surface was calculated after considering tilt angle as 30^{o} and area of 1.5 kW PV panels as 10.34 m^2. Daily power production on Julian day by 1.5 kWp of installed PV system was also estimated (Table 5.4).

To analyze the performance of PV system as a power source, the efficiency of PV modules must be determined. Efficiency in PV panels is measured by the ability of a panel to convert sunlight into usable energy for human consumption. Therefore, module operating efficiency of the installed 1.5 kWp PV system was calculated. It varied from 5.88% (May) to 12.7% (January) as shown in Table 5.4. This data verify the fact that silicon solar PV module operating efficiency is at optimum level in moderately low air temperatures [164].

5.3.2 Orientation of the Sun

The available solar radiation on a PV module is determined by two aspects: the angle at which the solar radiation meet the module's surface and the amount of available solar radiation. Although the available amount of solar radiation at any one time cannot be improved, there are options that can be implemented to increase the intensity of the solar radiation through concentrating collectors or by tracking the solar radiation through the use of PV trackers. Thus, the module's surface is always oriented so that it is consistently perpendicular to the sun. However, in the case of this research, the panel was mounted permanently at one angle, i.e., facing the equator at all times. The reason for this is that in almost all installations in the poor

rural regions of the world, the feasibility of employing concentrating or tracking systems is very low considering their high cost and miantenence requirements.

In this research, the PV panels were mounted at an angle equal to the latitude (~ 30^o N) with orientation in southward direction. This orientation was found to be an optimal design to absorb the maximum amount of solar radiation year-round [38, 98].

5.3.3 Solar Photovoltaic System Setup

The PV grid-connected system consisted of following major components (Figure 3.1):

- PV modules,
- Grid-connected inverter, and
- AC Distribution system

5.3.3.1 Photovoltaic Modules

A PV module is made up of multiple silicon cells. These silicon cells are doped to be able to convert the sun's energy into direct current (DC) electricity through the use of the photoelectric effect. However, the ability of PV modules to produce their rated power is dependent on both the ambient temperature and solar irradiance. The majority of panels around the world are presently rated at standard test conditions (STC). STC is considered to be 25°C cell temperature and 1000 Watts/m^2 of direct sunlight. The module's performance varies due to availability of the sun and the ambient temperature.

The eleven solar panels from Moserbaer Solar Ltd., with 1.5 kWp of total capacity was installed at the rooftop of the Department of Hydrology, Indian Institute of Technology Roorkee (Figure 5.8). Nominal maximum power output of each panel is 139.04W with an open circuit voltage (V_{oc}) of 22.3V and short circuit current (I_{sc}) of 8.39A. Its nominal operating voltage and current are 17.86V and 7.79A respectively. Detailed technical data of the installed PV system are given in Table 3.1. Fluctuation in monthly average of hourly current generated by 1.5 kW solar PV system are shown in Table 5.5. It is clearly indicated that the most productive hour for solar photovoltaic system is in between 8 AM to 3 PM (7 hours).

5.3.3.2 Solar Inverter

The DC electricity from the PV modules (1.5 kWp) passed through DC distribution network to a grid interactive DC/AC solar inverter, which converts the DC electricity into sinusoidal wave AC voltage (230V) of the same frequency (50 Hz) and phase (single phase) with that of the grid and fed through A/C distribution system linked to the electricity supplied by the grid AC (Figure 3.1). The DC/AC solar inverter had a power rating of 3 kW.

5.3.3.3 AC Distribution Board (ACDB)

ACDB received AC power output of DC/AC solar inverter and supplied its output to load distribution panel. One Energy meter (kWh) was fitted to record total power exported from solar system to load. The ACDB was made of dust and vermin proof metal sheet iron enclosure and had adequate cooling arrangement.

5.3.4 Data Logging System

To investigate the power generated by PV system, there are needs to acquire the input and output parameters of the PV array serving as the generation equipment. Data from acquisition system module are needed to produce useful information.

In this study, a PV generation monitoring system was employed for a 1.5 kWp PV generation. Input and output DC/AC power, voltage, and current of the array were acquired, processed and then transmitted so that it could be used for reviewing the performance of the generation plant. Acquired data were transmitted by RS-232 communication lines, while CEHE application program (computer software) was used to graphically display the acquired data. Figure 5.9 shows the screen shot of the software.

5.3.5 Comparison of Generated Current vs Required Current

The membrane filtration unit was designed to operate for about 6 to 8 hrs/day, depending on peak sun shine hours (PSSH) for 1.5 kW PV system as shown in Table 5.4. Hourly average value of AC current generated by 1.5 kW of PV system during June 2013 to May 2014, is presented in Figure 5.10. Monthly variation in current generation mainly depends on the sunny or cloudy nature of the sky. Generated current was compared with the current required by the hybrid membrane system (Figure 5.10). It was apparent that the amount of current generated

during the PSSH was enough to operate the NF-C-RO hybrid membrane unit. Excess energy, which was not utilized by membrane filtration system,could be utilized in maintaing the temperature of feed water and/or for pumping the water.

Table 5.4. Fluctuation in daily solar radiation in Roorkee throughout the year and efficiency of 1.5 kW solar PV system.

Month	**Daily solar radiation on horizontal surface* ($kWh/m^2/d$)**	**Daily solar radiation on Tilted surface ($kWh/m^2/d$)**	**Sunshine Hour (hr)**	**Daily power production on julian day (kWh/d)**	**Daily power production on julian day ($kWh/m^2/d$)**	**Efficiency (%)**
January	3.68	5.41	6	7.1	0.69	12.70
February	4.56	6.71	6	7.6	0.74	10.96
March	5.8	8.53	7	8.12	0.79	9.21
April	6.84	10.06	8	8.11	0.78	7.80
May	7.31	10.75	8	6.53	0.63	5.88
June	6.71	9.87	7	6.77	0.65	6.64
July	5.57	8.19	7	6.35	0.61	7.50
August	4.93	7.25	8	7.18	0.69	9.58
September	5.25	7.72	8	7.61	0.74	9.54
October	5.05	7.43	6	7.06	0.68	9.19
November	4.26	6.27	5	6.7	0.65	10.34
December	3.54	5.21	4	6.35	0.61	11.79

*NASA Surface meteorology and Solar Energy (SSE) Release 6.0 Data Set, Tilted angle= 30°, Area of 1.5 kW PV panels= 10.34 m^2

Table 5.5. Fluctuation in monthly average hourly current by 1.5 kW solar PV system.

							Time (hour) →									
Month ↓	5	6	7	8	9	10	11	12	13	14	15	16	17	18	19	
December			0.9	2.3	3.4	4.0	4.4	4.3	3.9	3.0	2.1	0.9	0.8			
January			1.4	3.1	4.1	4.6	5.3	5.2	4.6	4.1	3	1.9	0.8			
February		0.9	2.1	3.2	4.2	5.3	5.7	5.9	5.3	4.6	3.5	2.4	1.1	0.8		
March		0.9	2.1	3.2	4.2	4.8	5.6	5.4	4.8	4.5	4.2	2.5	1.5	0.8		
April	0.7	1.1	2.5	3.6	4.7	5.5	5.6	5.9	5.8	5.4	3.6	2.5	1.5	0.8		
May	0.8	1	2.2	3.7	5.3	4.6	5.6	5.9	5.1	4.7	3.3	2.4	1.1	0.8	0.9	
June	0.8	1	2	3.2	4.3	4.9	6	5.7	5	5.5	3.9	2.8	1.5	1	0.8	
July	0.8	1	1.7	3.4	4.7	5.9	6.1	6.3	5.9	4.8	3.9	3.1	2.1	0.9		
August	0.8	1.2	2.4	4.1	5.8	5.9	6.1	6.8	5.7	5.4	4.2	3.1	1.6	0.8		
September		1.2	2.4	4.5	5.1	5.5	6	5.8	5.4	4.8	3.8	2.6	1.2			
October		1	2.7	3.5	4.3	6.3	6.5	6.1	5.3	5.2	3.3	2.1	0.9			
November			1.2	2.6	3.6	4.3	4.5	4.4	3.7	3.0	1.9	0.9	0.5			

Green = Highest, Red = Lowest, Yellow = Moderate current

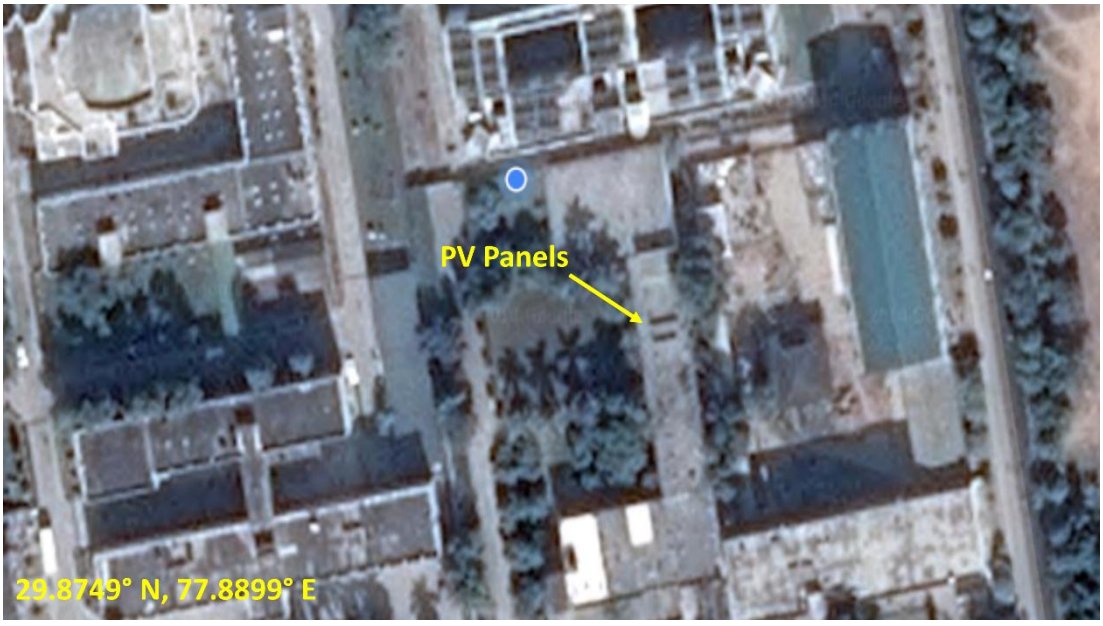

Figure 5.8. Location of the installed PV panels over the rooftop of the Department of Hydrology, IIT Roorkee.

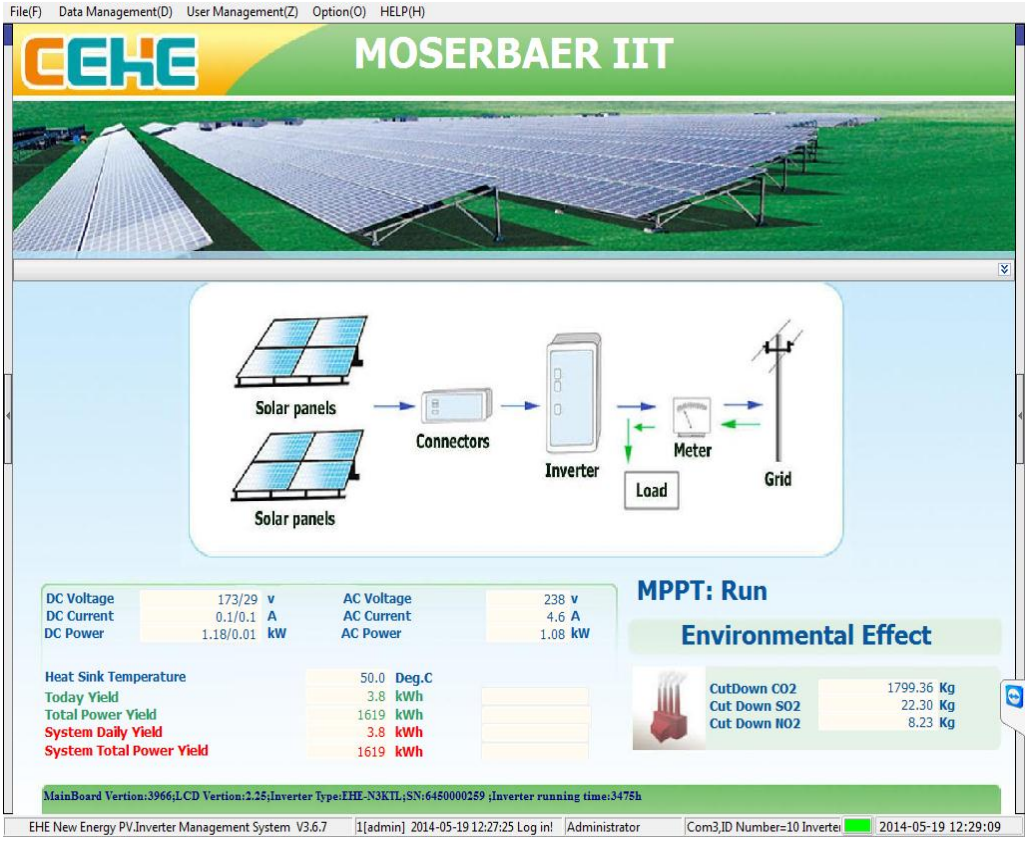

Figure 5.9. Screen Shot of data logging software.

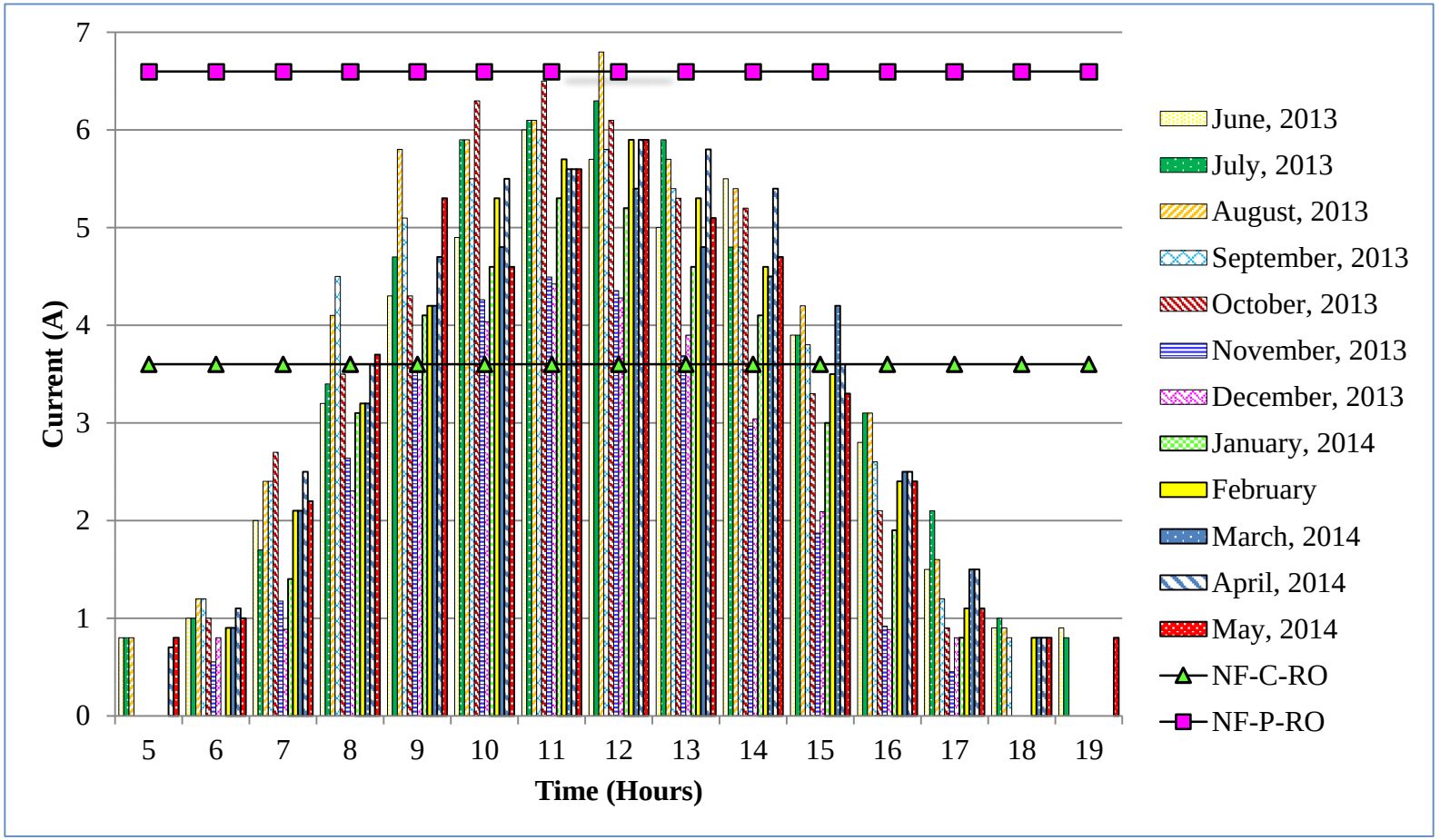

Figure 5.10. The hourly average generated AC current versus the required by the different hybrid membrane filtration schemes.

Chapter 6.
Economic Assessment

In this chapter, a method for determining the feasibility for community-scale PV assisted NF-RO systems is presented. A PV assisted NF-RO system is feasible if it is both technically and economically feasible [43]. Technical feasibility of community-scale PV assisted NF-RO systems has been established in the earlier chapter. Economic feasibility for the PV assisted NF-RO system is established based on a cost analysis of per cubic meter water production for remote locations.

6.1 Estimation of Water Production Cost

For estimation of water production cost, common technical assumptions, specifications and design parameters were considered for PV assisted RO and NF membrane systems in isolation and hybrid modes (Table 6.1). The following items were included:

(1) Capital cost
(2) Operation and maintenance cost
(3) Other cost and operating expenditure

6.1.1 Capital cost

Capital costs consists of the cost of the RO system and the cost of the energy production system. Total capital cost was converted into equivalent annual amortized cost and calculated by using following equation:

$$A = CC\frac{r(1+r)^n}{(1+r)^n-1} \tag{6.1}$$

Where, A is the periodic amortization payment, CC is the capital cost, r is the periodic interest rate divided by 100 and n is the total number of payments.

6.1.1.1 NF-RO system

Table 6.2 shows the total capital cost for the membrane system in hybrid, NF as well as RO configurations and PV system. The main components contributing to the total cost of the membrane system were high pressure pump and NF/RO membranes. The breakdown of the membrane system components are shown in Table 6.2. The capital cost of RO and NF membrane systems is 40% higher than hybrid membrane system.

6.1.1.2 Photovoltaic system

The capital cost of the entire PV system, including the costs of the PV modules, control electronics (solar inverter and ACDB), wiring, supporting structures and installation are shown in Table 6.2. Government incentives can substantially change these costs.

6.1.2 Operation and maintenance (O&M) cost

6.1.2.1 NF-RO system

Throughout the lifetime of the system, certain components of the NF-RO membrane system will require replacement. The major components that will require regular replacement are the membranes modules. Here, we assume that the membranes in the NF-RO system will be replaced once in two years [78, 160].

6.1.2.2 Photovoltaic system

The annual costs for the photovoltaic-power system are low since the energy for this system comes directly from the sun. The photovoltaic panels will not require replacement during the system lifetime since their expected life is 25 years (Table 6.1) [85, 88, 105]. Other portions of the photovoltaic-power system will require maintenance and repairing over the system operational life [88].

Earlier studies stated that annual O&M costs were about 20% of the plant annual amortized capital cost [30, 43, 105]. Therefore, in this study, annual O&M cost of NF-RO and PV system was assumed to be 20% of annual amortized capital cost.

Table 6.1. Technological specifications and design parameters for PV powered membrane system.

Specifications/Parameters	**PV-Hybrid**	**PV-NF**	**PV-RO**
Recovery (%)	35.79	19.92	20.05
Feed Flowrate (LPH)	435	435	171
Hours of operation/day	6	6	6
Water production (Liter/Day)	934.12	519.91	205.71
Annual product volume (m^3/year), Q	340.94	189.77	75.09
Total amount of water produced (m^3/25 years)	8523.84	4744.20	1877.13
SEC (kWh/m^3)	5.02	9.35	17.6
System Life (years) [2, 30, 105]	25	25	25
Membrane Life (years) [2, 30, 88]	2	2	2
Interest rate (%) [2, 30, 105]	5	5	5
RO plant availability (%), f [2, 30]	90	90	90
NF/RO membrane cost (Rs.)	10000	5000	5000
No. of PV module	11	11	11
Module rating of single module (Wp)	140	140	140
Total module rating (Wp)	1540	1540	1540
Cost of PV module (Rs./Wp)	166.88	166.88	166.88
Capital Recovery period (Years)	25	25	25

Table 6.2. Capital cost of PV powered membrane system.

Cost of membrane system (Rs.)			
Compoments	**Hybrid**	**NF**	**RO**
High pressure pump (with 1 HP motor)	15000	15000	15000
High pressure connecting pipes	5000	5000	5000
Membrane housing	5000	2500	2500
NF/RO membranes	10000	5000	5000
Feed/Permeate tank	2000	2000	2000
Temperature control unit	2000	2000	2000
Membrane system installation cost	5000	5000	5000
Total cost of membrane system	**44000**	**31500**	**31500**
PV system component wise cost (Rs.)			
PV module (11 x 140 W)	84233	84233	84233
AC distribution board	8294	8294	8294
Solar inverter (3 KW)	102512	102512	102512
Copper cable, Lightining arresters, Super earthing kit	12282	12282	12282
Module moulting structure	23979	23979	23979
Installation, Freight & Insuarance of PV system	25700	25700	25700
Total cost of PV system	**257000**	**257000**	**257000**
Total Capital cost	**301000**	**288500**	**288500**

Table 6.3. Calculation of annual per cubic meter water production cost (Rs.).

Parameters	**PV-Hybrid**	**PV-NF**	**PV-RO**
Membrane replacement cost per year, A1	5000	2500	2500
Annual amortized capital cost, A2	21357	20470	20470
O & M annual cost, A3 = A2*0.2	4271.34	4093.96	4093.96
Annual operating cost, C	30628.03	27063.74	27063.74
Unit production cost, Rs./m^3	**99.81**	**158.46**	**400.49**

6.1.3 Calculation of water production cost

The total per cubic meter water production cost includes the membrane replacement cost, annual amortized cost, operation and maintenance cost for the process and annual operating cost. Annual operating cost was estimated using [43]:

$$C = (A1+A2+A3) \quad (6.2)$$

Where A1 is the membrane replacement cost per year, A2 is the annual amortized capital cost, and A3 is the annual O&M cost.

The per cubic meter water production cost was calculated by dividing the sum of the membrane replacement cost, amortized capital costs and annual O&M costs by the annual water production and plant availability as given by Abraham and Luthra [2]:

$$C/(f \times Q) \quad (6.3)$$

Where C is the annual operating cost, f is the RO plant availability, Q is the annual product volume. The total water production cost at three selected configurations is depicted in Table 6.3.

Figure 6.1 shows the contribution of different components of membrane and PV systems in cost distribution of the PV-NF/RO system.

To stabilize the energy input to the membrane unit, to compensate the solar radiation variation and to provide backup during non-sunny days, most of the AC powered desalination systems use battery backup in the PV–RO system [54,55]. A 28 Ah capacity of battery bank with 4 kWh/day (Rs.8000/kWh) load along with 3 days of autonomy was used for calculation of the water production cost with battery storage.

The comparative results have been depicted for each configuration of membrane system and various interpretations and conclusions are presented below:

(1) The water production cost of PV-hybrid system (Rs.99.81 /m^3) was about 1.6 times lesser than PV-NF (Rs.158.46/m^3) and 4 times lesser than PV-RO (Rs.400.49/m^3) system. It depended mainly on water recovery and SEC.

(2) The major share of cost was of PV system, which contributed more than 50% of the overall cost (Figure 6.1).

(3) Annual water production cost with battery storage is about 34% more than the system without battery storage in case of hybrid system and 39% in case of single membrane system (Table 6.5)

6.2 Effect of Different Conditions on Photovoltaic Assisted Membrane Systems

6.2.1 Effect of Photovoltaic Fluctuation on the Performance of Hybrid Membrane System

Solar radiation and PSSH was highest in April and lowest in December. Average monthly water production cost was observed to be inversely proportional to solar radiation and sunshine hours, and it was highest in December and lowest in April (Table 6.4).

6.2.2 Effect of Subsidy on Water Production Cost

The Ministry of New and Renewable Energy of the Government of India provides subsidies for solar PV systems in the residential, commercial and industrial sectors under the national solar mission [172]. The main objective of the mission is to promote the use of PV system in the country through a combination of financial and promotional incentives, and other support measures so as to conserve electricity and other fossil fuels [135]. As of date the subsidy for rooftop solar PV systems is 30% of the actual cost. The capital subsidy has been increased to 90% for special category states (North Eastern states, Sikkim, Jammu & Kashmir, Himachal Pradesh, and Uttarakhand) [172].

The water production cost could be further reduced after increasing subsidy (or tax reduction to encourage using PV) provided by the government (Figure 6.3). The cost of per cubic meter water production varied from Rs.80/m^3 to Rs.35/m^3 in hybrid membrane configuration, Rs.122/m^3 to Rs.42/m^3 in NF and Rs.309/m^3 to Rs.107/m^3 in RO membrane systems (Table 6.6). Therefore, based on the water production cost corresponding to the provided subsidy, an incentive of 10% increment on subsidy may result in a reduction from 17% to 72% depending on configuration of the membrane system. However, on increasing the subsidy from 30% to 90%, the percentage reduction of water production cost from the hybrid membrane system would reduce from 34% to 17% in case of NF membrane and 74% to 67% in case of RO membrane.

6.2.3 Effect of the System Life on Water Produciton Cost

The life of different components in a solar powered membrane system encompassing raw material production, manufacturaing, quality of material and maintenance [123]. Good quality

PV modules are typically warranted for 20 to 25 years expectancies exceeding upto 40 years [88, 135].

The effect of increasing the system life on per cubic meter water production cost for the single and hybrid membrane system is shown in Figure 6.2. It is evident that the increasing system life reduced the cost of water production significantly. It was investigated that the water production cost of Rs.146.5/m^3, Rs.370.26/m^3 and Rs.92.87/m^3 for the PV-NF, PV-RO and PV-hybrid membrane systems, respectively, could be reached when the plant withstood 30 years. Further, it may be concluded that water production cost decreases at a much faster rate from 5 to 10 years followed with a steady decrease from 10 to 25 years and remains constant afterwards upto 30 years.

6.3 Cost Comparison with Earlier Studied Systems

Comparing cost of different membrane systems is complex and usually dependent significantly on specific conditions. The present PV powered NF-RO hybrid membrane system was compared with the previously studied PV powered brackish water RO systems (Table 6.7). It is evident that recovery, SEC and per cubic meter water production cost showed significant improvement over the previous systems.

Further, present system was compared with the other existing solar powered desalination technologies (Table 6.8). It was estimated that the per cubic meter water production cost of the present system came lower than that of all solar powered desalination technologies except solar pond [191]. This could be due to the high plant capacity of solar pond.

Moreover, on increasing the capacity of the membrane system, the cost of per unit water production would go down further [85].

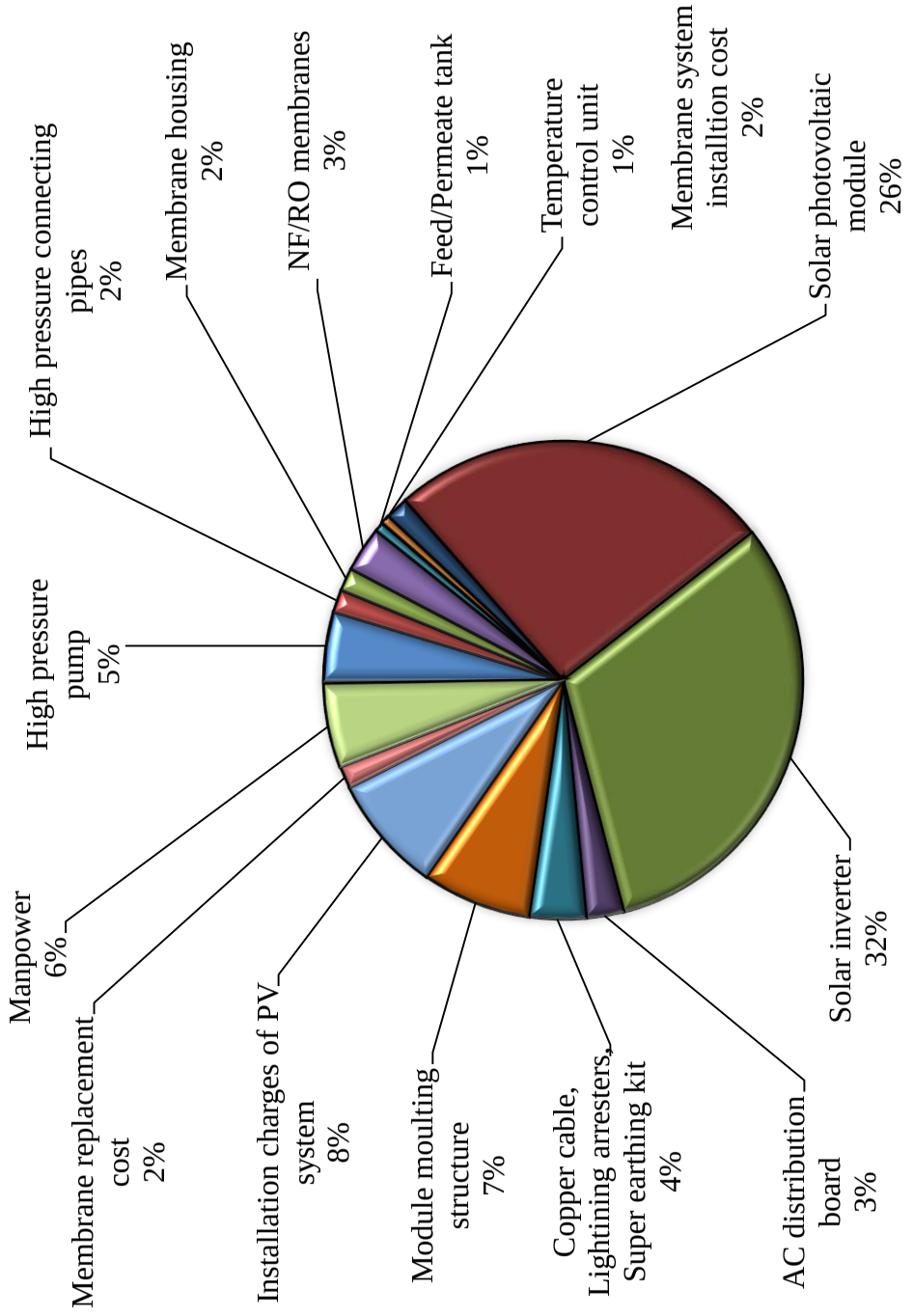

Figure 6.1. Cost distribution of hybrid PV-NF/RO water treatment system.

Table 6.4. Effect of monthly PSSH fluctuation on average monthly water production cost.

Month	PSSH	Water production cost (Rs./m^3)		
		PV-Hybrid	PV-NF	PV-RO
June	7.57	79.11	125.60	317.43
July	7.55	79.32	125.93	318.27
August	7.78	76.98	122.21	308.86
September	7.93	75.52	119.89	303.02
October	5.80	103.25	163.93	414.30
November	5.40	110.90	176.07	444.99
December	4.23	141.58	224.77	568.07
January	5.58	107.32	170.39	430.63
February	6.18	96.90	153.85	388.82
March	7.25	82.60	131.14	331.44
April	8.25	72.59	115.24	291.26
May	7.72	77.57	123.16	311.26

Table 6.5. Annual per cubic meter water production cost (Rs.) with and without battery storage

Scheme	Annual water production cost without battery storage (Rs./m^3)	Annual water production cost with battery storage (Rs./m^3)
Hybrid	99.81	133.88
NF	158.46	219.63
RO	400.49	555.08

Table 6.6. Effect of subsidy on per cubic meter water production cost.

Non-subsidized water production cost (Rs./m^3)	Subsidized water production cost (Rs./m^3)						
	30%	40%	50%	60%	70%	80%	90%
Hybrid 97.28	80.03	70.52	63.47	56.42	49.36	42.31	35.25
NF 154.44	122.49	106.06	93.39	80.71	68.04	55.37	42.69
RO 390.32	309.58	268.06	236.03	204.00	171.96	139.93	107.90

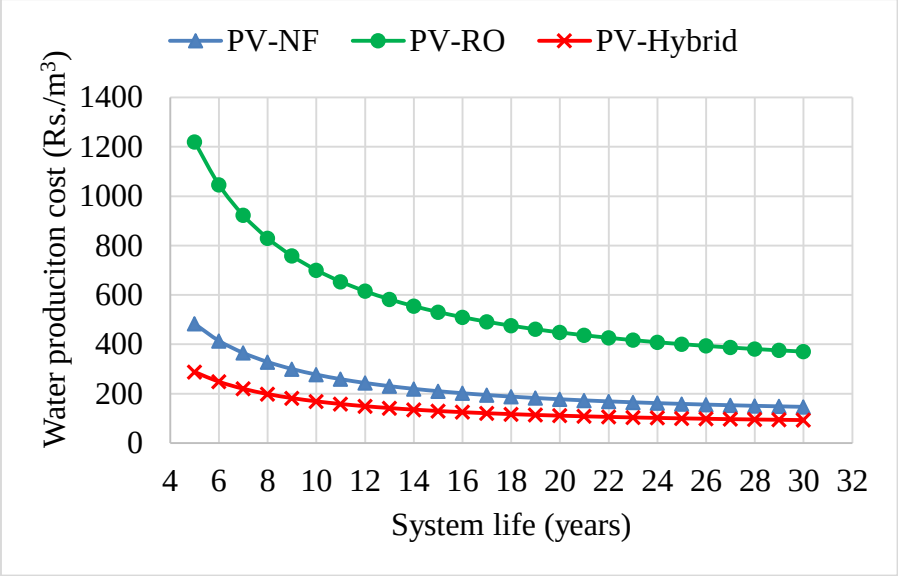

Figure 6.2. The effect of increasing system life on per cubic meter water production cost.

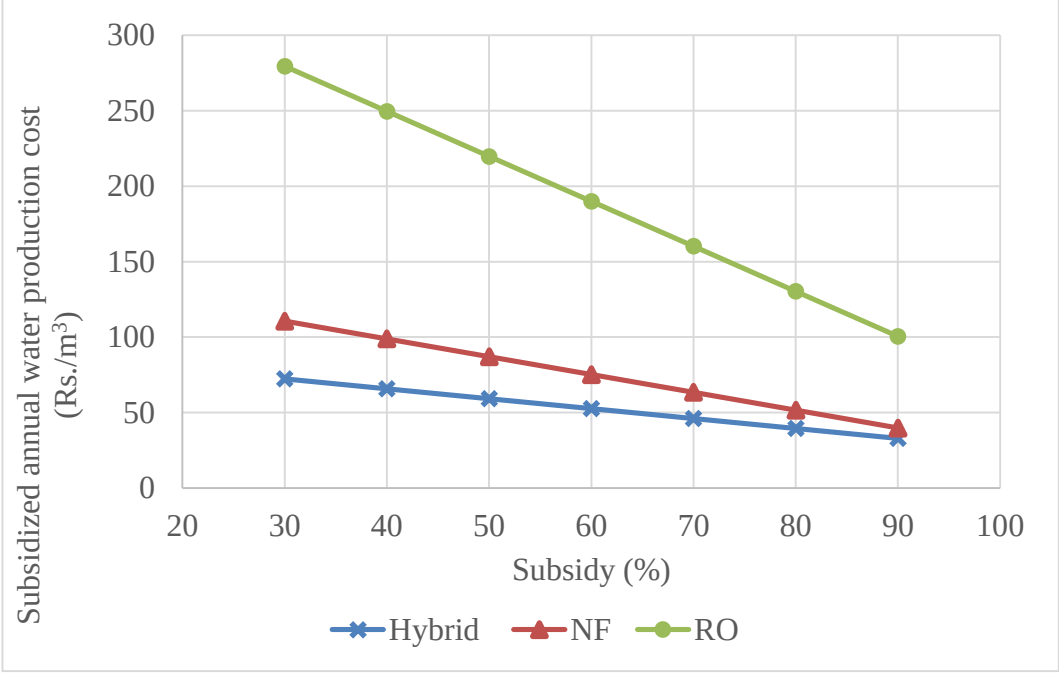

Figure 6.3. Effect of subsidy on per cubic meter water production cost

Table 6.7. Comparison of per cubic meter water production cost.

Reference	Year	Brackish water TDS (mg/l)	Recovery (%)	SEC (kWh/m^3)	Water production Cost (Rs./m^3)
Present Study		**1500**	**35.79**	**5.02**	**99.81 (without battery) 133.88 (with battery)**
[35]	2012	1700	30	32	-
[43]	2011	6000	-	-	145.02
[190]	2011	1700	29	13.82	-
[205]	2009	800	12.6	1.57	-
[30]	2008	1000	-	-	901.95
[52]	2004	1280-3200	27	3.03	767.26
[6]	2002	2000	-	-	224.28
[18]	2000	1000	-	-	392

Table 6.8. Water production cost of different solar powered desalination technologies.

Solar powered desalination techniques	Plant capacity (m^3/day)	Water production cost (Rs./m^3)	Reference
PV-NF/RO	**0.934**	**99.81 (without battery) 133.88 (with battery)**	**Present study**
PV-RO (SWRO)	120-12	480.58-1753.05	[6, 18, 99, 244]
PV-RO (BWRO)	250	438.26	[6, 18, 99, 244]
PV-ED	<100	350.61 - 967.2	[137, 245]
Solar pond	20000-200000	42.92 - 53.80	[191]
Solar-MEH	1-100	157.17-392.93	[159]
Solar-MD	0.15-10	634.73-1178.78	[20]
Solar-CSP/MED	>5000	145.08-169.26	[14]

Chapter 7.
Conclusions and Recommendations

7.1 Conclusions

The combination of photovoltaic (PV) system with nanofiltration - reverse osmosis (NF–RO) is one of the most promising solutions, especially in remote and arid regions. A techno-economic study was conducted on small scale hybrid NF and RO water desalination system powered by PV system.

Physical aspects of characterizing NF and RO membranes from various manufacturing brands have been investigated. Physical surface characteristics including surface roughness, occurrence of functional groups and hydrophobicity/hydrophilicity properties were determined by atomic force microscopy (AFM), fourier transform infrared spectroscopy (FTIR) and contact angle measurement respectively. A correlation between surface properties and membrane filtration results was obtained. Finally, the following conclusions could be drawn from this study:

1. The AFM technique has already proved earlier that rough surfaces are more vulnerable to fouling which causes decline in flux and salt rejection. The CSM RO membrane was found to be the smoothest, with an RMS (Rq) value of 33.99 µm.
2. Usually membrane materials having large contact angle are prone to adsorption of various solutes. The smaller contact angle (higher hydrophilicity) and smoother surface of CSM membrane among RO membranes and NF250 among NF membranes could be the reason of its better performance.
3. In order to authenticate functional groups on the membrane surfaces, FTIR analysis graphs were obtained for each virgin membrane. This analysis revealed that all RO and NF membranes contained thin polyamide layer with polysulfone support.
4. The X-Ray diffraction analysis (XRD) patterns of all inorganically fouled membranes were carried out and calcite ($CaCO_3$) was observed as a common element of the crystalline phase deposits observed on all membrane surfaces.

Experimental investigations were carried out to study the effect of feed water temperature, pressure, salt concentration and pH on the commercially available small-scale CSM RO membrane. The response surface methodology (RSM) approach using central composite design (CCD) was used for optimization of input process conditions in terms of increased water recovery, salt rejection, while simultaneously maintaining least energy consumption. The artificial neural network (ANN) model was developed and trained with data generated from RSM experimental design. The developed ANN model was used to validate RSM optimized process conditions. Furthermore, an experiment was conducted at optimum input process conditions to validate RSM and ANN predictions. Finally, the following conclusions could be drawn from the present study:

1. After using RSM optimization approach, CSM RO membrane showed the best performance among all RO membranes with 19.25% water recovery, 89.2% salt rejection and 17.6 kWh/m^3 of SEC. Also, NF250 showed the best performance among NF membranes with 18.98% water recovery, 70.64% salt rejection and 9.35 kWh/m^3 of SEC.
2. ANN predicted that the CSM RO membrane showed its best performance among all RO membranes with a maximum of 19.51% water recovery, 88.92% TDS rejection and 16.60 kWh/m^3 SEC. Also, NF250 showed the best performance among NF membranes with 18.59% water recovery, 71.4% salt rejection and 9.43 kWh/m^3 of SEC.
3. The values predicted by ANN model were closer to the experimental results than the values obtained by RSM.
4. NF-C-RO hybrid configuration showed an optimum performance with 35.79% water recovery, 78.51% salt rejection and 5.02 kWh/m^3 SEC.
5. In order to evaluate the feasibility of PV systems with brackish water NF-RO hybrid water treatment system, it could be concluded that amount of AC current generated by 1.5 kWh PV system during the PSSH was enough to operate the NF-C-RO hybrid membrane unit.

Economic feasibility for the PV assisted NF-RO system was established based on a cost analysis of per cubic meter water production. The comparative results were presented for each configuration of membrane system and various interpretations and conclusions are presented below:

1. The water production cost of NF-RO hybrid system (Rs.99.81/m^3) was about 1.6 times lesser than NF (Rs.158.46/m^3) and 4 times lesser than RO (Rs.400.49/m^3) system in isolation. It depended mainly on water recovery and SEC.

2. The major share of cost was of PV system, which contributed more than 50% of overall cost.
3. The water production cost of Rs.146.5/m^3, Rs.370.26/m^3 and Rs.92.87/m^3 for the PV-NF, PV-RO and PV-NF/RO hybrid membrane systems respectively could be reached when the plant life increased to 30 years.
4. The water production cost could be further reduced after increasing subsidy (or tax reduction to encourage using PV) provided by the government. Based on the water production cost corresponding to the provided subsidy, an incentive of 10% increment on subsidy could have resulted in a reduction from 17% to 72% depending on configuration of the membrane system. Therefore, on increasing the subsidy from 30% to 90%, the cost of per cubic meter water production varied from Rs.80/m^3 to Rs.35/m^3 in hybrid membrane configuration, Rs.122/m^3 to Rs.42/m^3 in NF and Rs.309/m^3 to Rs.107/m^3 in RO membrane system.
5. Annual water production cost with battery storage was about 34% more than the system without battery storage in case of hybrid system and 39% in case of single membrane system.

7.2 Recommendations for future study

A field level pilot plant is suggested based on the present findings as an extension of this study (Figure 7.1). Following features are recommended for the pilot study:

a) Brackish groundwater hybrid membrane treatment system with proposed NF-C-RO concentrate staging configuration.
b) Evaluation of the plant performance with actual groundwater of fluctuating water quality.
c) Utilization of surplus solar energy for water pumping.
d) Battery bank installation to facilitate stabilized power supply during fluctuation and non-sunny days.
e) Bigger size PV and NF-RO system to provide the drinking water for a small community (75-100 people).
f) Consideration of reject management issues.

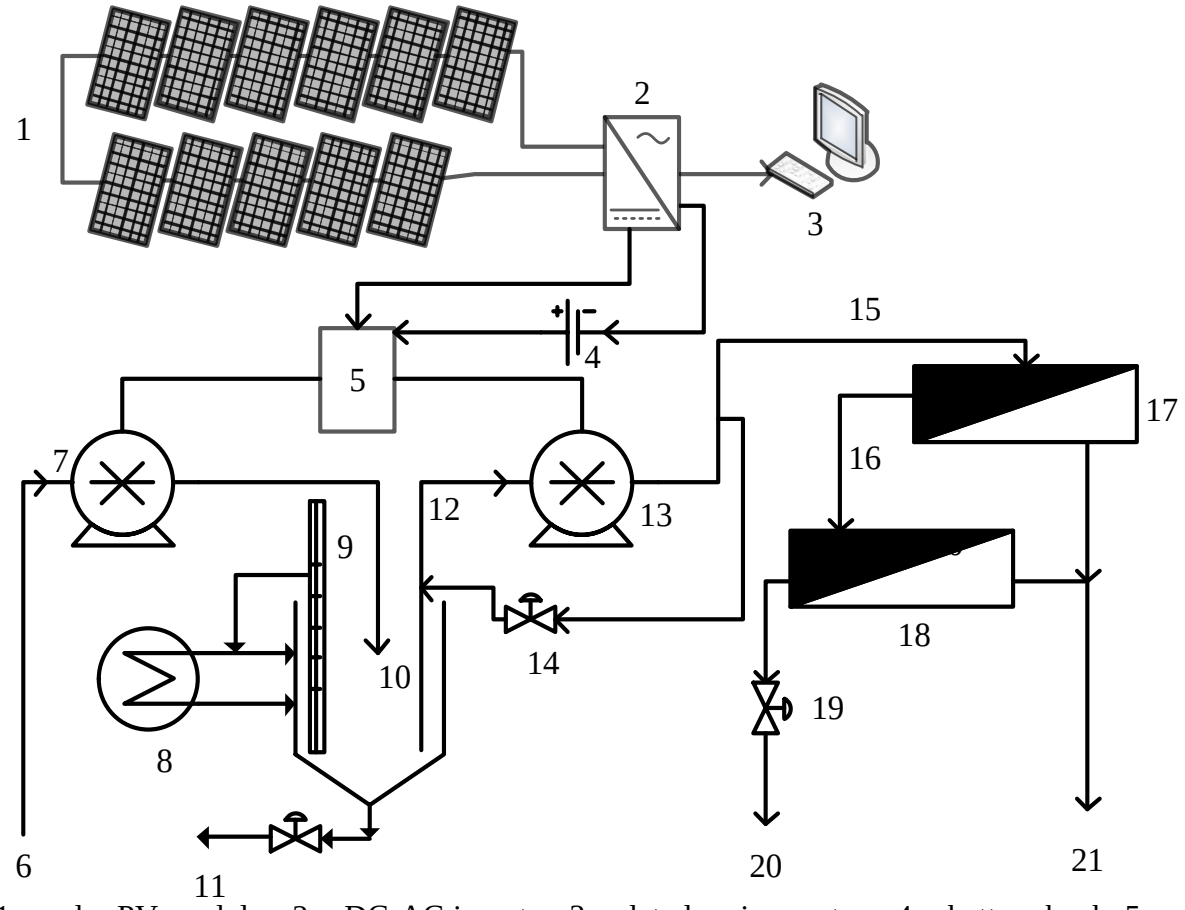

1 = solar PV modules, 2 = DC-AC inverter, 3 = data logging system, 4 = battery bank, 5 = AC distribution board, 6 = groundwater source, 7 = water pump, 8 = temperature controller, 9 = temperature probe, 10 = feed water tank, 11 = valve, 12 & 15 = feed water stream, 13 = high pressure pump, 14 = bypass valve, 16 = concentrate of NF, 17 = NF module, 18 = RO module, 19 = pressure control valve, 20 = concentrate stream, 21 = permeate stream.

Figure 7.1. Proposed pilot plant scheme of hybrid PV-NF/RO membrane system.

References

[1] Abdallah S., Abu-Hilal M., and Mohsen M. S., Performance of a photovoltaic powered reverse osmosis system under local climatic conditions, Desalination, 183, 95-104, 2005.

[2] Abraham T. and Luthra A., Socio-economic & technical assessment of photovoltaic powered membrane desalination processes for India, Desalination, 268, 238-248, 2011.

[3] Acra A., Raffoul Z., and Karahagopian Y., Solar Disinfection of Drinking Water and Oral Rehydration Solutions: Guidelines for Household Application in Developing Countries, UNICEF, Amman, Hashemite Kingdom of Jordan 1984.

[4] Adams G. and Bubucis P., Calculating an artificial sea water formulation using spreadsheet matrices, Aquarium Sciences and Conservation, 2, 35-41, 1998.

[5] Aglietti G. S., Redi S., Tatnall A. R., and Markvart T., Harnessing High-Altitude Solar Power, Energy Conversion, IEEE Transactions on, 24, 442-451, 2009.

[6] Ahmad G. E. and Schmid J., Feasibility study of brackish water desalination in the Egyptian deserts and rural regions using PV systems, Energy Conversion and Management, 43, 2641-2649, 2002.

[7] Ahmed M., Shayya W. H., Hoey D., and Al-Handaly J., Brine disposal from reverse osmosis desalination plants in Oman and the United Arab Emirates, Desalination, 133, 135-147, 2001.

[8] Akin O. and Temelli F., Probing the hydrophobicity of commercial reverse osmosis membranes produced by interfacial polymerization using contact angle, XPS, FTIR, FE-SEM and AFM, Desalination, 278, 387-396, 2011.

[9] Al-Juwayhel F., El-Dessouky H., and Ettouney H., Analysis of single-effect evaporator desalination systems combined with vapor compression heat pumps, Desalination, 114, 253-275, 1997.

[10] Al-Karaghouli A. and Kazmerski L. L., Energy consumption and water production cost of conventional and renewable-energy-powered desalination processes, Renewable and Sustainable Energy Reviews, 24, 343-356, 2013.

[11] Al-Karaghouli A., Renne D., and Kazmerski L. L., Technical and economic assessment of photovoltaic-driven desalination systems, Renewable Energy, 35, 323-328, 2010.

[12] Al-Mobayed A. S., Mubeen F. M., and Balaji S., Comparison of the performance of hollow fine fiber and spiral-wound membranes in the Al-Jubail SWRO desalination plant, Desalination, 178, 273-286, 2005.

[13] Al-Mutaz I. S. and Al-Namlah A. M., Characteristics of dual purpose MSF desalination plants, Desalination, 166, 287-294, 2004.

[14] Al-Shammiri M. and Safar M., Multi-effect distillation plants: state of the art, Desalination, 126, 45-59, 1999.

[15] Al-Sofi M. A. K., Hassan A. M., Hamed O. A., Dalvi A. G. I., Kither M. N. M., Mustafa G. M., and Bamardouf K., Optimization of hybridized seawater desalination process, Desalination, 131, 147-156, 2000.

[16] Al-Wazzan Y., Safar M., and Mesri A., Reverse osmosis brine staging treatment of subsurface water, Desalination, 155, 141-151, 2003.

[17] Al Malki A., Al Amri M., and Al Jabri H., Experimental study of using renewable energy in the rural areas of Oman, Renewable Energy, 14, 319-324, 1998.

[18] Al Suleimani Z. and Nair V. R., Desalination by solar-powered reverse osmosis in a remote area of the Sultanate of Oman, Applied Energy, 65, 367-380, 2000.

[19] Alayemieka E., Lee S., and Kim D., Effect of membrane surface characteristics on hydraulic flux balance and feed stream translation in concentrate multi-stage system, Desalination, 247, 64-76, 2009.

[20] Ali M. I., Summers E. K., Arafat H. A., and V J. H. L., Effects of membrane properties on water production cost in small scale membrane distillation systems, Desalination, 306, 60-71, 2012.

[21] Ali M. T., Fath H. E. S., and Armstrong P. R., A comprehensive techno-economical review of indirect solar desalination, Renewable and Sustainable Energy Reviews, 15, 4187-4199, 2011.

[22] AlMadani H. M. N., Water desalination by solar powered electrodialysis process, Renewable Energy, 28, 1915-1924, 2003.

[23] Appelo C. A. J., Multicomponent Ion Exchange and Chromatography in Natural Systems Mineralogical Society of America, United States, 1997.

[24] Arkhangelsky E., Kuzmenko D., and Gitis V., Impact of chemical cleaning on properties and functioning of polyethersulfone membranes, Journal of Membrane Science, 305, 176-184, 2007.

[25] Arnal J. M., Sancho M., Iborra I., Gozálvez J. M., Santafé A., and Lora J., Concentration of brines from RO desalination plants by natural evaporation, Desalination, 182, 435-439, 2005.

[26] Arora M., Maheshwari R. C., Jain S. K., and Gupta A., Use of membrane technology for potable water production, Desalination, 170, 105-112, 2004.

[27] Aybar H. S., Analysis of a mechanical vapor compression desalination system, Desalination, 142, 181-186, 2002.

[28] Aybar H. Ş., Akhatov J. S., Avezova N. R., and Halimov A. S., Solar powered RO desalination: Investigations on pilot project of PV powered RO desalination system, Appl. Sol. Energy, 46, 275-284, 2010.

[29] Balaban M., Guidebook details membrane desalination technology, Membrane Technology, 2007, 6, 2007.

[30] Banat F. and Jwaied N., Economic evaluation of desalination by small-scale autonomous solar-powered membrane distillation units, Desalination, 220, 566-573, 2008.

[31] Banat F. and Jwaied N., Exergy analysis of desalination by solar-powered membrane distillation units, Desalination, 230, 27-40, 2008.

[32] Banat F., Jwaied N., Rommel M., Koschikowski J., and Wieghaus M., Desalination by a "compact SMADES" autonomous solarpowered membrane distillation unit, Desalination, 217, 29-37, 2007.

[33] Banat F., Jwaied N., Rommel M., Koschikowski J., and Wieghaus M., Performance evaluation of the "large SMADES" autonomous desalination solar-driven membrane distillation plant in Aqaba, Jordan, Desalination, 217, 17-28, 2007.

[34] Banat F., Qiblawey H., and Al- Nasser Q., Design and Operation of Small-Scale Photovoltaic-Driven Reverse Osmosis (PV-RO) Desalination Plant for Water Supply in Rural Areas, Computational Water, Energy, and Environmental Engineering, 1, 31-36, 2012.

[35] Banat F., Qiblawey H., and Al-Nasser Q., Design and Operation of Small-Scale Photovoltaic-Driven Reverse Osmosis (PV-RO) Desalination Plant for Water Supply in Rural Areas Computational Water, Energy, and Environmental Engineering, 1, 31-36, 2012.

[36] Banerjee P., DasGupta S., and De S., Removal of dye from aqueous solution using a combination of advanced oxidation process and nanofiltration, Journal of Hazardous Materials, 140, 95-103, 2007.

[37] Bartels C., Franks R., Rybar S., Schierach M., and Wilf M., The effect of feed ionic strength on salt passage through reverse osmosis membranes, Desalination, 184, 185-195, 2005.

[38] Beringer S., Schilke H., Lohse I., and Seckmeyer G., Case study showing that the tilt angle of photovoltaic plants is nearly irrelevant, Solar Energy, 85, 470-476, 2011.

[39] Bezerra M. A., Santelli R. E., Oliveira E. P., Villar L. S., and Escaleira L. A., Response surface methodology (RSM) as a tool for optimization in analytical chemistry, Talanta, 76, 965-977, 2008.

[40] Bhattacharya P. K., Jayan R., and Bhattacharjee C., A combined biological and membrane-based treatment of prehydrolysis liquor from pulp mill, Separation and Purification Technology, 45, 119-130, 2005.

[41] Bhatti M. S., Reddy A. S., Kalia R. K., and Thukral A. K., Modeling and optimization of voltage and treatment time for electrocoagulation removal of hexavalent chromium, Desalination, 269, 157-162, 2011.

[42] Bilton A. M., Kelley L. C., and Dubowsky S., Photovoltaic reverse osmosis — Feasibility and a pathway to develop technology, Desalination and Water Treatment, 31, 24-34, 2011.

[43] Bilton A. M., Wiesman R., Arif A. F. M., Zubair S. M., and Dubowsky S., On the feasibility of community-scale photovoltaic-powered reverse osmosis desalination systems for remote locations, Renewable Energy, 36, 3246-3256, 2011.

[44] Boesch W. W., World's first solar powered reverse osmosis desalination plant, Desalination, 41, 233-237, 1982.

[45] Bohdziewicz J., Bodzek M., and Wąsik E., The application of reverse osmosis and nanofiltration to the removal of nitrates from groundwater, Desalination, 121, 139-147, 1999.

[46] Bou-Hamad S., Abdel-Jawad M., Al-Tabtabaei M., and Al-Shammari S., Comparative performance analysis of two seawater reverse osmosis plants: Twin hollow fine fiber and spiral wound membranes, Desalination, 120, 95-106, 1998.

[47] Bouguecha S., Hamrouni B., and Dhahbi M., Small scale desalination pilots powered by renewable energy sources: case studies, Desalination, 183, 151-165, 2005.

[48] Bowen W. R., Mohammad A. W., and Hilal N., Characterisation of nanofiltration membranes for predictive purposes — use of salts, uncharged solutes and atomic force microscopy, Journal of Membrane Science, 126, 91-105, 1997.

[49] Bundschuh J. and Hoinkis J., Renewable energy applications for freshwater production, CRC Press, Boca Raton, Florida, 2012.

[50] Bureau P. R., Annual Report 2009, The Population Reference Bureau, Washington, DC, USA, 2009.

[51] Buros O. K., The ABCs of Desalting, International Desalination Association, Topsfield, Massachusetts, USA, 2000.

[52] Carvalho P. C. M., Riffel D. B., Freire C., and Montenegro F. F. D., The Brazilian experience with a photovoltaic powered reverse osmosis plant, Progress in Photovoltaics: Research and Applications, 12, 373-385, 2004.

[53] Chafidz A., Al-Zahrani S., Al-Otaibi M. N., Hoong C. F., Lai T. F., and Prabu M., Portable and integrated solar-driven desalination system using membrane distillation for arid remote areas in Saudi Arabia, Desalination, 345, 36-49, 2014.

[54] Chakrabarty B., Ghoshal A. K., and Purkait M. K., SEM analysis and gas permeability test to characterize polysulfone membrane prepared with polyethylene glycol as additive, Journal of Colloid and Interface Science, 320, 245-253, 2008.

[55] Chakraborty S., Dasgupta J., Farooq U., Sikder J., Drioli E., and Curcio S., Experimental analysis, modeling and optimization of chromium (VI) removal from aqueous solutions by polymer-enhanced ultrafiltration, Journal of Membrane Science, 456, 139-154, 2014.

[56] Chakraborty S., Purkait M. K., DasGupta S., De S., and Basu J. K., Nanofiltration of textile plant effluent for color removal and reduction in COD, Separation and Purification Technology, 31, 141-151, 2003.

[57] Cheah S.-F., Photovoltaic Reverse Osmosis Desalination System, Bureau of Reclamation, Denver Federal Center, Denver, Colorado, Littleton, Colorado, USA, 30 pp., 2004.

[58] Chelme-Ayala P., Smith D. W., and El-Din M. G., Membrane concentrate management options: a comprehensive critical review, Canadian Journal of Civil Engineering, 36, 1107-1119, 2009.

[59] Chen S.-S., Taylor J. S., Mulford L. A., and Norris C. D., Influences of molecular weight, molecular size, flux, and recovery for aromatic pesticide removal by nanofiltration membranes, Desalination, 160, 103-111, 2004.

[60] Cherif H. and Belhadj J., Large-scale time evaluation for energy estimation of stand-alone hybrid photovoltaic–wind system feeding a reverse osmosis desalination unit, Energy, 36, 6058-6067, 2011.

[61] Childs W. D., Dabiri A. E., Al-Hinai H. A., and Abdullah H. A., VARI-RO solar-powered desalting technology, Desalination, 125, 155-166, 1999.

[62] Clarke D. P., Al-Abdeli Y. M., and Kothapalli G., The effects of including intricacies in the modelling of a small-scale solar-PV reverse osmosis desalination system, Desalination, 311, 127-136, 2013.

[63] Conesa A., Gumí T., Coello J., and Palet C., Near infrared spectroscopy: A novel technique for classifying and characterizing polysulfone membranes, Journal of Membrane Science, 300, 122-130, 2007.

[64] Dallas S., Sumiyoshi N., Kirk J., Mathew K., and Wilmot N., Efficiency analysis of the Solarflow – An innovative solar-powered desalination unit for treating brackish water, Renewable Energy, 34, 397-400, 2009.

[65] Darwish M. A., Thermal analysis of multi-stage flash desalting systems, Desalination, 85, 59-79, 1991.

[66] Darwish M. A., Thermal analysis of vapor compression desalination system, Desalination, 69, 275-295, 1988.

[67] Das C. and De S., Steady state modeling for membrane separation of pretreated liming effluent under cross-flow mode, Journal of Membrane Science, 338, 175-181, 2009.

[68] Das C., Patel P., De S., and DasGupta S., Treatment of tanning effluent using nanofiltration followed by reverse osmosis, Separation and Purification Technology, 50, 291-299, 2006.

[69] Draper N. R. and Smith H., Applied Regression Analysis Wiley, New York, 2004.

[70] Drioli E., Criscuoli A., and Curcio E., Integrated membrane operations for seawater desalination, Desalination, 147, 77-81, 2002.

[71] Drioli E., Curcio E., Di Profio G., Macedonio F., and Criscuoli A., Integrating Membrane Contactors Technology and Pressure-Driven Membrane Operations for Seawater Desalination: Energy, Exergy and Costs Analysis, Chemical Engineering Research and Design, 84, 209-220, 2006.

[72] Effendi Y., Three years experiences for PVRO-desalination, 1988 1988, 1194-1199 vol.1192.

[73] El-Manharawy S. and Hafez A., How to estimate inorganic fouling flux on RO membrane by using ROIFA-4?, Desalination, 277, 407-413, 2011.

[74] El-Manharawy S. and Hafez A., A new chemical classification system of natural waters for desalination and other industrial uses, Desalination, 156, 163-180, 2003.

[75] El-Manharawy S. and Hafez A., ROIFA-5 model and Spreadsheet for Predicting Total Hardness Fouling Flux and Saturation Factors on the RO-Membrane, Alexandria, Egypt2006, 685-702.

[76] Elimelech M., Chen W. H., and Waypa J. J., Measuring the zeta (electrokinetic) potential of reverse osmosis membranes by a streaming potential analyzer, Desalination, 95, 269-286, 1994.

[77] Elimelech M., Xiaohua Z., Childress A. E., and Seungkwan H., Role of membrane surface morphology in colloidal fouling of cellulose acetate and composite aromatic polyamide reverse osmosis membranes, Journal of Membrane Science, 127, 101-109, 1997.

[78] Eltawil M. A., Zhengming Z., and Yuan L., A review of renewable energy technologies integrated with desalination systems, Renewable and Sustainable Energy Reviews, 13, 2245-2262, 2009.

[79] Fahmy F. H., Ahmed N. M., and Farghally H. M., Optimization of Renewable Energy Power System for Small Scale Brackish Reverse Osmosis Desalination Unit and a Tourism Motel in Egypt, Smart Grid and Renewable Energy, 3, 43-50, 2012.

[80] Farahbod F., Mowla D., Jafari Nasr M. R., and Soltanieh M., Experimental study of a solar desalination pond as second stage in proposed zero discharge desalination process, Solar Energy, 97, 138-146, 2013.

[81] Faten Hosney F., Ninet Mohamed A., and Hanaa Mohamed F., Optimization of Renewable Energy Power System for Small Scale Brackish Reverse Osmosis Desalination Unit and a Tourism Motel in Egypt, Smart Grid and Renewable Energy, 03, 43-43, 2012.

[82] Fawell J. and Nieuwenhuijsen M. J., Contaminants in drinking water: Environmental pollution and health, British Medical Bulletin, 68, 199-208, 2003.

[83] Feitz A. J., Boyden B. H., and Waite T. D., Evaluation of two solar pilot scale fixed-bed photocatalytic reactors, Water Research, 34, 3927-3932, 2000.

[84] Ferreira S. L. C., Bruns R. E., da Silva E. G. P., dos Santos W. N. L., Quintella C. M., David J. M., de Andrade J. B., Breitkreitz M. C., Jardim I. C. S. F., and Neto B. B., Statistical designs and response surface techniques for the optimization of chromatographic systems, Journal of Chromatography A, 1158, 2-14, 2007.

[85] Fiorenza G., Sharma V. K., and Braccio G., Techno-economic evaluation of a solar powered water desalination plant, Energy Conversion and Management, 44, 2217-2240, 2003.

[86] Fischetti M., Fresh from the Sea, Sci Am, 297, 118-119, 2007.

[87] Foster S., Lawrence A., and Morris B., Groundwater in Urban Development: Assessing Management Needs and Formulating Policy Strategies, World Bank Publication, Washington DC, USA, 1998.

[88] Fu Y., Liu X., and Yuan Z., Life-cycle assessment of multi-crystalline photovoltaic (PV) systems in China, Journal of Cleaner Production, 86, 180-190, 2015.

[89] Gabelich C. J., Ishida K. P., Gerringer F. W., Evangelista R., Kalyan M., and Suffet I. H. M., Control of residual aluminum from conventional treatment to improve reverse osmosis performance, Desalination, 190, 147-160, 2006.

[90] Gabelich C. J., Xu P., and Cohen Y., Chapter 10 Concentrate Treatment for Inland Desalting. In: Sustainability Science and Engineering, Isabel, C. E. and Andrea, I. S. (Eds.), Elsevier, 2010.

[91] Gandhidasan P. and Al-Mojel S. A., Effect of feed pressure on the performance of the photovoltaic powered reverse osmosis seawater desalination system, Renewable Energy, 34, 2824-2830, 2009.

[92] Garmana M. A. and Muntasserb M. A., Sizing and thermal study of salinity gradient solar ponds connecting with the MED desalination unit, Desalination, 222, 689-695, 2008.

[93] Gedam V. V., Patil J. L., Kagne S., Sirsam R. S., and Labhasetwar P., Performance evaluation of polyamide reverse osmosis membrane for removal of contaminants in ground water collected from chandrapur district, Journal of membrane Science and Technology, 2, 2-5, 2012.

[94] Geyikçi F., Kılıç E., Çoruh S., and Elevli S., Modelling of lead adsorption from industrial sludge leachate on red mud by using RSM and ANN, Chemical Engineering Journal, 183, 53-59, 2012.

[95] Gilron J., Folkman Y., Savliev R., Waisman M., and Kedem O., WAIV — wind aided intensified evaporation for reduction of desalination brine volume, Desalination, 158, 205-214, 2003.

[96] Gryta M., Concentration of NaCl solution by membrane distillation integrated with crystallization, Separation Science and Technology, 37, 3535-3558, 2002.

[97] Gude V. G., Nirmalakhandan N., and Deng S., Renewable and sustainable approaches for desalination, Renewable and Sustainable Energy Reviews, 14, 2641-2654, 2010.

[98] Gunerhan H. and Hepbasli A., Determination of the optimum tilt angle of solar collectors for building applications, Building and Environment, 42, 779-783, 2007.

[99] Hafez A. and El-Manharawy S., Economics of seawater RO desalination in the Red Sea region, Egypt. Part 1. A case study, Desalination, 153, 335-347, 2003.

[100] Halaoui L. I., Abrams N. M., and Mallouk T. E., Increasing the Conversion Efficiency of Dye-Sensitized TiO2 Photoelectrochemical Cells by Coupling to Photonic Crystals, The Journal of Physical Chemistry B, 109, 6334-6342, 2005.

[101] Hanjra M. A. and Qureshi M. E., Global water crisis and future food security in an era of climate change, Food Policy, 35, 365-377, 2010.

[102] Hasnain S. M. and Alajlan S. A., Coupling of PV-powered RO brackish water desalination plant with solar stills, Desalination, 116, 57-64, 1998.

[103] Hassabou A. H., Spinnler M., and Polifke W., Tecnoeconomic Analysis of Medium and Large-sacle Desalination Plants Driven by Concentrated Solar Systems in the Mena Region, Energy Procedia, 42, 735-744, 2013.

[104] Hawlader M. N. A., Ho J. C., and Chua Kok T., Desalination of seawater: an experiment with RO membranes, Desalination, 132, 275-280, 2000.

[105] Helal A. M., Al-Malek S. A., and Al-Katheeri E. S., Economic feasibility of alternative designs of a PV-RO desalination unit for remote areas in the United Arab Emirates, Desalination, 221, 1-16, 2008.

[106] Hemat R. A. S., Air, Urotext, 2006.

[107] Hoffman E. J., 3 - Single-Stage Membrane Separations. In: Membrane Separations Technology, Hoffman, E. J. (Ed.), Gulf Professional Publishing, Burlington, 2003.

[108] Hrayshat E. S., Brackish water desalination by a stand alone reverse osmosis desalination unit powered by photovoltaic solar energy, Renewable Energy, 33, 1784-1790, 2008.

[109] Huiting H., Kappelhof J. W. N. M., and Bosklopper T. G. J., Operation of NF/RO plants: from reactive to proactive, Desalination, 139, 183-189, 2001.

[110] Iaquaniello G., Salladini A., Mari A., Mabrouk A. A., and Fath H. E. S., Concentrating solar power (CSP) system integrated with MED–RO hybrid desalination, Desalination, 336, 121-128, 2014.

[111] Ibáñez R., Pérez-González A., Gómez P., Urtiaga A. M., and Ortiz I., Acid and base recovery from softened reverse osmosis (RO) brines. Experimental assessment using model concentrates, Desalination, 309, 165-170, 2013.

[112] Idris A., Kormin F., and Noordin M. Y., Application of response surface methodology in describing the performance of thin film composite membrane, Separation and Purification Technology, 49, 271-280, 2006.

[113] ISA, Solar PV Industry 2010: Contemporary scenario and emerging trends, India, India Semiconductor Association, Bangalore, India, 56 pp., 2010.

[114] Jacobson M. Z., Review of solutions to global warming, air pollution, and energy security, Energy & Environmental Science, 2, 148-173, 2009.

[115] Jiang C., Wang Y., Zhang Z., and Xu T., Electrodialysis of concentrated brine from RO plant to produce coarse salt and freshwater, Journal of Membrane Science, 450, 323-330, 2014.

[116] Joyce A., Loureiro D., Rodrigues C., and Castro S., Small reverse osmosis units using PV systems for water purification in rural places, Desalination, 137, 39-44, 2001.

[117] Kalogirou, http://www.desware.net/desa7.aspx, 1996.

[118] Kamizono H., Congruent dissolution of high-level waste glass in synthetic groundwater, Journal of Nuclear Materials, 172, 319-324, 1990.

[119] Kapadia R. N. and Pandya V. P., Scanning electron microscopy study on reverse osmosis membranes prepared from Indian cellulosic polymers, Desalination, 34, 199-215, 1980.

[120] Karabelas A. J., Kostoglou M., and Koutsou C. P., Modeling of spiral wound membrane desalination modules and plants– review and research priorities, Desalination, doi: http://dx.doi.org/10.1016/j.desal.2014.10.002, 2015. 2015.

[121] Karabelas A. J., Koutsou C. P., and Kostoglou M., The effect of spiral wound membrane element design characteristics on its performance in steady state desalination — A parametric study, Desalination, 332, 76-90, 2014.

[122] Keeper B. G., Hembree R. D., and Schrack F. C., Optimized matching of solar photovoltaic power with reverse osmosis desalination, Desalination, 54, 89-103, 1985.

[123] Keoleian G. A. and Lewis G. M., Application of life-cycle energy analysis to photovoltaic module design, Progress in Photovoltaics: Research and Applications, 5, 287-300, 1997.

[124] Kershman S. A., Rheinländer J., Neumann T., and Goebel O., Hybrid wind/PV and conventional power for desalination in Libya—GECOL's facility for medium and small scale research at Ras Ejder, Desalination, 183, 1-12, 2005.

[125] Kesieme U. K., Milne N., Aral H., Cheng C. Y., and Duke M., Economic analysis of desalination technologies in the context of carbon pricing, and opportunities for membrane distillation, Desalination, 323, 66-74, 2013.

[126] Khayet M., Solar desalination by membrane distillation: Dispersion in energy consumption analysis and water production costs (a review), Desalination, 308, 89-101, 2013.

[127] Khayet M. and Cojocaru C., Artificial neural network model for desalination by sweeping gas membrane distillation, Desalination, 308, 102-110, 2013.

[128] Khayet M. and Cojocaru C., Artificial neural network modeling and optimization of desalination by air gap membrane distillation, Separation and Purification Technology, 86, 171-182, 2012.

[129] Khayet M., Cojocaru C., and Essalhi M., Artificial neural network modeling and response surface methodology of desalination by reverse osmosis, Journal of Membrane Science, 368, 202-214, 2011.

[130] Khayet M., Essalhi M., Armenta-Déu C., Cojocaru C., and Hilal N., Optimization of solar-powered reverse osmosis desalination pilot plant using response surface methodology, Desalination, 261, 284-292, 2010.

[131] Khayet M. and Mengual J. I., Effect of salt type on mass transfer in reverse osmosis thin film composite membranes, Desalination, 168, 383-390, 2004.

[132] Kolhe M., Techno-Economic Optimum Sizing of a Stand-Alone Solar Photovoltaic System, Energy Conversion, IEEE Transactions on, 24, 511-519, 2009.

[133] Koyuncu I., Yazgan M., Topacik D., and Sarikaya H. Z., Evaluation of the low pressure RO and NF membranes for an alternative treatment of Buyukcekmece Lake, Water Science and Technology: Water Supply, 1, 107-115, 2001.

[134] Krishna H. J., Introduction to Desalination Technologies, Texas Water Development, 2, 2004.

[135] Kumar S., Thermal–economic analysis of a hybrid photovoltaic thermal (PVT) active solar distillation system: Role of carbon credit, Urban Climate, 5, 112-124, 2013.

[136] Kumaravel M., Sulochana K., Gopalaswami R., and Saravanan G., Solar Photo Voltaics Powered Seawater Desalination Plants and their Techno-Economics. In: Proceedings of ISES World Congress 2007 (Vol. I – Vol. V), Goswami, D. Y. and Zhao, Y. (Eds.), Springer Berlin Heidelberg, 2009.

[137] Kuroda O., Takahashi S., Wakamatsu K., Itoh S., Kubota S., Kikuchi K., Eguchi Y., Ikenaga Y., Sohma N., and Nishinoiri K., An electrodialysis sea water desalination system powered by photovoltaic cells, Desalination, 65, 161-169, 1987.

[138] Kwak S.-Y. and Woo Ihm D., Use of atomic force microscopy and solid-state NMR spectroscopy to characterize structure-property-performance correlation in high-flux reverse osmosis (RO) membranes, Journal of Membrane Science, 158, 143-153, 1999.

[139] Kwak S.-Y., Yeom M.-O., Roh I. J., Kim D. Y., and Kim J.-J., Correlations of chemical structure, atomic force microscopy (AFM) morphology, and reverse osmosis (RO) characteristics in aromatic polyester high-flux RO membranes, Journal of Membrane Science, 132, 183-191, 1997.

[140] Laborde H. M., França K. B., Neff H., and Lima A. M. N., Optimization strategy for a small-scale reverse osmosis water desalination system based on solar energy, Desalination, 133, 1-12, 2001.

[141] Lalia B. S., Kochkodan V., Hashaikeh R., and Hilal N., A review on membrane fabrication: Structure, properties and performance relationship, Desalination, 326, 77-95, 2013.

[142] Lee H.-J., Sarfert F., Strathmann H., and Moon S.-H., Designing of an electrodialysis desalination plant, Desalination, 142, 267-286, 2002.

[143] Lee W., Ahn C. H., Hong S., Kim S., Lee S., Baek Y., and Yoon J., Evaluation of surface properties of reverse osmosis membranes on the initial biofouling stages under no filtration condition, Journal of Membrane Science, 351, 112-122, 2010.

[144] Legros G., Havet I., Bruce N., Bonjour S., Rijal K., Takada M., and Dora C., The Energy Access Situation in Developing Countries, A Review Focusing on the Least Developed Countries and Sub-Saharan Africa, New York, USA, 2009.

[145] Libotean D., Giralt J., Giralt F., Rallo R., Wolfe T., and Cohen Y., Neural network approach for modeling the performance of reverse osmosis membrane desalting, Journal of Membrane Science, 326, 408-419, 2009.

[146] Lutchmiah K., Verliefde A. R. D., Roest K., Rietveld L. C., and Cornelissen E. R., Forward osmosis for application in wastewater treatment: A review, Water Research, 58, 179-197, 2014.

[147] Mahbub F., Hawlader M. N. A., and Mujumdar A. S., Combined water and power plant (CWPP) — a novel desalination technology, Desalination and Water Treatment, 5, 172-177, 2009.

[148] Mahmoud M. M., Solar electric powered reverse osmosis water desalination system for the rural village, Al Maleh: design and simulation, International Journal of Sustainable Energy, 23, 51-62, 2003.

[149] Malaeb L. and Ayoub G. M., Reverse osmosis technology for water treatment: State of the art review, Desalination, 267, 1-8, 2011.

[150] Malek A., Hawlader M. N. A., and Ho J. C., Design and economics of RO seawater desalination, Desalination, 105, 245-261, 1996.

[151] Mallevialle J., Odendaal P., and Wiesner M. R., The Emergence of Membranes in Water and Wastewater Treatment. In: Membrane Processes in Water Treatment, J. Mallevialle, P. O., M.R. Wiesner (Ed.), McGraw-Hill, 1996.

[152] Mandal M. K. and Bhattacharya P. K., Poly(ether-block-amide) membrane for pervaporative separation of pyridine present in low concentration in aqueous solution, Journal of Membrane Science, 286, 115-124, 2006.

[153] Mandal M. K., Sant S. B., and Bhattacharya P. K., Dehydration of aqueous acetonitrile solution by pervaporation using PVA–iron oxide nanocomposite membrane, Colloids and Surfaces A: Physicochemical and Engineering Aspects, 373, 11-21, 2011.

[154] Manolakos D., Mohamed E. S., Karagiannis I., and Papadakis G., Technical and economic comparison between PV-RO system and RO-Solar Rankine system. Case study: Thirasia island, Desalination, 221, 37-46, 2008.

[155] Martinetti C. R., Childress A. E., and Cath T. Y., High recovery of concentrated RO brines using forward osmosis and membrane distillation, Journal of Membrane Science, 331, 31-39, 2009.

[156] Masson L., Richards B. S., and Schäfer A. I., System design and performance testing of a hybrid membrane — photovltaic desalination system, Desalination, 179, 51-59, 2005.

[157] Mehdizadeh H., Membrane desalination plants from an energy–exergy viewpoint, Desalination, 191, 200-209, 2006.

[158] Meneses M., Pasqualino J. C., Céspedes-Sánchez R., and Castells F., Alternatives for Reducing the Environmental Impact of the Main Residue From a Desalination Plant, Journal of Industrial Ecology, 14, 512-527, 2010.

[159] Michael P., Marcel W., and Charlotte B., Roadmap for the Development of Desalination Powered by Renewable Energy 2010.

[160] Miller E. J., Review of Water Resources and Desalination Technologies Sandia National Laboratories Sandia National Laboratories, Albuquerque, NewMexico 87185 and Livermore, California, 2003.

[161] Misra A. K. and Mishra A., Study of quaternary aquifers in Ganga Plain, India: Focus on groundwater salinity, fluoride and fluorosis, Journal of Hazardous Materials, 144, 438-448, 2007.

[162] Mohamed E. S. and Papadakis G., Design, simulation and economic analysis of a stand-alone reverse osmosis desalination unit powered by wind turbines and photovoltaics, Desalination, 164, 87-97, 2004.

[163] Mohamed E. S., Papadakis G., Mathioulakis E., and Belessiotis V., A direct coupled photovoltaic seawater reverse osmosis desalination system toward battery based systems — a technical and economical experimental comparative study, Desalination, 221, 17-22, 2008.

[164] Moharram K. A., Abd-Elhady M. S., Kandil H. A., and El-Sherif H., Enhancing the performance of photovoltaic panels by water cooling, Ain Shams Engineering Journal, 4, 869-877, 2013.

[165] Mohsen M. S., Jaber J. O., and Afonso M. D., Desalination of brackish water by nanofiltration and reverse osmosis, Desalination, 157, 167, 2003.

[166] Molden D., Water for food, water for life : a comprehensive assessment of water management in agriculture, International Water Management Institute, Earthscan, London ; Sterling, VA, 2007.

[167] Montgomery D. C., Design and Analysis of Experiments, Wiley, New York, 2004.

[168] Morillo J., Usero J., Rosado D., El Bakouri H., Riaza A., and Bernaola F.-J., Comparative study of brine management technologies for desalination plants, Desalination, 336, 32-49, 2014.

[169] Murthy Z. V. P. and Vora M. M., Prediction of reverse osmosis performance using artificial neural network, Indian Journal of Chemical Technology 11, 108-115, 2004.

[170] Nandi B. K., Moparthi A., Uppaluri R., and Purkait M. K., Treatment of oily wastewater using low cost ceramic membrane: Comparative assessment of pore blocking and artificial neural network models, Chemical Engineering Research and Design, 88, 881-892, 2010.

[171] Narayanan P. K., Harkare W. P., Adhikary S. K., Dave N. J., Chauhan D. K., and Govindan K. P., Performance of an electrodialysis desalination plant in rural area, Desalination, 54, 145-150, 1985.

[172] National Solar Mission N., http://indianpowersector.com/electricity-regulation/national-solar-mission/, 2010.

[173] Nayak J. K. and Prajapati J. A., Handbook on Energy Conscious Buildings Indian Institute of Technology, Bombay and Solar Energy Centre, Ministry of Non-conventional Energy Sources, Government of India. , 2006.

[174] Nemeth J. E., Innovative system designs to optimize performance of ultra-low pressure reverse osmosis membranes, Desalination, 118, 63-71, 1998.

[175] Nourbakhsh H., Emam-Djomeh Z., Omid M., Mirsaeedghazi H., and Moini S., Prediction of red plum juice permeate flux during membrane processing with ANN optimized using RSM, Computers and Electronics in Agriculture, 102, 1-9, 2014.

[176] Offodile M. E., The Development and Management of Ground Water for Water Supply in Nigeria, 2nd Fellow's Workshop of Nigerian Mining and Geosciences Society (NMGS), 2000.

[177] Owen G., Bandi M., Howell J. A., and Churchouse S. J., Economic assessment of membrane processes for water and waste water treatment, Journal of Membrane Science, 102, 77-91, 1995.

[178] Pacheco F. A., Pinnau I., Reinhard M., and Leckie J. O., Characterization of isolated polyamide thin films of RO and NF membranes using novel TEM techniques, Journal of Membrane Science, 358, 51-59, 2010.

[179] Palai T. and Bhattacharya P. K., Kinetics of lactose conversion to galacto-oligosaccharides by β-galactosidase immobilized on PVDF membrane, Journal of Bioscience and Bioengineering, 115, 668-673, 2013.

[180] Palenzuela P., Zaragoza G., Alarcón-Padilla D. C., Guillén E., Ibarra M., and Blanco J., Assessment of different configurations for combined parabolic-trough (PT) solar power and desalination plants in arid regions, Energy, 36, 4950-4958, 2011.

[181] Pastagia K. M., Chakraborty S., DasGupta S., Basu J. K., and De S., Prediction of permeate flux and concentration of two-component dye mixture in batch nanofiltration, Journal of Membrane Science, 218, 195-210, 2003.

[182] Patil A. S., Medhi M., Sadavarte N. V., Wadgaonkar P. P., and Maldar N. N., Synthesis and characterization of novel aromatic–aliphatic polyamides from bis-[(4-aminobenzyl)-4-benzamide] ether, Materials Science and Engineering: B, 168, 111-116, 2010.

[183] Pérez-González A., Urtiaga A. M., Ibáñez R., and Ortiz I., State of the art and review on the treatment technologies of water reverse osmosis concentrates, Water Research, 46, 267-283, 2012.

[184] Polasek V., Talo S., and Sharif T., Conversion from hollow fiber to spiral technology in large seawater RO systems — process design and economics, Desalination, 156, 239-247, 2003.

[185] Prakash Rao A., Joshi S. V., Trivedi J. J., Devmurari C. V., and Shah V. J., Structure–performance correlation of polyamide thin film composite membranes: effect of coating conditions on film formation, Journal of Membrane Science, 211, 13-24, 2003.

[186] PSUMRI, http://www.azonano.com/article.aspx?ArticleID=1972, 2007.

[187] Purkait M. K., Bhattacharya P. K., and De S., Membrane filtration of leather plant effluent: Flux decline mechanism, Journal of Membrane Science, 258, 85-96, 2005.

[188] Purkait M. K., Kumar V. D., and Maity D., Treatment of leather plant effluent using NF followed by RO and permeate flux prediction using artificial neural network, Chemical Engineering Journal, 151, 275-285, 2009.

[189] Qiblawey H., Banat F., and Al-Nasser Q., Laboratory setup for water purification using household PV-driven reverse osmosis unit, Desalination and Water Treatment, 7, 53-59, 2009.

[190] Qiblawey H., Banat F., and Al-Nasser Q., Performance of reverse osmosis pilot plant powered by Photovoltaic in Jordan, Renewable Energy, 36, 3452-3460, 2011.

[191] Qiblawey H. M. and Banat F., Solar thermal desalination technologies, Desalination, 220, 633-644, 2008.

[192] Qiu T. and Davies P. A., Comparison of Configurations for High-Recovery Inland Desalination Systems, Water, 4, 690-706, 2012.

[193] Qtaishat M. R. and Banat F., Desalination by solar powered membrane distillation systems, Desalination, 308, 186-197, 2013.

[194] Rahardianto A., Gao J., Gabelich C. J., Williams M. D., and Cohen Y., High recovery membrane desalting of low-salinity brackish water: Integration of accelerated precipitation softening with membrane RO, Journal of Membrane Science, 289, 123-137, 2007.

[195] Rahmanian B., Pakizeh M., Mansoori S. A. A., Esfandyari M., Jafari D., Maddah H., and Maskooki A., Prediction of MEUF process performance using artificial neural networks and ANFIS approaches, Journal of the Taiwan Institute of Chemical Engineers, 43, 558-565, 2012.

[196] Rautenbach R. and Dahm W., Design and optimization of spiral-wound and hollow fiber RO-modules, Desalination, 65, 259-275, 1987.

[197] Rautenbach R., Vossenkaul K., Linn T., and Katz T., Waste water treatment by membrane processes — New development in ultrafiltration, nanofiltration and reverse osmosis, Desalination, 108, 247-253, 1997.

[198] Razali N. F., Mohammad A. W., Hilal N., Leo C. P., and Alam J., Optimisation of polyethersulfone/polyaniline blended membranes using response surface methodology approach, Desalination, 311, 182-191, 2013.

[199] Reig M., Casas S., Aladjem C., Valderrama C., Gibert O., Valero F., Centeno C. M., Larrotcha E., and Cortina J. L., Concentration of NaCl from seawater reverse osmosis brines for the chlor-alkali industry by electrodialysis, Desalination, 342, 107-117, 2014.

[200] REN21, Renewables Global Futures Report, Paris: REN21, 2013.

[201] Richards B. S., CapÃo D. P. S., and SchÄfer A. I., Renewable Energy Powered Membrane Technology. 2. The Effect of Energy Fluctuations on Performance of a Photovoltaic Hybrid Membrane System, Environmental Science & Technology, 42, 4563-4569, 2008.

[202] Richards B. S., Masson L., and Schäfer A. I., Impact of Feedwater Salinity on Energy Requirements of a Small-Scale Membrane Filtration System. In: Appropriate Technologies for Environmental Protection in the Developing World, Yanful, E. (Ed.), Springer Netherlands, 2009.

[203] Richards B. S. and Schäfer A. I., Photovoltaic-powered desalination system for remote Australian communities, Renewable Energy, 28, 2013-2022, 2003.

[204] Richards L. A., Richards B. S., and Schäfer A. I., Renewable energy powered membrane technology: Salt and inorganic contaminant removal by nanofiltration/reverse osmosis, Journal of Membrane Science, 369, 188-195, 2011.

[205] Riffel D. B. and Carvalho P. C. M., Small-scale photovoltaic-powered reverse osmosis plant without batteries: Design and simulation, Desalination, 247, 378-389, 2009.

[206] Ritchie S. M. C. and Bhattacharyya D., Membrane-based hybrid processes for high water recovery and selective inorganic pollutant separation, Journal of Hazardous Materials, 92, 21-32, 2002.

[207] Roberts D. A., Johnston E. L., and Knott N. A., Impacts of desalination plant discharges on the marine environment: A critical review of published studies, Water Research, 44, 5117-5128, 2010.

[208] Rossiter H. M. A., Graham M. C., and Schäfer A. I., Impact of speciation on behaviour of uranium in a solar powered membrane system for treatment of brackish groundwater, Separation and Purification Technology, 71, 89-96, 2010.

[209] Saha N. K., Balakrishnan M., and Batra V. S., Improving industrial water use: case study for an Indian distillery, Resources, Conservation and Recycling, 43, 163-174, 2005.

[210] Saha N. K., Balakrishnan M., and Ulbricht M., Sugarcane juice ultrafiltration: FTIR and SEM analysis of polysaccharide fouling, Journal of Membrane Science, 306, 287-297, 2007.

[211] Saha N. K. and Joshi S. V., Performance evaluation of thin film composite polyamide nanofiltration membrane with variation in monomer type, Journal of Membrane Science, 342, 60-69, 2009.

[212] Sarver J. G. and Fournier R. L., Numerical investigation of a novel spiral wound membrane sandwich design for an implantable bioartificial pancreas, Computers in Biology and Medicine, 20, 105-119, 1990.

[213] Sassi K. M. and Mujtaba I. M., Simulation and Optimization of Full Scale Reverse Osmosis Desalination Plant. In: Computer Aided Chemical Engineering, Pierucci, S. and Ferraris, G. B. (Eds.), Elsevier, 2010.

[214] Schäfer A. I., Broeckmann A., and Richards B. S., Renewable Energy Powered Membrane Technology. 1. Development and Characterization of a Photovoltaic Hybrid Membrane System, Environmental Science & Technology, 41, 998-1003, 2007.

[215] Schäfer A. I., Fane A. G., and Waite T. D., Nanofiltration of natural organic matter: Removal, fouling and the influence of multivalent ions, Desalination, 118, 109-122, 1998.

[216] Schäfer A. I., Pihlajamäki A., Fane A. G., Waite T. D., and Nyström M., Natural organic matter removal by nanofiltration: effects of solution chemistry on retention of low molar mass acids versus bulk organic matter, Journal of Membrane Science, 242, 73-85, 2004.

[217] Schäfer A. I. and Richards B. S., Testing of a hybrid membrane system for groundwater desalination in an Australian national park, Desalination, 183, 55-62, 2005.

[218] Sen P. K., Sen P. V., Mudgal A., Singh S. N., Vyas S. K., and Davies P., A small scale Multi-effect Distillation (MED) unit for rural micro enterprises: Part I—design and fabrication, Desalination, 279, 15-26, 2011.

[219] Shojaeimehr T., Rahimpour F., Khadivi M. A., and Sadeghi M., A modeling study by response surface methodology (RSM) and artificial neural network (ANN) on Cu2+ adsorption optimization using light expended clay aggregate (LECA), Journal of Industrial and Engineering Chemistry, 20, 870-880, 2014.

[220] Shu L., Waite T. D., Bliss P. J., Fane A., and Jegatheesan V., Nanofiltration for the possible reuse of water and recovery of sodium chloride salt from textile effluent, Desalination, 172, 235-243, 2005.

[221] Shukla S. K., Kumar V., and Bansal M. C., Treatment of combined bleaching effluent by membrane filtration technology for system closure in paper industry, Desalination and Water Treatment, 14, 273-273, 2010.

[222] Shuman B., A Comparison of Response Surface Methodology and a One-factor-at-a-time Approach as Calibration Techniques for the Bioplume-II Simulation Model of Contaminant Degradation, Air Force Institute of Technology, 1995.

[223] Silverstein R. M., Webster F. X., and Kiemle D., Spectrometric Identification of Organic Compounds, John Wiley & Sons, Inc., 2005.

[224] Singh K., Singh A., Gupta S., and Rai P., Modeling and optimization of reductive degradation of chloramphenicol in aqueous solution by zero-valent bimetallic nanoparticles, Environmental Science and Pollution Research, 19, 2063-2078, 2012.

[225] Singh P. S., Rao A. P., Ray P., Bhattacharya A., Singh K., Saha N. K., and Reddy A. V. R., Techniques for characterization of polyamide thin film composite membranes, Desalination, 282, 78-86, 2011.

[226] Singh V. and Das C., Comparison of spiral wound UF membrane performance between turbulent and laminar flow regimes, Desalination, 337, 43-51, 2014.

[227] Singh V., Jain P. K., and Das C., Performance of spiral wound ultrafiltration membrane module for with and without permeate recycle: Experimental and theoretical consideration, Desalination, 322, 94-103, 2013.

[228] Singh V., Purkait M. K., Chandaliya V. K., Biswas P. P., Banerjee P. K., and Das C., Development of membrane based technology for the separation of coal from organic solvent, Desalination, 299, 123-128, 2012.

[229] Socrates G., Infrared characteristic group frequencies, Chichester:Wiley, New York 1980.

[230] SolarGIS, World map of global horizontal irradiation, http://solargis.info/doc/_pics/freemaps/1000px/ghi/SolarGIS-Solar-map-World-map-en.png. GeoModel Solar, 2013.

[231] Song Y., Gao X., and Gao C., Evaluation of scaling potential in a pilot-scale NF–SWRO integrated seawater desalination system, Journal of Membrane Science, 443, 201-209, 2013.

[232] Soric A., Cesaro R., Perez P., Guiol E., and Moulin P., Eausmose project desalination by reverse osmosis and batteryless solar energy: Design for a 1m3 per day delivery, Desalination, 301, 67-74, 2012.

[233] Sorrell S., Speirs J., Bentley R., Brandt A., and Miller R., Global Oil Depletion, An assessment of the evidence for a near-term peak in global oil production. A report produced by the Technology and Policy Assessment function of the UK Energy Research Centre, 198 pp., 2009.

[234] Spoolman G. T. M. S. E., 2008.

[235] Stoquart C., Servais P., Bérubé P. R., and Barbeau B., Hybrid Membrane Processes using activated carbon treatment for drinking water: A review, Journal of Membrane Science, 411–412, 1-12, 2012.

[236] Subramani A. and Jacangelo J. G., Treatment technologies for reverse osmosis concentrate volume minimization: A review, Separation and Purification Technology, 122, 472-489, 2014.

[237] Taha F. K. and Ismail S., Managing salinity in the developing world, 2nd International Salinity Forum, Salinity, Water and Society – Global issues, local action, Adelaide Convention Centre, Adelaide, South Australia, Australia, 2008.

[238] Tang C. Y., Kwon Y.-N., and Leckie J. O., Probing the nano- and micro-scales of reverse osmosis membranes—A comprehensive characterization of physiochemical properties of uncoated and coated membranes by XPS, TEM, ATR-FTIR, and streaming potential measurements, Journal of Membrane Science, 287, 146-156, 2007.

[239] Tang W. and Ng H. Y., Concentration of brine by forward osmosis: Performance and influence of membrane structure, Desalination, 224, 143-153, 2008.

[240] Tangsubkul N., Parameshwaran K., Lundie S., Fane A. G., and Waite T. D., Environmental life cycle assessment of the microfiltration process, Journal of Membrane Science, 284, 214-226, 2006.

[241] Tarboush B. J. A., Rana D., Matsuura T., Arafat H. A., and Narbaitz R. M., Preparation of thin-film-composite polyamide membranes for desalination using novel hydrophilic surface modifying macromolecules, Journal of Membrane Science, 325, 166-175, 2008.

[242] Thomson M., Reverse-osmosis desalination of seawater powered by photovoltaics without batteries, Ph.D., Loughborough University, U.K., 242 pp., 2003.

[243] Thomson M. and Infield D., Laboratory demonstration of a photovoltaic-powered seawater reverse-osmosis system without batteries, Desalination, 183, 105-111, 2005.

[244] Thomson M. and Infield D., A photovoltaic-powered seawater reverse-osmosis system without batteries, Desalination, 153, 1-8, 2003.

[245] Thomson M., Infield D., Lichtwardt, and Remmers, Water treatment using solar powered electrodialysis reversal, 11/1/ 1996, 105-111.

[246] Thomson M., Miranda M., Gwillim J., Rowbottom A., and Draisey I., Batteryless photovoltaic reverse osmosis desalination system, 25 pp., 2001.

[247] Tran A. T. K., Zhang Y., Jullok N., Meesschaert B., Pinoy L., and Van der Bruggen B., RO concentrate treatment by a hybrid system consisting of a pellet reactor and electrodialysis, Chemical Engineering Science, 79, 228-238, 2012.

[248] Tu K. L., Nghiem L. D., and Chivas A. R., Boron removal by reverse osmosis membranes in seawater desalination applications, Separation and Purification Technology, 75, 87-101, 2010.

[249] Tzen E., Perrakis K., and Baltas P., Design of a stand alone PV - desalination system for rural areas, Desalination, 119, 327-333, 1998.

[250] UNEP, 21 Issues for the 21st Century: Result of the UNEP Foresight Process on Emerging Environmental Issues., Nairobi, Kenya, 56 pp., 2012.

[251] Upadhyay V., Jain P. K., and Mehta N. K., Artificial Neural Network Modeling of Cutting Force in Turning of Ti-6Al-4V Alloy and Its Comparison with Response Surface Methodology, Roorkee, India2011, 761-768.

[252] Vinodia A. K., Promotion of renewable energy in rural india, Institute of Town Planners, India Journal, 3, 21-28, 2006.

[253] Vrijenhoek E. M., Hong S., and Elimelech M., Influence of membrane surface properties on initial rate of colloidal fouling of reverse osmosis and nanofiltration membranes, Journal of Membrane Science, 188, 115-128, 2001.

[254] Walha K., Amar R. B., Quemeneur F., and Jaouen P., Treatment by nanofiltration and reverse osmosis of high salinity drilling water for seafood washing and processing Abstract, Desalination, 219, 231-239, 2008.

[255] Weert F. V., Gun J. V. D., and Reckman J., Global Overview of Saline Groundwater Occurrence and Genesis, International Groundwater Resources Assessment Centre 107 pp., 2009.

[256] Wright N. C. and Winter V A. G., Justification for community-scale photovoltaic-powered electrodialysis desalination systems for inland rural villages in India, Desalination, 352, 82-91, 2014.

[257] Yangali-Quintanilla V., Verliefde A., Kim T. U., Sadmani A., Kennedy M., and Amy G., Artificial neural network models based on QSAR for predicting rejection of neutral organic compounds by polyamide nanofiltration and reverse osmosis membranes, J. of Memb. Sci., 342, 251-262, 2009.

[258] Yechieli Y. and Wood W. W., Hydrogeologic processes in saline systems: playas, sabkhas, and saline lakes, Earth-Science Reviews, 58, 343-365, 2002.

[259] Zhang X., Hu D., and Li Z., Performance analysis on a new multi-effect distillation combined with an open absorption heat transformer driven by waste heat, Applied Thermal Engineering, 62, 239-244, 2014.

[260] Zhao Y., Hu X.-m., Jiang B.-h., and Li L., Optimization of the operational parameters for desalination with response surface methodology during a capacitive deionization process, Desalination, 336, 64-71, 2014.

[261] Zulkali M. M. D., Ahmad A. L., and Derek C. J. C., Membrane application in proteomic studies: Preliminary studies on the effect of pH, ionic strength and pressure on protein fractionation, Desalination, 179, 381-390, 2005.

Author's Publications

International Journals

[1]. Garg M. C. and Joshi H., Optimization and economic analysis of small scale hybrid nanofiltration and reverse osmosis water desalination system powered by solar photovoltaic, Desalination, 353, 57-74, 2014.

[2]. Garg M. C. and Joshi H., New approach for optimization of small scale RO membrane using artificial groundwater, Environmental Technology, 35(23), 2988-2999, 2014.

[3]. Garg M. C. and Joshi H., Photovoltaic powered reverse osmosis process: solution to drinking water scarcity due to high salinity in non-electrified rural areas, Separation Science and Technology, Accepted (in Press), 2014.

International Journals (Communicated)

[1]. Garg M. C. and Joshi H., Comparative assessment and multivariate optimization of commercially available small scale reverse osmosis membranes, Communicated in Journal of Environmental Informatics (under review).

International Conferences

[1]. Garg M. C. and Joshi H., Optimization and economic analysis for a small scale nanofiltration and reverse osmosis water desalination system, International conference "4th IWA Regional Conference on Membrane Technology 2014", Ho Chi Minh City, Vietnam, 3-6 December, 2014.

[2]. Garg M. C. and Joshi H., The photovoltaic powered reverse osmosis: a critical review, International Symposium "Indian Desalination Association Congress-2011" (InDACON-2011), Vizianagaram, Andhara Pradesh, India, 24-25 March, 2011.